

Improved measurements of $D^0 \rightarrow K^- \ell^+ \nu_\ell$ and $D^+ \rightarrow \bar{K}^0 \ell^+ \nu_\ell$

M. Ablikim¹, M. N. Achasov^{4,c}, P. Adlarson⁷⁶, O. Afedulidis³, X. C. Ai⁸¹, R. Aliberti³⁵, A. Amoroso^{75A,75C}, Q. An^{72,58,a}, Y. Bai⁵⁷, O. Bakina³⁶, I. Balossino^{29A}, Y. Ban^{46,h}, H.-R. Bao⁶⁴, V. Batozskaya^{1,44}, K. Begzsuren³², N. Berger³⁵, M. Berlowski⁴⁴, M. Bertani^{28A}, D. Bettoni^{29A}, F. Bianchi^{75A,75C}, E. Bianco^{75A,75C}, A. Bortone^{75A,75C}, I. Boyko³⁶, R. A. Briere⁵, A. Brueggemann⁶⁹, H. Cai⁷⁷, X. Cai^{1,58}, A. Calcaterra^{28A}, G. F. Cao^{1,64}, N. Cao^{1,64}, S. A. Cetin^{62A}, X. Y. Chai^{46,h}, J. F. Chang^{1,58}, G. R. Che⁴³, Y. Z. Che^{1,58,64}, G. Chelkov^{36,b}, C. Chen⁴³, C. H. Chen⁹, Chao Chen⁵⁵, G. Chen¹, H. S. Chen^{1,64}, H. Y. Chen²⁰, M. L. Chen^{1,58,64}, S. J. Chen⁴², S. L. Chen⁴⁵, S. M. Chen⁶¹, T. Chen^{1,64}, X. R. Chen^{31,64}, X. T. Chen^{1,64}, Y. B. Chen^{1,58}, Y. Q. Chen³⁴, Z. J. Chen^{25,i}, Z. Y. Chen^{1,64}, S. K. Choi¹⁰, G. Cibinetto^{29A}, F. Cossio^{75C}, J. J. Cui⁵⁰, H. L. Dai^{1,58}, J. P. Dai⁷⁹, A. Dbeyssi¹⁸, R. E. de Boer³, D. Dedovich³⁶, C. Q. Deng⁷³, Z. Y. Deng¹, A. Denig³⁵, I. Denysenko³⁶, M. Destefanis^{75A,75C}, F. De Mori^{75A,75C}, B. Ding^{67,1}, X. X. Ding^{46,h}, Y. Ding³⁴, Y. Ding⁴⁰, J. Dong^{1,58}, L. Y. Dong^{1,64}, M. Y. Dong^{1,58,64}, X. Dong⁷⁷, M. C. Du¹, S. X. Du⁸¹, Y. Y. Duan⁵⁵, Z. H. Duan⁴², P. Egorov^{36,b}, Y. H. Fan⁴⁵, J. Fang^{1,58}, J. Fang⁵⁹, S. S. Fang^{1,64}, W. X. Fang¹, Y. Fang¹, Y. Q. Fang^{1,58}, R. Farinelli^{29A}, L. Fava^{75B,75C}, F. Feldbauer³, G. Felici^{28A}, C. Q. Feng^{72,58}, J. H. Feng⁵⁹, Y. T. Feng^{72,58}, M. Fritsch³, C. D. Fu¹, J. L. Fu⁶⁴, Y. W. Fu^{1,64}, H. Gao⁶⁴, X. B. Gao⁴¹, Y. N. Gao^{46,h}, Yang Gao^{72,58}, S. Garbolino^{75C}, I. Garzia^{29A,29B}, L. Ge⁸¹, P. T. Ge¹⁹, Z. W. Ge⁴², C. Geng⁵⁹, E. M. Gersabeck⁶⁸, A. Gilman⁷⁰, K. Goetzen¹³, L. Gong⁴⁰, W. X. Gong^{1,58}, W. Gradl³⁵, S. Gramigna^{29A,29B}, M. Greco^{75A,75C}, M. H. Gu^{1,58}, Y. T. Gu¹⁵, C. Y. Guan^{1,64}, A. Q. Guo^{31,64}, L. B. Guo⁴¹, M. J. Guo⁵⁰, R. P. Guo⁴⁹, Y. P. Guo^{12,g}, A. Guskov^{36,b}, J. Gutierrez²⁷, K. L. Han⁶⁴, T. T. Han¹, F. Hanisch³, X. Q. Hao¹⁹, F. A. Harris⁶⁶, K. K. He^{55,16}, K. L. He^{1,64}, F. H. Heinsius³, C. H. Heinz³⁵, Y. K. Heng^{1,58,64}, C. Herold⁶⁰, T. Holtmann³, P. C. Hong³⁴, G. Y. Hou^{1,64}, X. T. Hou^{1,64}, Y. R. Hou⁶⁴, Z. L. Hou¹, B. Y. Hu⁵⁹, H. M. Hu^{1,64}, J. F. Hu^{56,j}, S. L. Hu^{12,g}, T. Hu^{1,58,64}, Y. Hu¹, G. S. Huang^{72,58}, K. X. Huang⁵⁹, L. Q. Huang^{31,64}, X. T. Huang⁵⁰, Y. P. Huang¹, Y. S. Huang⁵⁹, T. Hussain⁷⁴, F. Hölzken³, N. Hüsken³⁵, N. in der Wiesche⁶⁹, J. Jackson²⁷, S. Janchiv³², J. H. Jeong¹⁰, Q. Ji¹, Q. P. Ji¹⁹, W. Ji^{1,64}, X. B. Ji^{1,64}, X. L. Ji^{1,58}, Y. Y. Ji⁵⁰, X. Q. Jia⁵⁰, Z. K. Jia^{72,58}, D. Jiang^{1,64}, H. B. Jiang⁷⁷, P. C. Jiang^{46,h}, S. S. Jiang³⁹, T. J. Jiang¹⁶, X. S. Jiang^{1,58,64}, Y. Jiang⁶⁴, J. B. Jiao⁵⁰, J. K. Jiao³⁴, Z. Jiao²³, S. Jin⁴², Y. Jin⁶⁷, M. Q. Jing^{1,64}, X. M. Jing⁶⁴, T. Johansson⁷⁶, S. Kabana³³, N. Kalantar-Nayestanaki⁶⁵, X. L. Kang⁹, X. S. Kang⁴⁰, M. Kavatsyuk⁶⁵, B. C. Ke⁸¹, V. Khachatryan²⁷, A. Khoukaz⁶⁹, R. Kiuchi¹, O. B. Kolcu^{62A}, B. Kopf³, M. Kuessner³, X. Kui^{1,64}, N. Kumar²⁶, A. Kupsc^{44,76}, W. Kühn³⁷, J. J. Lane⁶⁸, L. Lavezzi^{75A,75C}, T. T. Lei^{72,58}, Z. H. Lei^{72,58}, M. Lellmann³⁵, T. Lenz³⁵, C. Li⁴³, C. Li⁴⁷, C. H. Li³⁹, Cheng Li^{72,58}, D. M. Li⁸¹, F. Li^{1,58}, G. Li¹, H. B. Li^{1,64}, H. J. Li¹⁹, H. N. Li^{56,j}, Hui Li⁴³, J. R. Li⁶¹, J. S. Li⁵⁹, K. Li¹, K. L. Li¹⁹, L. J. Li^{1,64}, L. K. Li¹, Lei Li⁴⁸, M. H. Li⁴³, P. R. Li^{38,k,l}, Q. M. Li^{1,64}, Q. X. Li⁵⁰, R. Li^{17,31}, S. X. Li¹², T. Li⁵⁰, W. D. Li^{1,64}, W. G. Li^{1,a}, X. Li^{1,64}, X. H. Li^{72,58}, X. L. Li⁵⁰, X. Y. Li^{1,64}, X. Z. Li⁵⁹, Y. G. Li^{46,h}, Z. J. Li⁵⁹, Z. Y. Li⁷⁹, C. Liang⁴², H. Liang^{72,58}, H. Liang^{1,64}, Y. F. Liang⁵⁴, Y. T. Liang^{31,64}, G. R. Liao¹⁴, Y. P. Liao^{1,64}, J. Libby²⁶, A. Limphirat⁶⁰, C. C. Lin⁵⁵, D. X. Lin^{31,64}, T. Lin¹, B. J. Liu¹, B. X. Liu⁷⁷, C. Liu³⁴, C. X. Liu¹, F. Liu¹, F. H. Liu⁵³, Feng Liu⁶, G. M. Liu^{56,j}, H. Liu^{38,k,l}, H. B. Liu¹⁵, H. H. Liu¹, H. M. Liu^{1,64}, Huihui Liu²¹, J. B. Liu^{72,58}, J. Y. Liu^{1,64}, K. Liu^{38,k,l}, K. Y. Liu⁴⁰, Ke Liu²², L. Liu^{72,58}, L. C. Liu⁴³, Lu Liu⁴³, M. H. Liu^{12,g}, P. L. Liu¹, Q. Liu⁶⁴, S. B. Liu^{72,58}, T. Liu^{12,g}, W. K. Liu⁴³, W. M. Liu^{72,58}, X. Liu³⁹, X. Liu^{38,k,l}, Y. Liu⁸¹, Y. Liu^{38,k,l}, Y. B. Liu⁴³, Z. A. Liu^{1,58,64}, Z. D. Liu⁹, Z. Q. Liu⁵⁰, X. C. Lou^{1,58,64}, F. X. Lu⁵⁹, H. J. Lu²³, J. G. Lu^{1,58}, X. L. Lu¹, Y. Lu⁷, Y. P. Lu^{1,58}, Z. H. Lu^{1,64}, C. L. Luo⁴¹, J. R. Luo⁵⁹, M. X. Luo⁸⁰, T. Luo^{12,g}, X. L. Luo^{1,58}, X. R. Lyu⁶⁴, Y. F. Lyu⁴³, F. C. Ma⁴⁰, H. Ma⁷⁹, H. L. Ma¹, J. L. Ma^{1,64}, L. L. Ma⁵⁰, L. R. Ma⁶⁷, M. M. Ma^{1,64}, Q. M. Ma¹, R. Q. Ma^{1,64}, T. Ma^{72,58}, X. T. Ma^{1,64}, X. Y. Ma^{1,58}, Y. M. Ma³¹, F. E. Maas¹⁸, I. MacKay⁷⁰, M. Maggiora^{75A,75C}, S. Malde⁷⁰, Y. J. Mao^{46,h}, Z. P. Mao¹, S. Marcello^{75A,75C}, Z. X. Meng⁶⁷, J. G. Messchendorp^{13,65}, G. Mezzadri^{29A}, H. Miao^{1,64}, T. J. Min⁴², R. E. Mitchell²⁷, X. H. Mo^{1,58,64}, B. Moses²⁷, N. Yu. Muchnoi^{4,c}, J. Muskalla³⁵, Y. Nefedov³⁶, F. Nerling^{18,e}, L. S. Nie²⁰, I. B. Nikolaev^{4,c}, Z. Ning^{1,58}, S. Nisar^{11,m}, Q. L. Niu^{38,k,l}, W. D. Niu⁵⁵, Y. Niu⁵⁰, S. L. Olsen⁶⁴, S. L. Olsen^{10,64}, Q. Ouyang^{1,58,64}, S. Pacetti^{28B,28C}, X. Pan⁵⁵, Y. Pan⁵⁷, A. Pathak³⁴, Y. P. Pei^{72,58}, M. Pelizaeus³, H. P. Peng^{72,58}, Y. Y. Peng^{38,k,l}, K. Peters^{13,e}, J. L. Ping⁴¹, R. G. Ping^{1,64}, S. Plura³⁵, V. Prasad³³, F. Z. Qi¹, H. Qi^{72,58}, H. R. Qi⁶¹, M. Qi⁴², T. Y. Qi^{12,g}, S. Qian^{1,58}, W. B. Qian⁶⁴, C. F. Qiao⁶⁴, X. K. Qiao⁸¹, J. J. Qin⁷³, L. Q. Qin¹⁴, L. Y. Qin^{72,58}, X. P. Qin^{12,g}, X. S. Qin⁵⁰, Z. H. Qin^{1,58}, J. F. Qiu¹, Z. H. Qu⁷³, C. F. Redmer³⁵, K. J. Ren³⁹, A. Rivetti^{75C}, M. Rolo^{75C}, G. Rong^{1,64}, Ch. Rosner¹⁸, M. Q. Ruan^{1,58}, S. N. Ruan⁴³, N. Salone⁴⁴, A. Sarantsev^{36,d}, Y. Schelhaas³⁵, K. Schoenning⁷⁶, M. Scodeggio^{29A}, K. Y. Shan^{12,g}, W. Shan²⁴, X. Y. Shan^{72,58}, Z. J. Shang^{38,k,l}, J. F. Shangguan¹⁶, L. G. Shao^{1,64}, M. Shao^{72,58}, C. P. Shen^{12,g}, H. F. Shen^{1,8}, W. H. Shen⁶⁴, X. Y. Shen^{1,64}, B. A. Shi⁶⁴, H. Shi^{72,58}, H. C. Shi^{72,58}, J. L. Shi^{12,g}, J. Y. Shi¹, Q. Q. Shi⁵⁵, S. Y. Shi⁷³, X. Shi^{1,58}, J. J. Song¹⁹, T. Z. Song⁵⁹, W. M. Song^{34,1}, Y. J. Song^{12,g}, Y. X. Song^{46,h,n}, S. Sosio^{75A,75C}, S. Spataro^{75A,75C},

F. Stierl³⁵, S. S. Su⁴⁰, Y. J. Su⁶⁴, G. B. Sun⁷⁷, G. X. Sun¹, H. Sun⁶⁴, H. K. Sun¹, J. F. Sun¹⁹, K. Sun⁶¹, L. Sun⁷⁷, S. S. Sun^{1,64}, T. Sun^{51,f}, W. Y. Sun³⁴, Y. Sun⁹, Y. J. Sun^{72,58}, Y. Z. Sun¹, Z. Q. Sun^{1,64}, Z. T. Sun⁵⁰, C. J. Tang⁵⁴, G. Y. Tang¹, J. Tang⁵⁹, M. Tang^{72,58}, Y. A. Tang⁷⁷, L. Y. Tao⁷³, Q. T. Tao^{25,i}, M. Tat⁷⁰, J. X. Teng^{72,58}, V. Thoren⁷⁶, W. H. Tian⁵⁹, Y. Tian^{31,64}, Z. F. Tian⁷⁷, I. Uman^{62B}, Y. Wan⁵⁵, S. J. Wang⁵⁰, B. Wang¹, B. L. Wang⁶⁴, Bo Wang^{72,58}, D. Y. Wang^{46,h}, F. Wang⁷³, H. J. Wang^{38,k,l}, J. J. Wang⁷⁷, J. P. Wang⁵⁰, K. Wang^{1,58}, L. L. Wang¹, M. Wang⁵⁰, N. Y. Wang⁶⁴, S. Wang^{38,k,l}, S. Wang^{12,g}, T. Wang^{12,g}, T. J. Wang⁴³, W. Wang⁵⁹, W. Wang⁷³, W. P. Wang^{35,58,72,o}, X. Wang^{46,h}, X. F. Wang^{38,k,l}, X. J. Wang³⁹, X. L. Wang^{12,g}, X. N. Wang¹, Y. Wang⁶¹, Y. D. Wang⁴⁵, Y. F. Wang^{1,58,64}, Y. L. Wang¹⁹, Y. N. Wang⁴⁵, Y. Q. Wang¹, Yaqian Wang¹⁷, Yi Wang⁶¹, Z. Wang^{1,58}, Z. L. Wang⁷³, Z. Y. Wang^{1,64}, Ziyi Wang⁶⁴, D. H. Wei¹⁴, F. Weidner⁶⁹, S. P. Wen¹, Y. R. Wen³⁹, U. Wiedner³, G. Wilkinson⁷⁰, M. Wolke⁷⁶, L. Wollenberg³, C. Wu³⁹, J. F. Wu^{1,8}, L. H. Wu¹, L. J. Wu^{1,64}, X. Wu^{12,g}, X. H. Wu³⁴, Y. Wu^{72,58}, Y. H. Wu⁵⁵, Y. J. Wu³¹, Z. Wu^{1,58}, L. Xia^{72,58}, X. M. Xian³⁹, B. H. Xiang^{1,64}, T. Xiang^{46,h}, D. Xiao^{38,k,l}, G. Y. Xiao⁴², S. Y. Xiao¹, Y. L. Xiao^{12,g}, Z. J. Xiao⁴¹, C. Xie⁴², X. H. Xie^{46,h}, Y. Xie⁵⁰, Y. G. Xie^{1,58}, Y. H. Xie⁶, Z. P. Xie^{72,58}, T. Y. Xing^{1,64}, C. F. Xu^{1,64}, C. J. Xu⁵⁹, G. F. Xu¹, H. Y. Xu^{67,2,p}, M. Xu^{72,58}, Q. J. Xu¹⁶, Q. N. Xu³⁰, W. Xu¹, W. L. Xu⁶⁷, X. P. Xu⁵⁵, Y. Xu⁴⁰, Y. C. Xu⁷⁸, Z. S. Xu⁶⁴, F. Yan^{12,g}, L. Yan^{12,g}, W. B. Yan^{72,58}, W. C. Yan⁸¹, X. Q. Yan^{1,64}, H. J. Yang^{51,f}, H. L. Yang³⁴, H. X. Yang¹, J. H. Yang⁴², T. Yang¹, Y. Yang^{12,g}, Y. F. Yang⁴³, Y. F. Yang^{1,64}, Y. X. Yang^{1,64}, Z. W. Yang^{38,k,l}, Z. P. Yao⁵⁰, M. Ye^{1,58}, M. H. Ye⁸, J. H. Yin¹, Junhao Yin⁴³, Z. Y. You⁵⁹, B. X. Yu^{1,58,64}, C. X. Yu⁴³, G. Yu^{1,64}, J. S. Yu^{25,i}, M. C. Yu⁴⁰, T. Yu⁷³, X. D. Yu^{46,h}, Y. C. Yu⁸¹, C. Z. Yuan^{1,64}, J. Yuan³⁴, J. Yuan⁴⁵, L. Yuan², S. C. Yuan^{1,64}, Y. Yuan^{1,64}, Z. Y. Yuan⁵⁹, C. X. Yue³⁹, A. A. Zafar⁷⁴, F. R. Zeng⁵⁰, S. H. Zeng^{63A,63B,63C,63D}, X. Zeng^{12,g}, Y. Zeng^{25,i}, Y. J. Zeng⁵⁹, Y. J. Zeng^{1,64}, X. Y. Zhai³⁴, Y. C. Zhai⁵⁰, Y. H. Zhan⁵⁹, A. Q. Zhang^{1,64}, B. L. Zhang^{1,64}, B. X. Zhang¹, D. H. Zhang⁴³, G. Y. Zhang¹⁹, H. Zhang⁸¹, H. Zhang^{72,58}, H. C. Zhang^{1,58,64}, H. H. Zhang⁵⁹, H. H. Zhang³⁴, H. Q. Zhang^{1,58,64}, H. R. Zhang^{72,58}, H. Y. Zhang^{1,58}, J. Zhang⁸¹, J. Zhang⁵⁹, J. J. Zhang⁵², J. L. Zhang²⁰, J. Q. Zhang⁴¹, J. S. Zhang^{12,g}, J. W. Zhang^{1,58,64}, J. X. Zhang^{38,k,l}, J. Y. Zhang¹, J. Z. Zhang^{1,64}, Jianyu Zhang⁶⁴, L. M. Zhang⁶¹, Lei Zhang⁴², P. Zhang^{1,64}, Q. Y. Zhang³⁴, R. Y. Zhang^{38,k,l}, S. H. Zhang^{1,64}, Shulei Zhang^{25,i}, X. M. Zhang¹, X. Y. Zhang⁴⁰, X. Y. Zhang⁵⁰, Y. Zhang¹, Y. Zhang⁷³, Y. T. Zhang⁸¹, Y. H. Zhang^{1,58}, Y. M. Zhang³⁹, Yan Zhang^{72,58}, Z. D. Zhang¹, Z. H. Zhang¹, Z. L. Zhang³⁴, Z. Y. Zhang⁷⁷, Z. Y. Zhang⁴³, Z. Z. Zhang⁴⁵, G. Zhao¹, J. Y. Zhao^{1,64}, J. Z. Zhao^{1,58}, L. Zhao¹, Lei Zhao^{72,58}, M. G. Zhao⁴³, N. Zhao⁷⁹, R. P. Zhao⁶⁴, S. J. Zhao⁸¹, Y. B. Zhao^{1,58}, Y. X. Zhao^{31,64}, Z. G. Zhao^{72,58}, A. Zhemchugov^{36,b}, B. Zheng⁷³, B. M. Zheng³⁴, J. P. Zheng^{1,58}, W. J. Zheng^{1,64}, Y. H. Zheng⁶⁴, B. Zhong⁴¹, X. Zhong⁵⁹, H. Zhou⁵⁰, J. Y. Zhou³⁴, L. P. Zhou^{1,64}, S. Zhou⁶, X. Zhou⁷⁷, X. K. Zhou⁶, X. R. Zhou^{72,58}, X. Y. Zhou³⁹, Y. Z. Zhou^{12,g}, Z. C. Zhou²⁰, A. N. Zhu⁶⁴, J. Zhu⁴³, K. Zhu¹, K. J. Zhu^{1,58,64}, K. S. Zhu^{12,g}, L. Zhu³⁴, L. X. Zhu⁶⁴, S. H. Zhu⁷¹, T. J. Zhu^{12,g}, W. D. Zhu⁴¹, Y. C. Zhu^{72,58}, Z. A. Zhu^{1,64}, J. H. Zou¹, J. Zu^{72,58}

(BESIII Collaboration)

¹ *Institute of High Energy Physics, Beijing 100049, People's Republic of China*

² *Beihang University, Beijing 100191, People's Republic of China*

³ *Bochum Ruhr-University, D-44780 Bochum, Germany*

⁴ *Budker Institute of Nuclear Physics SB RAS (BINP), Novosibirsk 630090, Russia*

⁵ *Carnegie Mellon University, Pittsburgh, Pennsylvania 15213, USA*

⁶ *Central China Normal University, Wuhan 430079, People's Republic of China*

⁷ *Central South University, Changsha 410083, People's Republic of China*

⁸ *China Center of Advanced Science and Technology, Beijing 100190, People's Republic of China*

⁹ *China University of Geosciences, Wuhan 430074, People's Republic of China*

¹⁰ *Chung-Ang University, Seoul, 06974, Republic of Korea*

¹¹ *COMSATS University Islamabad, Lahore Campus, Defence Road, Off Raiwind Road, 54000 Lahore, Pakistan*

¹² *Fudan University, Shanghai 200433, People's Republic of China*

¹³ *GSI Helmholtzcentre for Heavy Ion Research GmbH, D-64291 Darmstadt, Germany*

¹⁴ *Guangxi Normal University, Guilin 541004, People's Republic of China*

¹⁵ *Guangxi University, Nanning 530004, People's Republic of China*

¹⁶ *Hangzhou Normal University, Hangzhou 310036, People's Republic of China*

¹⁷ *Hebei University, Baoding 071002, People's Republic of China*

¹⁸ *Helmholtz Institute Mainz, Staudinger Weg 18, D-55099 Mainz, Germany*

¹⁹ *Henan Normal University, Xinxiang 453007, People's Republic of China*

²⁰ *Henan University, Kaifeng 475004, People's Republic of China*

- ²¹ Henan University of Science and Technology, Luoyang 471003, People's Republic of China
- ²² Henan University of Technology, Zhengzhou 450001, People's Republic of China
- ²³ Huangshan College, Huangshan 245000, People's Republic of China
- ²⁴ Hunan Normal University, Changsha 410081, People's Republic of China
- ²⁵ Hunan University, Changsha 410082, People's Republic of China
- ²⁶ Indian Institute of Technology Madras, Chennai 600036, India
- ²⁷ Indiana University, Bloomington, Indiana 47405, USA
- ²⁸ INFN Laboratori Nazionali di Frascati, (A)INFN Laboratori Nazionali di Frascati, I-00044, Frascati, Italy; (B)INFN Sezione di Perugia, I-06100, Perugia, Italy; (C)University of Perugia, I-06100, Perugia, Italy
- ²⁹ INFN Sezione di Ferrara, (A)INFN Sezione di Ferrara, I-44122, Ferrara, Italy; (B)University of Ferrara, I-44122, Ferrara, Italy
- ³⁰ Inner Mongolia University, Hohhot 010021, People's Republic of China
- ³¹ Institute of Modern Physics, Lanzhou 730000, People's Republic of China
- ³² Institute of Physics and Technology, Peace Avenue 54B, Ulaanbaatar 13330, Mongolia
- ³³ Instituto de Alta Investigación, Universidad de Tarapacá, Casilla 7D, Arica 1000000, Chile
- ³⁴ Jilin University, Changchun 130012, People's Republic of China
- ³⁵ Johannes Gutenberg University of Mainz, Johann-Joachim-Becher-Weg 45, D-55099 Mainz, Germany
- ³⁶ Joint Institute for Nuclear Research, 141980 Dubna, Moscow region, Russia
- ³⁷ Justus-Liebig-Universität Giessen, II. Physikalisches Institut, Heinrich-Buff-Ring 16, D-35392 Giessen, Germany
- ³⁸ Lanzhou University, Lanzhou 730000, People's Republic of China
- ³⁹ Liaoning Normal University, Dalian 116029, People's Republic of China
- ⁴⁰ Liaoning University, Shenyang 110036, People's Republic of China
- ⁴¹ Nanjing Normal University, Nanjing 210023, People's Republic of China
- ⁴² Nanjing University, Nanjing 210093, People's Republic of China
- ⁴³ Nankai University, Tianjin 300071, People's Republic of China
- ⁴⁴ National Centre for Nuclear Research, Warsaw 02-093, Poland
- ⁴⁵ North China Electric Power University, Beijing 102206, People's Republic of China
- ⁴⁶ Peking University, Beijing 100871, People's Republic of China
- ⁴⁷ Qufu Normal University, Qufu 273165, People's Republic of China
- ⁴⁸ Renmin University of China, Beijing 100872, People's Republic of China
- ⁴⁹ Shandong Normal University, Jinan 250014, People's Republic of China
- ⁵⁰ Shandong University, Jinan 250100, People's Republic of China
- ⁵¹ Shanghai Jiao Tong University, Shanghai 200240, People's Republic of China
- ⁵² Shanxi Normal University, Linfen 041004, People's Republic of China
- ⁵³ Shanxi University, Taiyuan 030006, People's Republic of China
- ⁵⁴ Sichuan University, Chengdu 610064, People's Republic of China
- ⁵⁵ Soochow University, Suzhou 215006, People's Republic of China
- ⁵⁶ South China Normal University, Guangzhou 510006, People's Republic of China
- ⁵⁷ Southeast University, Nanjing 211100, People's Republic of China
- ⁵⁸ State Key Laboratory of Particle Detection and Electronics, Beijing 100049, Hefei 230026, People's Republic of China
- ⁵⁹ Sun Yat-Sen University, Guangzhou 510275, People's Republic of China
- ⁶⁰ Suranaree University of Technology, University Avenue 111, Nakhon Ratchasima 30000, Thailand
- ⁶¹ Tsinghua University, Beijing 100084, People's Republic of China
- ⁶² Turkish Accelerator Center Particle Factory Group, (A)Istinye University, 34010, Istanbul, Turkey; (B)Near East University, Nicosia, North Cyprus, 99138, Mersin 10, Turkey
- ⁶³ University of Bristol, (A)H H Wills Physics Laboratory; (B)Tyndall Avenue; (C)Bristol; (D)BS8 1TL
- ⁶⁴ University of Chinese Academy of Sciences, Beijing 100049, People's Republic of China
- ⁶⁵ University of Groningen, NL-9747 AA Groningen, The Netherlands
- ⁶⁶ University of Hawaii, Honolulu, Hawaii 96822, USA
- ⁶⁷ University of Jinan, Jinan 250022, People's Republic of China
- ⁶⁸ University of Manchester, Oxford Road, Manchester, M13 9PL, United Kingdom
- ⁶⁹ University of Muenster, Wilhelm-Klemm-Strasse 9, 48149 Muenster, Germany

⁷⁰ *University of Oxford, Keble Road, Oxford OX13RH, United Kingdom*

⁷¹ *University of Science and Technology Liaoning, Anshan 114051, People's Republic of China*

⁷² *University of Science and Technology of China, Hefei 230026, People's Republic of China*

⁷³ *University of South China, Hengyang 421001, People's Republic of China*

⁷⁴ *University of the Punjab, Lahore-54590, Pakistan*

⁷⁵ *University of Turin and INFN, (A)University of Turin, I-10125, Turin, Italy; (B)University of Eastern Piedmont, I-15121, Alessandria, Italy; (C)INFN, I-10125, Turin, Italy*

⁷⁶ *Uppsala University, Box 516, SE-75120 Uppsala, Sweden*

⁷⁷ *Wuhan University, Wuhan 430072, People's Republic of China*

⁷⁸ *Yantai University, Yantai 264005, People's Republic of China*

⁷⁹ *Yunnan University, Kunming 650500, People's Republic of China*

⁸⁰ *Zhejiang University, Hangzhou 310027, People's Republic of China*

⁸¹ *Zhengzhou University, Zhengzhou 450001, People's Republic of China*

^a *Deceased*

^b *Also at the Moscow Institute of Physics and Technology, Moscow 141700, Russia*

^c *Also at the Novosibirsk State University, Novosibirsk, 630090, Russia*

^d *Also at the NRC "Kurchatov Institute", PNPI, 188300, Gatchina, Russia*

^e *Also at Goethe University Frankfurt, 60323 Frankfurt am Main, Germany*

^f *Also at Key Laboratory for Particle Physics, Astrophysics and Cosmology, Ministry of Education; Shanghai Key Laboratory for Particle Physics and Cosmology; Institute of Nuclear and Particle Physics, Shanghai 200240, People's Republic of China*

^g *Also at Key Laboratory of Nuclear Physics and Ion-beam Application (MOE) and Institute of Modern Physics, Fudan University, Shanghai 200443, People's Republic of China*

^h *Also at State Key Laboratory of Nuclear Physics and Technology, Peking University, Beijing 100871, People's Republic of China*

ⁱ *Also at School of Physics and Electronics, Hunan University, Changsha 410082, China*

^j *Also at Guangdong Provincial Key Laboratory of Nuclear Science, Institute of Quantum Matter, South China Normal University, Guangzhou 510006, China*

^k *Also at MOE Frontiers Science Center for Rare Isotopes, Lanzhou University, Lanzhou 730000, People's Republic of China*

^l *Also at Lanzhou Center for Theoretical Physics, Lanzhou University, Lanzhou 730000, People's Republic of China*

^m *Also at the Department of Mathematical Sciences, IBA, Karachi 75270, Pakistan*

ⁿ *Also at Ecole Polytechnique Federale de Lausanne (EPFL), CH-1015 Lausanne, Switzerland*

^o *Also at Helmholtz Institute Mainz, Staudinger Weg 18, D-55099 Mainz, Germany*

^p *Also at School of Physics, Beihang University, Beijing 100191, China*

Using 7.93 fb^{-1} of e^+e^- collision data collected at the center-of-mass energy of 3.773 GeV with the BESIII detector, we measure the absolute branching fractions of $D^0 \rightarrow K^- e^+ \nu_e$, $D^0 \rightarrow K^- \mu^+ \nu_\mu$, $D^+ \rightarrow \bar{K}^0 e^+ \nu_e$, and $D^+ \rightarrow \bar{K}^0 \mu^+ \nu_\mu$ to be $(3.521 \pm 0.009_{\text{stat.}} \pm 0.016_{\text{syst.}})\%$, $(3.419 \pm 0.011_{\text{stat.}} \pm 0.016_{\text{syst.}})\%$, $(8.864 \pm 0.039_{\text{stat.}} \pm 0.082_{\text{syst.}})\%$, and $(8.665 \pm 0.046_{\text{stat.}} \pm 0.084_{\text{syst.}})\%$, respectively. By performing a simultaneous fit to the partial decay rates of these four decays, the product of the hadronic form factor $f_+^K(0)$ and the modulus of the $c \rightarrow s$ CKM matrix element $|V_{cs}|$ is determined to be $f_+^K(0)|V_{cs}| = 0.7171 \pm 0.0011_{\text{stat.}} \pm 0.0013_{\text{syst.}}$. Taking the value of $|V_{cs}| = 0.97349 \pm 0.00016$ from the standard model global fit or that of $f_+^K(0) = 0.7452 \pm 0.0031$ from the LQCD calculation as input, we derive the results $f_+^K(0) = 0.7366 \pm 0.0011_{\text{stat.}} \pm 0.0013_{\text{syst.}}$ and $|V_{cs}| = 0.9623 \pm 0.0015_{\text{stat.}} \pm 0.0017_{\text{syst.}} \pm 0.0040_{\text{LQCD}}$.

I. INTRODUCTION

Improved measurements of semileptonic decays of charmed mesons provide important inputs to further the understanding of weak and strong interactions in the charm sector. By analyzing their decay dynamics, one can determine the product of the modulus of the Cabibbo-Kobayashi-Maskawa (CKM) matrix element

$|V_{cs(d)}|$ and the hadronic transition form factor. Taking $D \rightarrow \bar{K} e^+ \nu_e$ as an example, the hadronic transition form factors at zero-momentum transfer $f_+^K(0)$ [1–9] can be calculated via several theoretical approaches, *e.g.*, lattice quantum chromodynamics (LQCD) [1–4], QCD light-cone sum rules (LCSR) [5], covariant light-front quark model (LFQM) [6], the covariant confined quark model (CCQM) [7], and the relativistic quark model (RQM)

[8]. Using the value of $|V_{cs}|$ provided by the CKMFitter group [10], the hadronic transition form factor $f_+^K(0)$ can be calculated, resulting in a stringent test of the theoretical predictions. Conversely, using the $f_+^K(0)$ value predicted by theory allows the determination of $|V_{cs}|$, which is important to test CKM matrix unitarity. Furthermore, measurements of the branching fractions of $D^0 \rightarrow K^- \ell^+ \nu_\ell$ and $D^+ \rightarrow \bar{K}^0 \ell^+ \nu_\ell$ ($\ell = e$ or μ) are important to test lepton flavor universality and isospin conservation in $D \rightarrow K \ell^+ \nu_\ell$.

Previously, the branching fractions of $D^0 \rightarrow K^- \ell^+ \nu_\ell$ and $D^+ \rightarrow \bar{K}^0 \ell^+ \nu_\ell$ were measured by BESII [11–13], BaBar [14], Belle [15], CLEO-c [16–19], and BESIII [20–26]. Studies of the decay dynamics of $D \rightarrow \bar{K} \ell^+ \nu_\ell$ were reported by BaBar [14], CLEO-c [19], and BESIII [21–24]. The previous BESIII analysis used 2.93 fb^{-1} of e^+e^- collision data taken at the center-of-mass energy $\sqrt{s} = 3.773 \text{ GeV}$. This paper reports improved measurements of the branching fractions and decay dynamics of $D^0 \rightarrow K^- \ell^+ \nu_\ell$ and $D^+ \rightarrow \bar{K}^0 \ell^+ \nu_\ell$ by using 7.93 fb^{-1} of e^+e^- collision data collected by the BESIII detector at $\sqrt{s} = 3.773 \text{ GeV}$ [27]. Throughout this paper, charge conjugate modes are implied.

II. BESIII DETECTOR AND MONTE CARLO SIMULATIONS

The BESIII detector [28] records symmetric e^+e^- collisions provided by the BEPCII storage ring [29] in the center-of-mass energy range from 1.84 to 4.95 GeV, with a peak luminosity of $1.1 \times 10^{33} \text{ cm}^{-2}\text{s}^{-1}$ achieved at $\sqrt{s} = 3.773 \text{ GeV}$. BESIII has collected large data samples in this energy region [30, 31]. The cylindrical core of the BESIII detector covers 93% of the full solid angle and consists of a helium-based multilayer drift chamber (MDC), a time-of-flight system (TOF), and a CsI(Tl) electromagnetic calorimeter (EMC), which are all enclosed in a superconducting solenoidal magnet providing a 1.0 T magnetic field. The solenoid is supported by an octagonal flux-return yoke with resistive plate muon identification counters (MUC) interleaved with steel. The main function of the MUC is to separate muons from charged pions, other hadrons and backgrounds based on their hit patterns in the instrumented flux-return yoke. The charged-particle momentum resolution at $1 \text{ GeV}/c$ is 0.5%, and the dE/dx resolution is 6% for electrons from Bhabha scattering. The EMC measures photon energies with a resolution of 2.5% (5%) at 1 GeV in the barrel (end-cap) region. The time resolution in the plastic scintillator TOF barrel region is 68 ps, while that in the end-cap region was 110 ps. The end-cap TOF system was upgraded in 2015 using multi-gap resistive plate chamber technology, providing a time resolution of 60 ps [32]. Approximately 67% of the data used here was collected after this upgrade.

Simulated samples produced with GEANT4-based [33]

Monte Carlo (MC) software, which includes the geometric description [34] of the BESIII detector and the detector response, are used to determine detection efficiencies and to estimate backgrounds. The simulation models the beam energy spread and initial state radiation (ISR) in the e^+e^- annihilations with the generator KKMC [35]. Signal MC samples of the decays $D \rightarrow \bar{K} \ell^+ \nu_\ell$ are simulated with a specific two-parameter series expansion model [36]. The background is studied using an inclusive MC sample that consists of the production of $D\bar{D}$ pairs from the $\psi(3770)$ (including quantum coherence for the neutral D channels), the non- $D\bar{D}$ decays of the $\psi(3770)$, the ISR production of the charmonium states, and the continuum processes. These processes are also generated with KKMC. The known decay modes are modeled by EVTGEN [37] with branching fractions taken from the Particle Data Group (PDG) [10], while the remaining unknown charmonium decays are modeled with LUNDCHARM [38]. Final state radiation from charged final-state particles is incorporated using PHOTOS [39].

III. MEASUREMENT METHOD

At $\sqrt{s} = 3.773 \text{ GeV}$, the D and \bar{D} mesons are produced in pairs from the $e^+e^- \rightarrow \psi(3770) \rightarrow D\bar{D}$ process, where D stands for D^0 or D^+ . This property allows us to do absolute branching fraction measurement with the well established double-tag (DT) method [40]. In this method, the single-tag (ST) candidate events are selected by reconstructing a \bar{D}^0 in the six hadronic final states $\bar{D}^0 \rightarrow K^+\pi^-$, $K^+\pi^-\pi^0$, $K^+\pi^-\pi^-\pi^+$, $K^+\pi^-\pi^0\pi^0$, $K^+\pi^-\pi^-\pi^+\pi^0$, and $K_S^0\pi^+\pi^-$, or a D^- in the six hadronic final states $D^- \rightarrow K^+\pi^-\pi^-$, $K_S^0\pi^-$, $K^+\pi^-\pi^-\pi^0$, $K_S^0\pi^-\pi^0$, $K_S^0\pi^+\pi^-\pi^-$, and $K^+K^-\pi^-$. These inclusively selected candidates are referred to as ST \bar{D} mesons. In the presence of the ST \bar{D} mesons, candidates for the signal decays are selected to form DT events. The branching fraction of the signal decay is determined by

$$\mathcal{B}_{\text{sig}} = N_{\text{DT}} / (N_{\text{ST}}^{\text{tot}} \cdot \bar{\epsilon}_{\text{sig}}), \quad (1)$$

where N_{DT} is the total DT yield in data, $N_{\text{ST}}^{\text{tot}}$ is the total ST yield

$$N_{\text{ST}}^{\text{tot}} = \sum_{i=1}^6 N_{\text{ST}}^i, \quad (2)$$

where N_{ST}^i is the ST yield of tag mode i , and $\bar{\epsilon}_{\text{sig}}$ is the weighted efficiency of detecting the semileptonic decay, calculated by

$$\bar{\epsilon}_{\text{sig}} = \sum_{i=1}^6 \frac{N_{\text{ST}}^i \epsilon_{\text{sig}}^i}{N_{\text{ST}}^{\text{tot}}}. \quad (3)$$

Here, $\varepsilon_{\text{sig}}^i = \varepsilon_{\text{DT}}^i / \varepsilon_{\text{ST}}^i$, is the efficiency of detecting the semileptonic decay in the presence of the ST \bar{D} meson of tag mode i , where $\varepsilon_{\text{DT}}^i$ and $\varepsilon_{\text{ST}}^i$ are the DT efficiency and ST efficiency, respectively.

IV. SELECTION OF SINGLE TAG \bar{D} MESONS

For each charged track (except for those used for K_S^0 reconstruction), the polar angle (θ) with respect to the MDC axis is required to satisfy $|\cos\theta| < 0.93$, and the point of closest approach to the interaction point must be within 1 cm in the plane perpendicular to the MDC axis, $|V_{xy}|$, and within 10 cm along the MDC axis, $|V_z|$. Charged tracks are identified by using the dE/dx and TOF information, with which the combined confidence levels under the pion and kaon hypotheses are computed separately. Charged tracks are assigned to the particle type that has the higher probability.

Candidate K_S^0 mesons are reconstructed from pairs of oppositely charged tracks. For these two tracks, their polar angles are required to satisfy $|\cos\theta| < 0.93$ and the distance of closest approach to the interaction point is required to be less than 20 cm along the MDC axis. There is no requirement on the distance of closest approach in the transverse plane, and no particle identification (PID) criteria are required. The two charged tracks are constrained to originate from the same vertex, which is required to be away from the interaction point by a flight distance of at least twice the vertex resolution. The quality of the vertex fit is ensured by the requirement of $\chi^2 < 100$, and the invariant mass of the $\pi^+\pi^-$ pair is required to be within $(0.487, 0.511)$ GeV/c^2 .

Neutral pion candidates are reconstructed via the $\pi^0 \rightarrow \gamma\gamma$ decay. Photon candidates are identified from EMC showers. The EMC time difference from the event start time is required to be within $(0, 700)$ ns. The energy deposited in the EMC is required to be greater than 25 MeV in the barrel region ($|\cos\theta| < 0.80$) and 50 MeV in the end-cap region ($0.86 < |\cos\theta| < 0.92$). The opening angle between the photon candidate and the nearest charged track in the EMC is required to be greater than 10° . For any π^0 candidate, the invariant mass of the photon pair is required to be within $(0.115, 0.150)$ GeV/c^2 . To improve the momentum resolution, a mass-constrained (1C) fit to the known π^0 mass [10] is imposed on the photon pair, and the χ^2 of the 1C kinematic fit is required to be less than 50. The four-momentum of the π^0 candidate from this kinematic fit is used for further analysis.

For the two-body tag mode of $\bar{D}^0 \rightarrow K^+\pi^-$, the backgrounds originating from cosmic rays, Bhabha and dimuon events are vetoed with the following procedure defined in Ref. [41]. It is required that the TOF time difference between the two charged tracks is less than 5 ns, and at least one EMC shower with energy greater than 50 MeV or at least one additional charged track detected in the MDC survives in each event. Further, it

is required that the two charged tracks are not consistent with being a muon pair or an electron-positron pair, identified using the TOF, dE/dx , EMC, and MUC measurement information with the combined confidence levels \mathcal{L}_e , \mathcal{L}_μ , \mathcal{L}_K , and \mathcal{L}_π for electron, muon, kaon, and pion hypotheses, respectively. To be identified as an electron, \mathcal{L}_e is required to be greater than 0 and larger than \mathcal{L}_K , \mathcal{L}_π , as well as $0.8 \cdot (\mathcal{L}_e + \mathcal{L}_\pi + \mathcal{L}_K)$. To identify a track as a muon, \mathcal{L}_μ is required to be greater than 0, the deposited energy in the EMC should fall within the range of 0.15 to 0.30 GeV, and the hit depth in the MUC needs to be either greater than $(80 \times |p_{\text{trk}}| - 60)$ cm or greater than 40 cm, where p_{trk} is the track momentum.

To identify the ST \bar{D} mesons, we use two kinematic variables: the energy difference $\Delta E \equiv E_{\bar{D}} - E_{\text{beam}}$ and the beam-constrained mass $M_{\text{BC}} \equiv \sqrt{E_{\text{beam}}^2/c^4 - |\vec{p}_{\bar{D}}|^2/c^2}$, where E_{beam} is the beam energy, and $E_{\bar{D}}$ and $\vec{p}_{\bar{D}}$ are the total energy and momentum of the ST \bar{D} meson in the e^+e^- center-of-mass frame, respectively. If there are multiple \bar{D} candidates for a specific tag mode, the one giving the least $|\Delta E|$ is chosen for further analysis. To suppress combinatorial backgrounds in the M_{BC} distribution, tag dependent ΔE requirements are imposed on the ST candidates. The detailed ΔE requirements and the ST efficiencies estimated by analyzing the inclusive MC sample are summarized in Table 1.

For each tag mode, the yield of ST \bar{D} mesons is obtained by the maximum likelihood fit to the corresponding M_{BC} distribution. In the fit, the \bar{D} signal shape is described by the sum of an MC-simulated signal shape, made by RooHistPdf in Rootclass [42], convolved with a double-Gaussian resolution function plus a single-Gaussian function, to account for resolution difference between data and MC simulation and initial state radiation (ISR) effects. The parameters of those functions are free. The background shape is described by an ARGUS function [43] with the endpoint fixed at the E_{beam} value. Figure 1 shows the results of the fits to the M_{BC} distributions of the accepted ST candidates in data for different tag modes. The candidates with M_{BC} within $(1.859, 1.873)$ GeV/c^2 for \bar{D}^0 tags and $(1.863, 1.877)$ GeV/c^2 for D^- tags are kept for further analysis. Summing over the tag modes gives the total yields of ST \bar{D}^0 and D^- mesons ($N_{\text{ST}}^{\text{tot}}$) to be $(7922.7 \pm 3.4_{\text{stat.}}) \times 10^3$ and $(4135.4 \pm 2.4_{\text{stat.}}) \times 10^3$, respectively.

V. SELECTION OF DOUBLE TAG EVENTS

The candidates for $D^0 \rightarrow K^-e^+\nu_e$, $D^0 \rightarrow K^-\mu^+\nu_\mu$, $D^+ \rightarrow \bar{K}^0e^+\nu_e$, and $D^+ \rightarrow \bar{K}^0\mu^+\nu_\mu$ are selected from the remaining tracks in the presence of the ST \bar{D} candidates. Candidates for K^- and K_S^0 are selected with the same criteria as those used in the ST selection. The positron and muon are identified using the TOF, dE/dx , and EMC measurements with the combined confidence levels \mathcal{L}_e , \mathcal{L}_μ , \mathcal{L}_K , and \mathcal{L}_π , which are calculated for

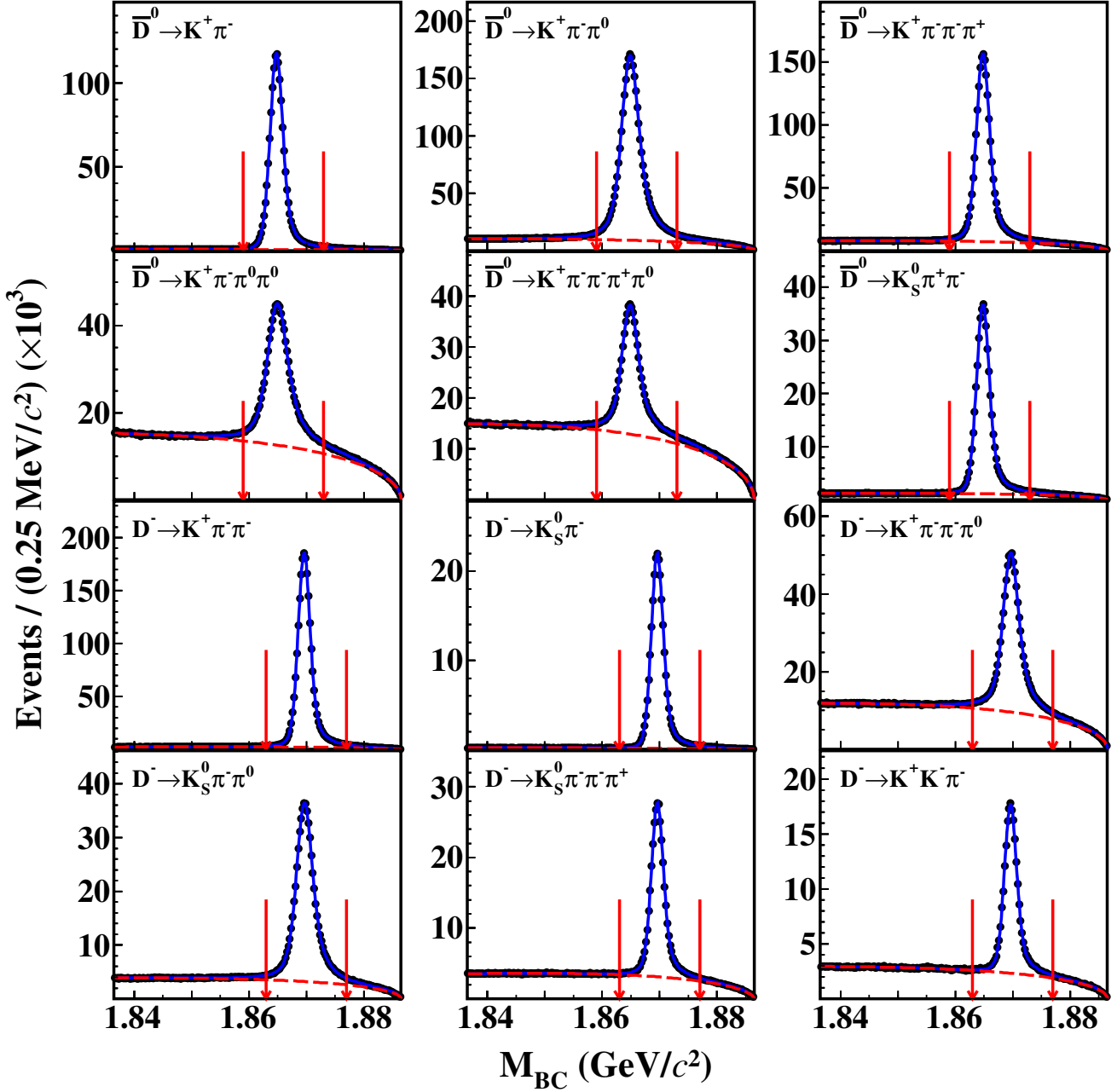


Fig. 1. Fits to the M_{BC} distributions of the ST \bar{D} candidates. The points with error bars are data, the blue curves are the best fits, and the red dashed curves are the fitted combinatorial background shapes. The pairs of red arrows show the M_{BC} signal window.

electron, muon, kaon, and pion hypotheses, respectively. The positron candidate is required to satisfy $\mathcal{L}_e > 0.8 \cdot (\mathcal{L}_e + \mathcal{L}_\pi + \mathcal{L}_K)$ and $\mathcal{L}_e > 0.001$. The muon candidate is required to satisfy $\mathcal{L}_\mu > \mathcal{L}_e$ and $\mathcal{L}_\mu > 0.001$, and the energy of the muon deposited in the EMC is required to be within (0.1, 0.3) GeV.

To suppress backgrounds associated with hadronic D decays, it is required that there are no additional good

charged tracks on the signal side ($N_{\text{extra}}^{\text{trk}} = 0$). To reject the backgrounds from hadronic decays involving π^0 , the maximum energy of extra photons ($E_{\text{extra}}^{\text{max}} \gamma$) not used in the event reconstruction is required to be less than 0.25 GeV. Requirements on the \bar{K} and ℓ^+ ($M_{\bar{K}\ell}$) invariant mass, which are $M_{K^-e^+} < 1.83 \text{ GeV}/c^2$ for $D^0 \rightarrow K^-e^+\nu_e$, $M_{K^-e^+} < 1.50 \text{ GeV}/c^2$ for $D^0 \rightarrow K^-e^+\nu_e$, $M_{K_S^0e^+} < 1.84 \text{ GeV}/c^2$ for $D^+ \rightarrow \bar{K}^0e^+\nu_e$,

Table 1. The ΔE requirements, the ST \bar{D} yields in data of the tag mode i (N_{ST}^i), and the ST efficiencies of tag mode i ($\varepsilon_{\text{ST}}^i$). The uncertainties are statistical only.

D	Tag mode	ΔE (MeV)	N_{ST}^i ($\times 10^3$)	$\varepsilon_{\text{ST}}^i$ (%)
D^0	$K^+\pi^-$	(-27, 27)	1452.5 ± 1.3	65.28 ± 0.01
	$K^+\pi^-\pi^0$	(-62, 49)	2908.1 ± 2.0	35.69 ± 0.01
	$K^+\pi^-\pi^-\pi^+$	(-26, 24)	1957.5 ± 1.6	41.17 ± 0.01
	$K^+\pi^-\pi^0\pi^0$	(-68, 53)	698.8 ± 1.3	15.24 ± 0.01
	$K^+\pi^-\pi^-\pi^+\pi^0$	(-57, 51)	457.1 ± 1.1	16.49 ± 0.01
	$K_S^0\pi^+\pi^-$	(-24, 24)	448.7 ± 0.7	37.60 ± 0.01
D^-	$K^+\pi^-\pi^-$	(-25, 24)	2164.4 ± 1.6	51.09 ± 0.01
	$K_S^0\pi^-$	(-25, 26)	249.4 ± 0.5	50.72 ± 0.02
	$K^+\pi^-\pi^-\pi^0$	(-57, 46)	676.0 ± 1.1	25.04 ± 0.01
	$K_S^0\pi^-\pi^0$	(-62, 49)	554.3 ± 0.9	26.23 ± 0.01
	$K_S^0\pi^-\pi^-\pi^+$	(-28, 27)	304.0 ± 0.7	29.53 ± 0.01
	$K^+K^-\pi^-$	(-24, 23)	187.3 ± 0.5	41.12 ± 0.02

and $M_{K_S^0\mu^+} < 1.56$ GeV/ c^2 for $D^+ \rightarrow \bar{K}^0\mu^+\nu_\mu$, are used to suppress the backgrounds associated with the misidentification between π^+ and ℓ^+ .

The neutrino is not detectable by the BESIII detector. In order to determine the number of semileptonic D candidates, we define $U_{\text{miss}} \equiv E_{\text{miss}} - |\vec{p}_{\text{miss}}|c$, where E_{miss} and \vec{p}_{miss} are the missing energy and momentum of a DT event in the e^+e^- center-of-mass frame, respectively. They are calculated by $E_{\text{miss}} \equiv E_{\text{beam}} - E_{\bar{K}} - E_{\ell^+}$ and $\vec{p}_{\text{miss}} \equiv \vec{p}_D - \vec{p}_{\bar{K}} - \vec{p}_{\ell^+}$, where $E_{\bar{K}(\ell^+)}$ and $\vec{p}_{\bar{K}(\ell^+)}$ are the measured energy and momentum of the $\bar{K}(\ell^+)$ candidate in an event. Here to improve the U_{miss} resolution, \vec{p}_D is evaluated as $\vec{p}_D = -\hat{p}_D \sqrt{E_{\text{beam}}^2/c^2 - m_D^2}$, where \hat{p}_D is the unit vector in the momentum direction of the ST \bar{D} meson and $m_{\bar{D}}$ is the known \bar{D} mass [10].

VI. BRANCHING FRACTIONS

A. Results on branching fractions

After imposing all selection criteria, the U_{miss} distributions of the accepted candidates for $D \rightarrow \bar{K}\ell^+\nu_\ell$ in data are shown in Fig. 2. Studies of the inclusive MC sample show that main backgrounds are caused mainly due to mis-identifying μ^+ or π^+ as e^+ for e channels; mis-identifying π^+ as μ^+ for μ channels; or missing π^0 (s) for all signal decays. The main sources of backgrounds, normalized yields and fractions, which are estimated from the inclusive MC sample, are listed in Table 2.

For each signal decay, the signal yields in data are obtained from the maximum likelihood fits to the corresponding U_{miss} distributions. In the fit, the signal shape is determined from the simulated shape convolved with a Gaussian function with free parameters, which

accounts for different resolutions between data and MC simulation. For the $D \rightarrow \bar{K}\mu^+\nu_\mu$ decays, the main peaking backgrounds $D \rightarrow \bar{K}\pi^+\pi^0$ are modeled by the simulated shapes convolved with the same Gaussian function as the corresponding signal, and their yields are free. In the U_{miss} distributions, there are also small peaking backgrounds from $D \rightarrow \bar{K}\mu^+\nu_\mu$ around 0.03 GeV for $D \rightarrow \bar{K}e^+\nu_e$, and small peaking background $D^0 \rightarrow \pi^-e^+\nu_e$ around -0.13 GeV for $D^0 \rightarrow K^-e^+\nu_e$. Their shapes and yields are fixed in the fits and merged into other backgrounds in the plots. The shapes of signal and all backgrounds are derived from signal and inclusive MC samples, respectively, and all of them are made by RooHistPdf in Rootclass [42]. From these fits, we obtain the signal yields of each signal decay in data (N_{DT}).

The DT efficiencies are obtained by analyzing the corresponding signal MC samples. The obtained DT efficiencies and signal efficiencies for different signal decays in each tag mode as well as the weighted signal efficiencies ($\bar{\varepsilon}_{\text{sig}}$) are listed in Table 3.

Table 2. Main sources of backgrounds, normalized yields (N_{bkg}) and fractions in all backgrounds (f_{bkg}) for each signal decay estimated from the inclusive MC sample.

Signal decay	Background source	N_{bkg}	f_{bkg} (%)
$D^0 \rightarrow K^-e^+\nu_e$	$D^0 \rightarrow K^{*-}e^+\nu_e$	9820	46.7
	$D^0 \rightarrow K^-\mu^+\nu_\mu$	5421	25.8
	$D^0 \rightarrow K^-\pi^+\pi^0$	2756	13.1
	$D^0 \rightarrow \pi^-e^+\nu_e$	458	2.2
$D^0 \rightarrow K^-\mu^+\nu_\mu$	$D^0 \rightarrow K^-\pi^+\pi^0$	44932	44.2
	$D^0 \rightarrow K^-\pi^+\pi^0\pi^0$	28815	28.3
	$D^0 \rightarrow K^{*-}\mu^+\nu_\mu$	8285	8.2
$D^+ \rightarrow \bar{K}^0e^+\nu_e$	$D^+ \rightarrow \bar{K}^{*0}e^+\nu_e$	2821	51.6
	$D^+ \rightarrow \bar{K}^0\mu^+\nu_\mu$	1558	28.5
	$D^+ \rightarrow K_S^0\pi^+\pi^0$	261	4.8
$D^+ \rightarrow \bar{K}^0\mu^+\nu_\mu$	$D^+ \rightarrow K_S^0\pi^+\pi^0$	8760	50.3
	$D^+ \rightarrow \bar{K}^{*0}\mu^+\nu_\mu$	2546	14.6
	$D^+ \rightarrow K_S^0\pi^+\pi^0\pi^0$	2072	11.9

With the signal yields in data N_{DT} , the weighted signal efficiencies $\bar{\varepsilon}_{\text{sig}}$, as well as the ST yield in data, the branching fractions of $D^0 \rightarrow K^-e^+\nu_e$, $D^0 \rightarrow K^-\mu^+\nu_\mu$, $D^+ \rightarrow \bar{K}^0e^+\nu_e$, and $D^+ \rightarrow \bar{K}^0\mu^+\nu_\mu$ are determined with Eq. (1) and listed in Table 4.

B. Systematic uncertainties on branching fractions

Table 5 summarizes the sources of the systematic uncertainties in the branching fraction measurements. They are assigned relative to the measured branching fractions and are discussed below.

a. ST \bar{D} yields The systematic uncertainty of the fits to the M_{BC} spectra is estimated by varying the

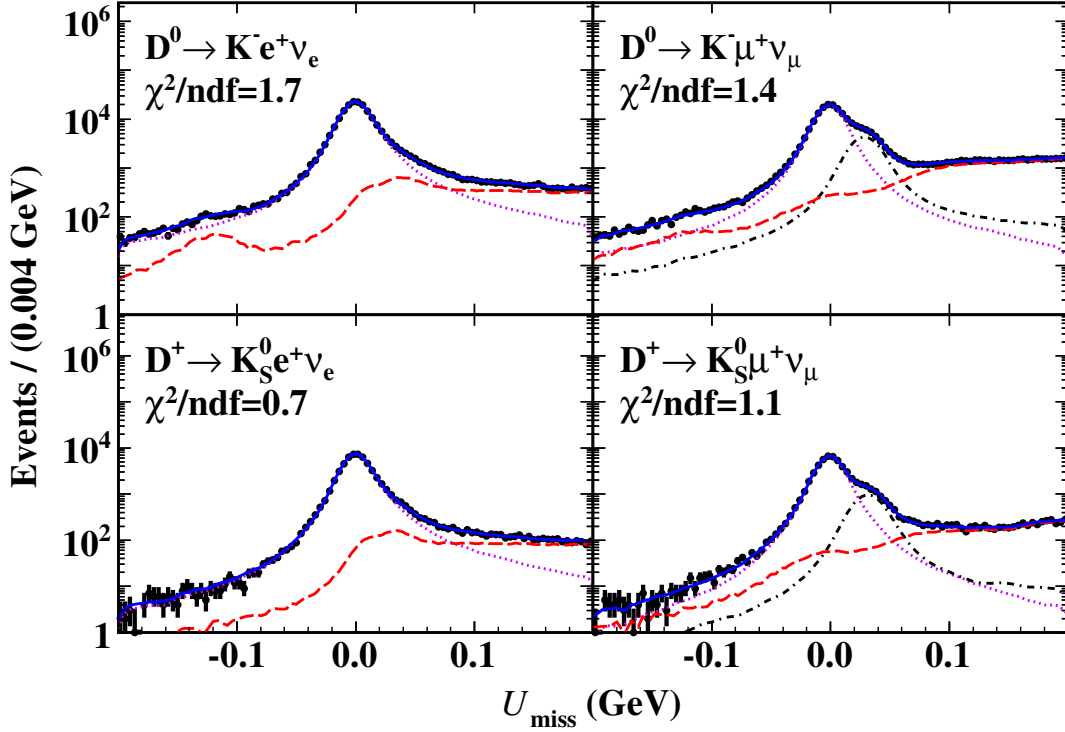


Fig. 2. Fits to the U_{miss} distributions of the accepted candidates for $D \rightarrow \bar{K}\ell^+\nu_\ell$ in data. The points with error bars are data. The violet dotted lines are the fitted signals. The black dash-dotted lines are the fitted peaking backgrounds, and the red dashed lines are the fitted combinatorial background shapes.

Table 3. The DT efficiencies ε_{DT} , signal efficiencies ε for different signal decays in each tag mode, as well as the weighted signal efficiencies $\bar{\varepsilon}_{\text{sig}}$. The listed efficiencies are all in unit of % and have taken into account corrections from data-MC differences originating from tracking and PID. For the D^+ signal decays, the efficiencies also include the branching fraction of $\bar{K}^0 \rightarrow \pi^+\pi^-$. The uncertainties are statistical only.

D^0 decay				D^+ decay					
Tag mode	$\varepsilon_{\text{DT},K^-e^+\nu_e}$	$\varepsilon_{K^-e^+\nu_e}$	$\varepsilon_{\text{DT},K^-\mu^+\nu_\mu}$	$\varepsilon_{K^-\mu^+\nu_\mu}$	Tag mode	$\varepsilon_{\text{DT},\bar{K}^0e^+\nu_e}$	$\varepsilon_{\bar{K}^0e^+\nu_e}$	$\varepsilon_{\text{DT},\bar{K}^0\mu^+\nu_\mu}$	$\varepsilon_{\bar{K}^0\mu^+\nu_\mu}$
$K^+\pi^-$	43.45 ± 0.03	66.57 ± 0.05	34.76 ± 0.03	53.26 ± 0.04	$K^+\pi^-\pi^-$	8.14 ± 0.01	15.94 ± 0.02	6.78 ± 0.01	13.26 ± 0.02
$K^+\pi^-\pi^0$	24.69 ± 0.03	69.17 ± 0.07	19.81 ± 0.02	55.51 ± 0.06	$K_S^0\pi^-$	8.10 ± 0.01	15.98 ± 0.02	6.75 ± 0.01	13.31 ± 0.02
$K^+\pi^-\pi^-\pi^+$	27.28 ± 0.03	66.26 ± 0.06	21.41 ± 0.02	51.99 ± 0.06	$K^+\pi^-\pi^-\pi^0$	3.91 ± 0.01	15.60 ± 0.03	3.27 ± 0.01	13.06 ± 0.02
$K^+\pi^-\pi^0\pi^0$	11.20 ± 0.02	73.50 ± 0.12	9.08 ± 0.02	59.56 ± 0.11	$K_S^0\pi^-\pi^0$	4.11 ± 0.01	15.67 ± 0.02	3.48 ± 0.01	13.28 ± 0.02
$K^+\pi^-\pi^-\pi^+\pi^0$	11.81 ± 0.02	71.59 ± 0.12	9.40 ± 0.02	57.03 ± 0.11	$K_S^0\pi^-\pi^-\pi^+$	4.48 ± 0.01	15.18 ± 0.02	3.71 ± 0.01	12.56 ± 0.02
$K_S^0\pi^+\pi^-$	24.89 ± 0.03	66.19 ± 0.07	19.59 ± 0.02	52.07 ± 0.06	$K^+K^-\pi^-$	6.45 ± 0.01	15.67 ± 0.02	5.38 ± 0.01	13.07 ± 0.02
$\bar{\varepsilon}_{\text{sig}}$		68.32 ± 0.03		54.48 ± 0.03	$\bar{\varepsilon}_{\text{sig}}$		15.78 ± 0.01		13.18 ± 0.01

Table 4. The signal yields in data N_{DT} , the weighted signal efficiency $\bar{\varepsilon}_{\text{sig}}$, as well as the branching fractions of the four signal decays \mathcal{B}_{sig} . For \mathcal{B}_{sig} , the first uncertainties are statistical and the second are systematic. For other quantities, the uncertainties are statistical only.

Signal decay	N_{DT}	$\bar{\varepsilon}_{\text{sig}}$ (%)	\mathcal{B}_{sig} (%)
$D^0 \rightarrow K^-e^+\nu_e$	190605 ± 471	68.32 ± 0.03	$3.521 \pm 0.009 \pm 0.016$
$D^0 \rightarrow K^-\mu^+\nu_\mu$	147596 ± 488	54.48 ± 0.03	$3.419 \pm 0.011 \pm 0.016$
$D^+ \rightarrow \bar{K}^0e^+\nu_e$	57846 ± 256	15.78 ± 0.01	$8.864 \pm 0.039 \pm 0.082$
$D^+ \rightarrow \bar{K}^0\mu^+\nu_\mu$	47229 ± 248	13.18 ± 0.01	$8.665 \pm 0.046 \pm 0.084$

signal and background shapes and repeating the fits for both data and the inclusive MC sample. A variation of the signal shape is obtained by modifying the matching requirement between generated and reconstructed angles from 15° to 10° or 20° . The uncertainty related to the background shape is obtained by varying the endpoint by ± 0.2 MeV. In addition, the effect of removing the M_{BC} requirements from the ST selection is evaluated, and the difference with the nominal measurement is taken as a systematic uncertainty accounting for possible mismodelling of the M_{BC} distribution in simulation. Adding these three effects quadratically leads to a 0.3% variation, which is taken as the systematic uncertainty on N_{ST} . The uncertainty in the ST \bar{D}^0 yield is correlated for $D^0 \rightarrow K^- e^+ \nu_e$ and $D^0 \rightarrow K^- \mu^+ \nu_\mu$, while that for the ST D^- yield is correlated for $D^+ \rightarrow \bar{K}^0 e^+ \nu_e$ and $D^+ \rightarrow \bar{K}^0 \mu^+ \nu_\mu$.

b. K^- tracking and PID The K^- tracking and PID efficiencies are studied by using a control sample of hadronic $D\bar{D}$ events, with D^0 decaying into $K^- \pi^+$, $K^- \pi^+ \pi^+ \pi^-$ and \bar{D}^0 decaying into $K^+ \pi^-$, $K^+ \pi^- \pi^- \pi^+$, as well as D^+ decaying into $K^- \pi^+ \pi^+$ and D^- decaying into $K^+ \pi^- \pi^-$. The ratios of the momentum weighted data and MC efficiencies are 0.999 ± 0.001 and 1.000 ± 0.001 for tracking and PID, respectively. The signal efficiencies are corrected by these ratios, and their uncertainties, which are correlated for $D^0 \rightarrow K^- e^+ \nu_e$ and $D^0 \rightarrow K^- \mu^+ \nu_\mu$, are assigned as systematic uncertainties.

c. K_S^0 reconstruction The K_S^0 reconstruction efficiencies are examined in two aspects. The π^\pm tracking efficiencies are determined by using the control samples used in the studies of K^- tracking and PID, but with a missing π^\pm . The efficiencies associated with the K_S^0 mass window and K_S^0 decay vertex fit are examined using the hadronic $D\bar{D}$ events, with D^0 or D^+ decaying into $K_S^0 \pi^+ \pi^-$, $K_S^0 \pi^+ \pi^- \pi^0$, $K_S^0 \pi^0$, $K_S^0 \pi^+$, $K_S^0 \pi^+ \pi^0$, and $K_S^0 \pi^+ \pi^+ \pi^-$. The polar angle distribution of the control sample is consistent with that in the signal decays, therefore its effect on the K_S^0 reconstruction efficiency is negligible. The momentum weighted difference between the K_S^0 reconstruction efficiency of data and MC is 0.84% for $D^+ \rightarrow \bar{K}^0 e^+ \nu_e$ and 0.88% for $D^+ \rightarrow \bar{K}^0 \mu^+ \nu_\mu$, which are taken as the systematic uncertainties. These uncertainties are correlated for $D^+ \rightarrow \bar{K}^0 e^+ \nu_e$ and $D^+ \rightarrow \bar{K}^0 \mu^+ \nu_\mu$.

d. ℓ^+ tracking and PID The tracking and PID efficiencies of e^+ and μ^+ are studied by using the control samples of $e^+ e^- \rightarrow \gamma e^+ e^-$ and $e^+ e^- \rightarrow \gamma \mu^+ \mu^-$, respectively. The ratios of the data and MC efficiencies weighted by momentum and $\cos\theta$ are 0.999 ± 0.001 for e^+ tracking and 0.983 ± 0.001 for e^+ PID; while they are 1.001 ± 0.001 for μ^+ tracking and 0.985 ± 0.002 for μ^+ PID. The signal efficiencies are corrected by these factors. After correction, the uncertainties of ratios are assigned as the systematic uncertainties, and these uncertainties are correlated for the four signal decays.

e. MC model The detection efficiencies are estimated by using signal MC events generated with the hadronic transition form factors measured in this work. The corresponding systematic uncertainties are estimated by varying the parameters by $\pm 1\sigma$. These uncertainties are independent for each signal decay.

f. $M_{\bar{K}\ell^+}$ requirement The uncertainty due to the $M_{\bar{K}\ell^+}$ upper bound in each signal decay is studied by scanning the requirement from 1.74-1.84 GeV/ c^2 for semielectronic decay and 1.46-1.56 GeV/ c^2 for semimuonic decay with a step of 0.01 GeV/ c^2 . We find the changes of branching fractions $|\mathcal{B}_{\text{alternative}} - \mathcal{B}_{\text{nominal}}|$ are smaller than the statistical uncertainty difference $\sqrt{|\sigma_{\text{alternative}}^2 - \sigma_{\text{nominal}}^2|}$. Therefore, we neglect this systematic uncertainty.

g. $E_{\text{extra}}^{\text{max } \gamma}$ and $N_{\text{extra}}^{\text{trk}}$ requirements The systematic uncertainty of the $E_{\text{extra}}^{\text{max } \gamma}$ and $N_{\text{extra}}^{\text{trk}}$ requirements is estimated by control samples of hadronic $D\bar{D}$ events, with both D and \bar{D} decaying into one of the used ST hadronic final states. The difference of the acceptance efficiencies between data and MC simulation is assigned as the systematic uncertainty. These uncertainties are correlated for $D^0 \rightarrow K^- e^+ \nu_e$ and $D^0 \rightarrow K^- \mu^+ \nu_\mu$ or $D^+ \rightarrow \bar{K}^0 e^+ \nu_e$ and $D^+ \rightarrow \bar{K}^0 \mu^+ \nu_\mu$.

h. U_{miss} fit The systematic uncertainty due to the U_{miss} fit is considered in two parts. Since a Gaussian function is convolved with the simulated signal shapes to account for the resolution difference between data and MC simulation, the systematic uncertainty from the signal shape is ignored. The systematic uncertainty due to the background shape is assigned by varying the relative fractions of backgrounds from $e^+ e^- \rightarrow q\bar{q}$ and the dominant background channels in the inclusive MC sample within the uncertainties of their input branching fractions. The changes in the branching fractions are taken as the corresponding systematic uncertainties. These uncertainties are independent for the four signal decays.

i. MC statistics The relative uncertainties on the signal efficiencies are assigned as systematic uncertainties due to MC statistics. These uncertainties are independent for the four signal decays.

j. Quoted branching fractions For the $D^+ \rightarrow \bar{K}^0 e^+ \nu_e$ and $D^+ \rightarrow \bar{K}^0 \mu^+ \nu_\mu$ decays, the uncertainty of the quoted branching fraction of $K_S^0 \rightarrow \pi^+ \pi^-$ is 0.07% [10]. These uncertainties are correlated for $D^+ \rightarrow \bar{K}^0 e^+ \nu_e$ and $D^+ \rightarrow \bar{K}^0 \mu^+ \nu_\mu$.

Table 5. Relative systematic uncertainties (in %) in the measurements of the branching fractions.

Source	$D^0 \rightarrow K^- e^+ \nu_e$	$D^0 \rightarrow K^- \mu^+ \nu_\mu$	$D^+ \rightarrow \bar{K}^0 e^+ \nu_e$	$D^+ \rightarrow \bar{K}^0 \mu^+ \nu_\mu$
N_{ST}	0.30	0.30	0.30	0.30
K^- tracking	0.10	0.10	–	–
K^- PID	0.10	0.10	–	–
K_S^0 reconstruction	–	–	0.85	0.89
ℓ^+ tracking	0.10	0.10	0.10	0.10
ℓ^+ PID	0.10	0.16	0.10	0.15
MC model	0.20	0.19	0.10	0.05
$M_{\bar{K}\ell}$ requirement	–	–	–	–
$E_{\text{extra}}^{\text{max}} \gamma$ and $N_{\text{extra}}^{\text{trk}}$ requirement	0.10	0.10	0.10	0.10
U_{miss} fit	0.18	0.14	0.06	0.05
MC statistics	0.05	0.06	0.07	0.07
Quoted branching fractions	–	–	0.07	0.07
Total	0.46	0.46	0.93	0.97

VII. HADRONIC TRANSITION FORM FACTORS

A. Theoretical formula

The differential decay width of the semileptonic decay $D \rightarrow \bar{K} \ell^+ \nu_\ell$ can be expressed as [8]

$$\frac{d\Gamma_i}{dq^2} = \frac{G_F^2 |V_{cs}|^2 (q^2 - m_\ell^2)^2 |\vec{p}_K|}{24\pi^3 q^4 m_D^2} \left[\left(1 + \frac{m_\ell^2}{2q^2}\right) m_D^2 |\vec{p}_K|^2 \times |f_+^K(q^2)|^2 + \frac{3m_\ell^2}{8q^2} (m_D^2 - m_K^2)^2 |f_0^K(q^2)|^2 \right], \quad (4)$$

where q is the four-momentum transfer to the $\ell^+ \nu_\ell$ system, $|\vec{p}_K|$ is the modulus of the meson three-momentum in the D rest frame, G_F is the Fermi constant, $f_+^K(q^2)$ is the vector form factor, and $f_0^K(q^2)$ is the scalar form factor. The series expansion [36] is the most popular parameterization to describe the hadronic transition form factor, which has the form

$$f_+^K(q^2) = \frac{1}{P(q^2)\Phi(q^2)} \sum_{k=0}^{\infty} a_k(t_0) [z(q^2, t_0)]^k. \quad (5)$$

Here, $a_k(t_0)$ are the real coefficients, and $P(q^2) = z(q^2, m_{D_s^{*+}}^2)$, where $z(q^2, t_0) = \frac{\sqrt{t_+ - q^2} - \sqrt{t_+ - t_0}}{\sqrt{t_+ - q^2} + \sqrt{t_+ - t_0}}$. The function Φ is given by

$$\Phi(q^2) = \sqrt{\frac{1}{24\pi\chi_V}} \left(\frac{t_+ - q^2}{t_+ - t_0}\right)^{1/4} \left(\sqrt{t_+ - q^2} + \sqrt{t_+}\right)^{-5} \times \left(\sqrt{t_+ - q^2} + \sqrt{t_+ - t_0}\right) \left(\sqrt{t_+ - q^2} + \sqrt{t_+ - t_-}\right)^{3/2} \times (t_+ - q^2)^{3/4}, \quad (6)$$

where $t_\pm = (m_D \pm m_K)^2$, $t_0 = t_+(1 - \sqrt{1 - t_-/t_+})$, m_D and m_K are the masses of D and K particles, $m_{D_s^{*+}}$ is the pole mass of the vector form factor $f_+^K(q^2)$ accounting for the strong interaction between D and K mesons and usually taken as the mass of the lowest lying $c\bar{s}$ vector meson D_s^{*+} , which is 2112.2 MeV [10]. The χ_V parameter is obtained from dispersion relations using perturbative QCD [44],

$$\chi_V = \frac{3}{32\pi^2 m_c^2}, \quad (7)$$

where $m_c = 1.27$ GeV is the c -quark mass.

In this analyses, the two-parameter series expansion is enough to describe the data, i.e.

$$f_+^K(q^2) = \frac{1}{P(q^2)\Phi(q^2)} [a_0(t_0) + a_1(t_0)z(q^2, t_0)]. \quad (8)$$

By setting $r_1(t_0) = a_1(t_0)/a_0(t_0)$, the vector form factor $f_+^K(q^2)$ can be written as

$$f_+^K(q^2) = \frac{1}{P(q^2)\Phi(q^2)} \frac{f_+^K(0)P(0)\Phi(0)}{1 + r_1(t_0)z(0, t_0)} \times (1 + r_1(t_0)[z(q^2, t_0)]). \quad (9)$$

The scalar form factor $f_0^K(q^2)$ is similar to $f_+^K(q^2)$ but with a one-parameter series expansion, which is given by [8]

$$f_0^K(q^2) = \frac{1}{P(q^2)\Phi(q^2)} f_0^K(0)P(0)\Phi(0). \quad (10)$$

Here, $f_0^K(q^2)$ has the same normalization at $q^2 = 0$ as $f_+^K(q^2)$, i.e.

$$f_0^K(0) = f_+^K(0), \quad (11)$$

but with a different pole mass $m_{D_{s0}^*(2317)^+}$ in $P(q^2)$, which is 2317.8 MeV [10].

B. Partial decay rates in data

To obtain the hadronic transition form factors of the semileptonic decays, the whole q^2 range is divided into 18 intervals for each signal decay. The differential decay rate in the i -th q^2 interval is determined as

$$\frac{d\Gamma_i}{dq_i^2} = \frac{\Delta\Gamma_i}{\Delta q_i^2}, \quad (12)$$

where $\Delta\Gamma_i = N_{\text{prd}}^i/(\tau_D \cdot N_{\text{ST}}^{\text{tot}})$ is the partial decay rate in the i -th q^2 interval, N_{prd}^i is the number of events produced in the i -th q^2 interval, and τ_D is the D lifetime [10].

In the i -th q^2 interval, the number of events produced in data is calculated as

$$N_{\text{prd}}^i = \sum_j^{N_{\text{intervals}}} (\varepsilon^{-1})_{ij} N_{\text{DT}}^j, \quad (13)$$

where $(\varepsilon^{-1})_{ij}$ is the element of the inverse efficiency matrix, obtained by analyzing the signal MC events. The statistical uncertainty of N_{prd}^i is given by

$$[\sigma(N_{\text{prd}}^i)]^2 = \sum_j^{N_{\text{intervals}}} (\varepsilon^{-1})_{ij}^2 \left[\sigma_{\text{stat}}(N_{\text{DT}}^j) \right]^2, \quad (14)$$

where $\sigma_{\text{stat}}(N_{\text{DT}}^j)$ is the statistical uncertainty of N_{DT}^j . The element ε_{ij}^α of the efficiency matrix with tag mode α is given by

$$\varepsilon_{ij}^\alpha = \frac{N_{ij}^{\text{rec}}}{N_j^{\text{gen}}} \cdot \frac{1}{\varepsilon_{\text{ST}}^\alpha}, \quad (15)$$

where N_{ij}^{rec} is the number of events generated in the j -th q^2 interval and reconstructed in the i -th q^2 interval, N_j^{gen} is the number of events generated in the j -th q^2 interval, and $\varepsilon_{\text{ST}}^\alpha$ is the ST efficiency with tag mode α . The efficiency matrix elements ε_{ij} weighted by the ST yields of data, which are presented in Tables 9–12 in Appendix, are given by

$$\varepsilon_{ij} = \sum_{\alpha=1}^6 \frac{N_{\text{ST}}^\alpha \varepsilon_{ij}^\alpha}{N_{\text{ST}}^{\text{tot}}}. \quad (16)$$

For each signal decay, the signal yield observed in each reconstructed q^2 interval is obtained from a fit to the U_{miss} distribution. The fitting method is the same as mentioned in Section VIA. Figure 3 shows the results of the fits to the U_{miss} distributions in reconstructed q^2 intervals for $D^0 \rightarrow K^- e^+ \nu_e$ semileptonic D decays. Similar figures for $D^0 \rightarrow K^- \mu^+ \nu_\mu$, $D^+ \rightarrow \bar{K}^0 e^+ \nu_e$, and

$D^+ \rightarrow \bar{K}^0 \mu^+ \nu_\mu$ decays are available in Figs. 7–9 in Appendix.

Table 6 lists the q^2 ranges, the fitted numbers of observed DT events (N_{DT}), the numbers of produced events (N_{prd}) calculated by the weighted efficiency matrix and the decay rates ($\Delta\Gamma$) of $D^0 \rightarrow K^- e^+ \nu_e$ semileptonic D decays in individual q^2 intervals. Similar tables for $D^0 \rightarrow K^- \mu^+ \nu_\mu$, $D^+ \rightarrow \bar{K}^0 e^+ \nu_e$, and $D^+ \rightarrow \bar{K}^0 \mu^+ \nu_\mu$ decays are available in Tables 13–15 in Appendix.

Table 6. The observed yields (N_{DT}^i), the produced yields (N_{prd}^i) and the partial decay rates ($\Delta\Gamma$) of $D^0 \rightarrow K^- e^+ \nu_e$ in different q^2 intervals of data, where the uncertainties are statistical only.

q^2 (GeV ² /c ⁴)	N_{DT}^i	N_{prd}^i	$\Delta\Gamma$ (ns ⁻¹)
(0.00, 0.10)	21356 ± 160	29580 ± 236	9.100 ± 0.073
(0.10, 0.20)	19982 ± 154	28248 ± 247	8.690 ± 0.076
(0.20, 0.30)	18675 ± 149	26707 ± 249	8.216 ± 0.076
(0.30, 0.40)	17406 ± 143	25180 ± 244	7.746 ± 0.075
(0.40, 0.50)	16176 ± 137	23475 ± 238	7.221 ± 0.073
(0.50, 0.60)	14896 ± 132	21685 ± 231	6.671 ± 0.071
(0.60, 0.70)	13682 ± 126	20003 ± 222	6.153 ± 0.068
(0.70, 0.80)	12372 ± 119	18119 ± 211	5.574 ± 0.065
(0.80, 0.90)	11140 ± 112	16357 ± 198	5.032 ± 0.061
(0.90, 1.00)	9997 ± 105	14719 ± 187	4.528 ± 0.057
(1.00, 1.10)	8691 ± 98	13040 ± 176	4.011 ± 0.054
(1.10, 1.20)	7394 ± 90	11091 ± 162	3.412 ± 0.050
(1.20, 1.30)	6135 ± 83	9459 ± 150	2.910 ± 0.046
(1.30, 1.40)	4797 ± 73	7644 ± 136	2.352 ± 0.042
(1.40, 1.50)	3499 ± 63	5627 ± 118	1.731 ± 0.036
(1.50, 1.60)	2521 ± 53	4356 ± 105	1.340 ± 0.032
(1.60, 1.70)	1418 ± 41	2621 ± 86	0.806 ± 0.026
(1.70, 1.88)	554 ± 26	1378 ± 72	0.424 ± 0.022

C. Construction of χ^2 and statistical covariance matrices

To determine the hadronic transition form factor and $|V_{cs}|$, a least χ^2 method is used to fit the partial decay rates of the different signal decays. Considering the correlations of the measured partial decay rates ($\Delta\Gamma_i^{\text{msr}}$) among different q^2 intervals, the χ^2 is given by

$$\chi^2 = \sum_{i,j=1}^{N_{\text{intervals}}} (\Delta\Gamma_i^{\text{msr}} - \Delta\Gamma_i^{\text{th}}) (C^{-1})_{ij} (\Delta\Gamma_j^{\text{msr}} - \Delta\Gamma_j^{\text{th}}), \quad (17)$$

where $\Delta\Gamma_i^{\text{th}}$ is the theoretically expected decay rate in the i -th interval, $(C^{-1})_{ij}$ is the element of the inverse covariance matrix of the measured partial decay rates

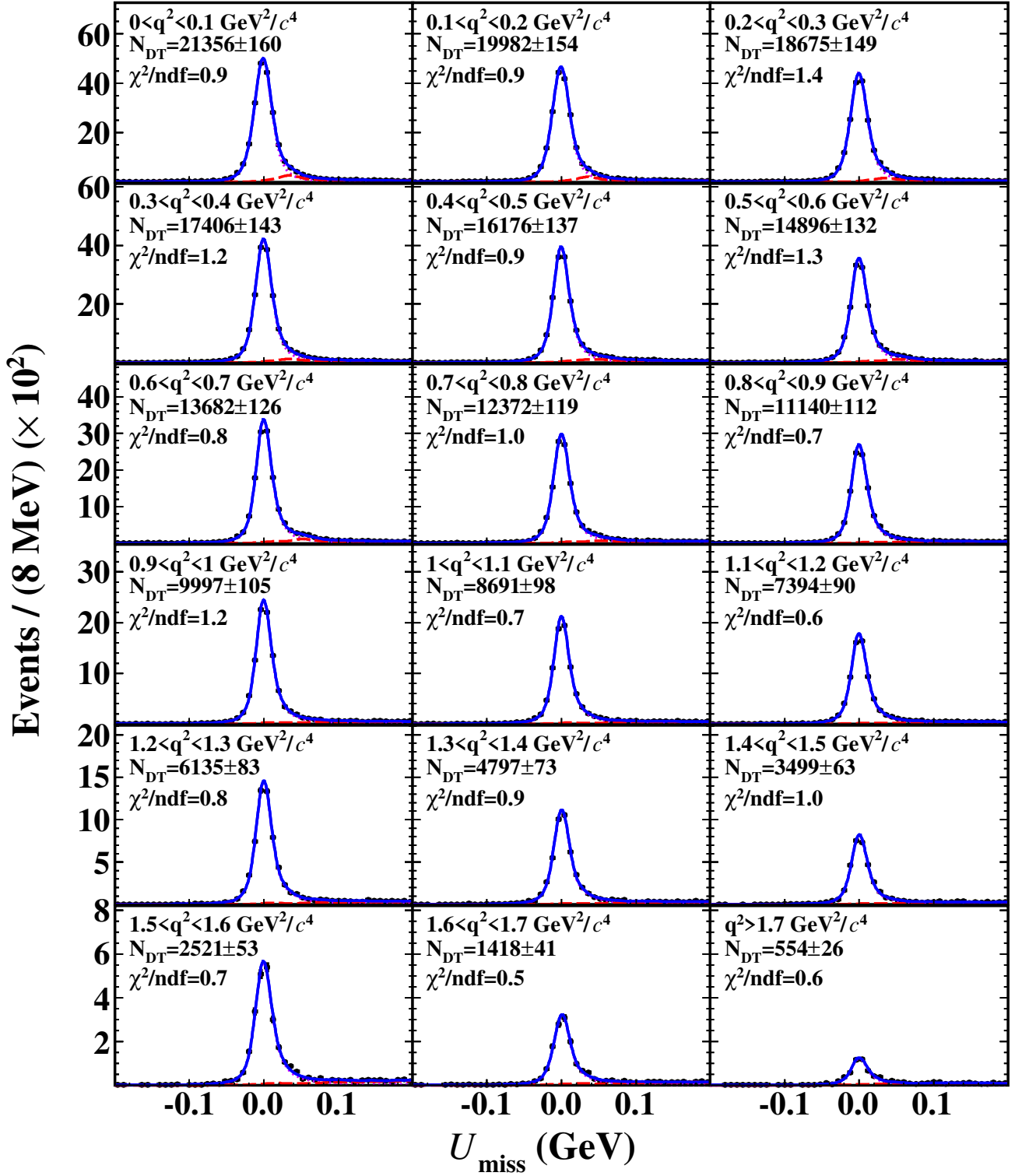


Fig. 3. Fits to the U_{miss} distributions of the accepted $D^0 \rightarrow K^- e^+ \nu_e$ candidates in different q^2 bins. The points with error bars are data. The blue solid curves are the fit results. The violet dotted curves are the signal shapes, and the red dashed curves are the fitted combinatorial background shapes.

and is given by $C_{ij} = C_{ij}^{\text{stat}} + C_{ij}^{\text{syst}}$. Here, C_{ij}^{stat} and C_{ij}^{syst} are elements of the statistical and systematic covariance matrices, respectively. The elements of the statistical covariance matrix are defined as

$$C_{ij}^{\text{stat}} = \left(\frac{1}{\tau_D N_{\text{ST}}^{\text{tot}}} \right)^2 \sum_{\alpha} (\varepsilon^{-1})_{i\alpha} (\varepsilon^{-1})_{j\alpha} (\sigma(N_{\text{DT}}^{\alpha}))^2, \quad (18)$$

where $\sigma(N_{\text{DT}}^{\alpha})$ is the statistical uncertainty of the signal yield observed in the α -th interval. The elements of the statistical covariance density matrices of $D^0 \rightarrow K^- e^+ \nu_e$, $D^0 \rightarrow K^- \mu^+ \nu_{\mu}$, $D^+ \rightarrow \bar{K}^0 e^+ \nu_e$ and $D^+ \rightarrow \bar{K}^0 \mu^+ \nu_{\mu}$ decays are presented in Tables 16–19 in [Appendix](#).

D. Systematic uncertainties on partial decay rates

The sources of systematic uncertainties are discussed below.

a. ST \bar{D} yields The systematic uncertainties associated with the number of $\bar{D}^0(D^-)$ tags are fully correlated across q^2 intervals. The element of the related systematic covariance matrix is calculated by

$$C_{ij}^{\text{syst}}(N_{\text{ST}}) = \Delta\Gamma_i \Delta\Gamma_j \left(\frac{\sigma(N_{\text{ST}})}{N_{\text{ST}}} \right)^2, \quad (19)$$

where $\sigma(N_{\text{ST}})/N_{\text{ST}}$ is the relative uncertainty on the number of $\bar{D}^0(D^-)$ tags.

b. D lifetime The systematic uncertainties associated with the D lifetime are fully correlated across the q^2 intervals. The element of the related systematic covariance matrix is calculated by

$$C_{ij}^{\text{syst}}(\tau_D) = \sigma(\Delta\Gamma_i) \sigma(\Delta\Gamma_j), \quad (20)$$

where $\sigma(\Delta\Gamma_i) = \sigma\tau_D \cdot \Delta\Gamma_i$ and $\sigma\tau_D$ is the uncertainty on the D lifetime [10].

c. MC statistics The elements of the covariance matrix which accounts for the systematic uncertainties and correlations between the q^2 intervals are calculated by

$$C_{ij}^{\text{syst}}(\text{MC}^{\text{stat}}) = \left(\frac{1}{\tau_D N_{\text{ST}}} \right)^2 \times \sum_{\alpha\beta} N_{\text{DT}}^{\alpha} N_{\text{DT}}^{\beta} \text{Cov} \left((\varepsilon^{-1})_{i\alpha}, (\varepsilon^{-1})_{j\beta} \right), \quad (21)$$

where $N_{\text{DT}}^{\alpha(\beta)}$ is the signal yield observed in the interval $\alpha(\beta)$, and the covariances of the inverse efficiency matrix elements are given by

$$\text{Cov} \left((\varepsilon^{-1})_{i\alpha}, (\varepsilon^{-1})_{j\beta} \right) = \sum_{mn} \left((\varepsilon^{-1})_{im} (\varepsilon^{-1})_{jm} \right) [\sigma(\varepsilon_{mn})]^2 \left((\varepsilon^{-1})_{\alpha n} (\varepsilon^{-1})_{\beta n} \right). \quad (22)$$

d. MC model To estimate the uncertainty from the MC model, we vary the parameters of the two-parameter series expansion model by $\pm 1\sigma$. The difference between the alternative and nominal efficiencies is taken as the systematic uncertainty for each signal decay. The element of the covariance matrix is defined as

$$C_{ij}^{\text{syst}}(\text{MC model}) = \delta(\Delta\Gamma_i) \delta(\Delta\Gamma_j), \quad (23)$$

where $\delta(\Delta\Gamma_i)$ denotes the change of the partial decay rate in the i -th q^2 interval.

e. Tracking, PID The systematic uncertainties associated with the e^+ or μ^+ tracking and PID efficiencies, and K^- tracking and PID efficiencies are estimated by varying the corresponding correction factors for efficiencies within $\pm 1\sigma$. Using the new efficiency matrix, the element of the corresponding systematic covariance matrix is calculated by

$$C_{ij}^{\text{syst}}(\text{Tracking, PID}) = \delta(\Delta\Gamma_i) \delta(\Delta\Gamma_j), \quad (24)$$

where $\delta(\Delta\Gamma_i)$ denotes the change of the partial decay rate in the i -th q^2 interval.

f. U_{miss} fit The systematic covariance matrix arising from the uncertainty in the U_{miss} fit has elements

$$C_{ij}^{\text{syst}}(U_{\text{miss}} \text{ fit}) = \left(\frac{1}{\tau_D N_{\text{ST}}^{\text{tot}}} \right)^2 \sum_{\alpha} \varepsilon_{i\alpha}^{-1} \varepsilon_{j\alpha}^{-1} (\sigma_{\alpha}^{\text{Fit}})^2, \quad (25)$$

where $\sigma_{\alpha}^{\text{Fit}}$ is the systematic uncertainty of the signal yield observed in the interval α obtained by varying the background shape in the U_{miss} fit as described in Section [VIB](#).

g. Remaining uncertainties The remaining systematic uncertainties, include the $E_{\text{extra}}^{\text{max}} \gamma$ and $N_{\text{extra}}^{\text{trk}}$ requirements, K_S^0 reconstruction, and quoted branching fractions, are assumed to be fully correlated across q^2 intervals, and the element of the corresponding systematic covariance matrix is calculated by

$$C_{ij}^{\text{syst}} = \sigma(\Delta\Gamma_i) \sigma(\Delta\Gamma_j), \quad (26)$$

where $\sigma(\Delta\Gamma_i) = \sigma_{\text{syst}} \cdot \Delta\Gamma_i$. The systematic uncertainties σ_{syst} on $D^0 \rightarrow K^- e^+ \nu_e$ semileptonic D decays in different q^2 intervals are shown in Table 7, and those of $D^0 \rightarrow K^- \mu^+ \nu_{\mu}$, $D^+ \rightarrow \bar{K}^0 e^+ \nu_e$, and $D^+ \rightarrow \bar{K}^0 \mu^+ \nu_{\mu}$ decays are available in Tables 20–22 in [Appendix](#), as well as the elements of the systematic covariance density matrices for all signal decays.

E. Results based on individual fits

With the statistical and systematic covariance matrices described previously, we fit individually the partial decay rates of $D^0 \rightarrow K^- e^+ \nu_e$, $D^0 \rightarrow K^- \mu^+ \nu_{\mu}$, $D^+ \rightarrow \bar{K}^0 e^+ \nu_e$, and $D^+ \rightarrow \bar{K}^0 \mu^+ \nu_{\mu}$ to obtain the fit parameters $f_+^K(0)|V_{cs}|$ and $r_1(t_0)$ from Eq. (9). The

Table 7. The systematic uncertainties (in %) of the measured decay rates of $D^0 \rightarrow K^- e^+ \nu_e$ in different q^2 bins.

i -th q^2 bin	1	2	3	4	5	6	7	8	9	10	11	12	13	14	15	16	17	18
N_{ST}	0.30	0.30	0.30	0.30	0.30	0.30	0.30	0.30	0.30	0.30	0.30	0.30	0.30	0.30	0.30	0.30	0.30	0.30
D^0 lifetime	0.24	0.24	0.24	0.24	0.24	0.24	0.24	0.24	0.24	0.24	0.24	0.24	0.24	0.24	0.24	0.24	0.24	0.24
MC statistics	0.14	0.15	0.15	0.16	0.17	0.17	0.18	0.19	0.20	0.21	0.23	0.25	0.28	0.31	0.36	0.45	0.60	0.99
MC model	0.21	0.19	0.56	0.28	0.06	0.46	1.50	0.25	1.58	0.31	0.44	0.04	0.57	1.33	0.31	0.29	3.63	1.04
K^- tracking	0.10	0.10	0.10	0.10	0.10	0.10	0.10	0.10	0.10	0.10	0.10	0.11	0.11	0.13	0.13	0.18	0.23	0.43
K^- PID	0.10	0.10	0.10	0.10	0.10	0.10	0.10	0.10	0.10	0.10	0.10	0.10	0.10	0.10	0.10	0.10	0.10	0.13
e^+ tracking	0.10	0.10	0.10	0.10	0.10	0.10	0.10	0.10	0.10	0.10	0.10	0.10	0.10	0.10	0.10	0.10	0.10	0.10
e^+ PID	0.10	0.10	0.10	0.10	0.10	0.10	0.10	0.10	0.10	0.10	0.10	0.10	0.10	0.10	0.10	0.10	0.10	0.10
U_{miss} fit	0.18	0.16	0.18	0.16	0.15	0.17	0.15	0.16	0.10	0.11	0.10	0.09	0.09	0.11	0.08	0.14	0.18	0.34
$E_{\text{extra}}^{\text{max}} \gamma$ and $N_{\text{extra}}^{\text{trk}}$ cut	0.10	0.10	0.10	0.10	0.10	0.10	0.10	0.10	0.10	0.10	0.10	0.10	0.10	0.10	0.10	0.10	0.10	0.10
Total	0.54	0.53	0.75	0.57	0.50	0.68	1.58	0.57	1.65	0.59	0.67	0.52	0.78	1.44	0.66	0.73	3.71	1.60

statistical uncertainties on the fit parameters are taken from the fit with the statistical covariance matrix, and the systematic uncertainties on the fit parameters are obtained by calculating the quadrature difference between the uncertainties of the fit parameters using the statistical covariance matrix and the uncertainties using the combined statistical and systematic covariance matrix.

The sub-figures on the left of Fig. 4 show the individual fit results of $D^0 \rightarrow K^- e^+ \nu_e$, $D^0 \rightarrow K^- \mu^+ \nu_\mu$, $D^+ \rightarrow \bar{K}^0 e^+ \nu_e$, and $D^+ \rightarrow \bar{K}^0 \mu^+ \nu_\mu$. The sub-figures on the right of Fig. 4 show the projections of the form factor fits as a function of q^2 , where the points with error bars show the measured values of the form factor, which are obtained with

$$f_+^{\text{data}}(q_i^2) = \sqrt{\frac{(\Delta\Gamma_i^{\text{measured}} - B) \cdot |f_+(q_i^2)|^2}{A}}, \quad (27)$$

with

$$A = \int_{q_{\text{min}}^2}^{q_{\text{max}}^2} \frac{G_F^2 |V_{cs}|^2 (q^2 - m_\ell^2)^2 |\vec{p}_K|}{24\pi^3 q^4 m_D^2} \times \left(1 + \frac{m_\ell^2}{2q^2}\right) m_D^2 |\vec{p}_K|^2 |f_+(q^2)|^2 dq^2, \quad (28)$$

$$B = \int_{q_{\text{min}}^2}^{q_{\text{max}}^2} \frac{G_F^2 |V_{cs}|^2 (q^2 - m_\ell^2)^2 |\vec{p}_K|}{24\pi^3 q^4 m_D^2} \times \frac{3m_\ell^2}{8q^2} (m_D^2 - m_K^2)^2 |f_0(q^2)|^2 dq^2, \quad (29)$$

where q_{min}^2 and q_{max}^2 are the low and high boundaries of the i -th q^2 bin. Both functions $f_+(q^2)$ and $f_0(q^2)$ are calculated using the two-parameter series expansion model.

The parameters obtained from the individual fits to the differential decay rates of $D^0 \rightarrow K^- e^+ \nu_e$, $D^0 \rightarrow K^- \mu^+ \nu_\mu$, $D^+ \rightarrow \bar{K}^0 e^+ \nu_e$, and $D^+ \rightarrow \bar{K}^0 \mu^+ \nu_\mu$ are listed

in Table 8.

F. Results based on a simultaneous fit

To consider the correlation effects in the measurements of the hadronic form factor among the four signal decays, we perform a simultaneous fit to the partial decay rates of $D^0 \rightarrow K^- e^+ \nu_e$, $D^0 \rightarrow K^- \mu^+ \nu_\mu$, $D^+ \rightarrow \bar{K}^0 e^+ \nu_e$, and $D^+ \rightarrow \bar{K}^0 \mu^+ \nu_\mu$ to obtain the product $f_+^K(0)|V_{cs}|$ and $r_1(t_0)$.

In the simultaneous fit, the values of $f_+^K(0)|V_{cs}|$ and $r_1(t_0)$ are shared among the four signal decays. We still use the least χ^2 method from Eq. (17) to obtain the fit parameters. The $\Delta\Gamma_i$ for these four semileptonic decay modes are combined into one vector with 72 components and the elements of the covariance matrix for the combined $\Delta\Gamma_i$ are redefined as $C_{ij} = C_{ij}^{\text{stat}} + C_{ij}^{\text{csyst}} + C_{ij}^{\text{usyst}}$, ($i, j = 1, 2, 3, \dots, 71, 72$), where C_{ij}^{stat} is the element of statistical covariance matrix, which is diagonal in blocks, *i.e.*

$$C^{\text{stat}} = \begin{pmatrix} A & 0 & 0 & 0 \\ 0 & B & 0 & 0 \\ 0 & 0 & C & 0 \\ 0 & 0 & 0 & D \end{pmatrix}.$$

Here A , B , C , and D are the statistical covariance matrices obtained from each signal channel. The element of the correlated systematic covariance matrix is

$$C_{ij}^{\text{csyst}} = \delta(\Delta\Gamma_i)\delta(\Delta\Gamma_j). \quad (30)$$

The uncorrelated systematic covariance matrix is defined

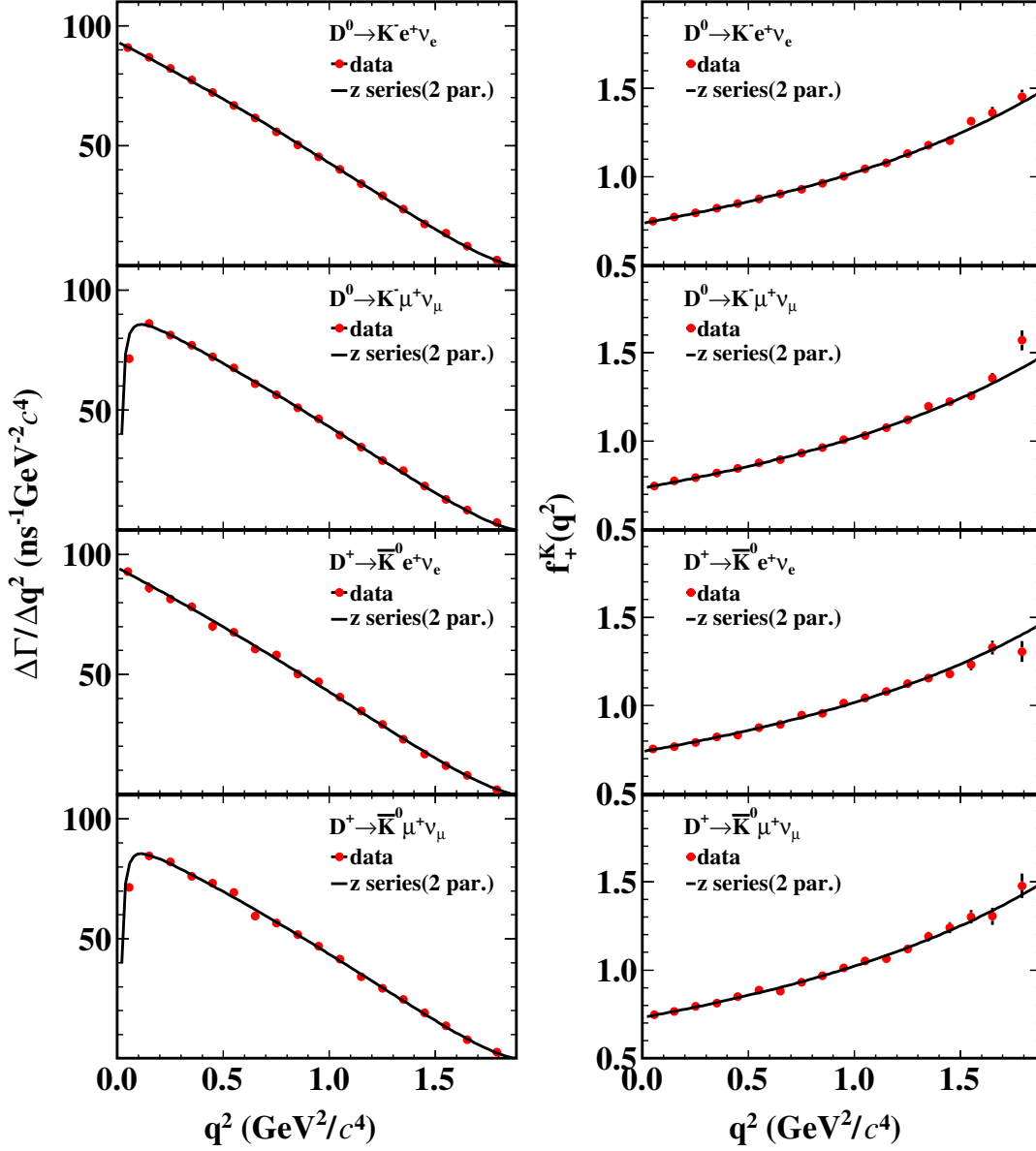


Fig. 4. (Left) Fits to the partial decay rates of $D \rightarrow \bar{K} \ell^+ \nu_\ell$ and (Right) projections of the form factor as functions of q^2 , where the red points with error bars are the measured partial decay rates and the solid curves are the fits.

Table 8. The parameters ($f_+^K(0)|V_{cs}|$, $r_1(t_0)$) of the hadronic form factors from the fits to the partial decay rates of the semileptonic decays, where the first and second uncertainties are statistical and systematic, respectively. The column labeled $\rho_{2\text{par}}$ gives the correlation coefficients of the two parameters, and ndf denotes the number of degrees of freedom.

Case	Signal decay	$f_+^K(0) V_{cs} $	$r_1(t_0)$	$\rho_{2\text{par}}$	χ^2/ndf
Individual fit	$D^0 \rightarrow K^- e^+ \nu_e$	$0.7179 \pm 0.0016 \pm 0.0017$	$-2.30 \pm 0.05 \pm 0.03$	0.48	16.3/16
	$D^0 \rightarrow K^- \mu^+ \nu_\mu$	$0.7162 \pm 0.0022 \pm 0.0019$	$-2.28 \pm 0.08 \pm 0.02$	0.62	17.1/16
	$D^+ \rightarrow \bar{K}^0 e^+ \nu_e$	$0.7207 \pm 0.0027 \pm 0.0035$	$-2.13 \pm 0.10 \pm 0.07$	0.29	13.0/16
	$D^+ \rightarrow \bar{K}^0 \mu^+ \nu_\mu$	$0.7124 \pm 0.0035 \pm 0.0032$	$-2.41 \pm 0.12 \pm 0.08$	0.45	10.6/16
Simultaneous fit	$D \rightarrow \bar{K} \ell^+ \nu_\ell$	$0.7171 \pm 0.0011 \pm 0.0013$	$-2.28 \pm 0.04 \pm 0.02$	0.44	60.9/70

in blocks as

$$C^{\text{usyst}} = \begin{pmatrix} a & 0 & 0 & 0 \\ 0 & b & 0 & 0 \\ 0 & 0 & c & 0 \\ 0 & 0 & 0 & d \end{pmatrix},$$

where a , b , c , and d are the uncorrelated systematic covariance matrices obtained from each signal channel.

Then, the elements of covariance density matrix for the simultaneous fit are available in Tables 27–30 in Appendix.

With the modified $\Delta\Gamma_i$ and C_{ij} , we do the simultaneous fit to the partial decay rates of $D \rightarrow \bar{K}\ell^+\nu_\ell$, which is shown in Fig. 5. The fitted parameters are $f_+^K(0)|V_{cs}| = 0.7171 \pm 0.0011 \pm 0.0013$ and $r_1(t_0) = -2.28 \pm 0.04 \pm 0.02$, which are summarized in Table 8.

VIII. SUMMARY

In summary, by analyzing 7.93 fb^{-1} of e^+e^- collision data collected at $\sqrt{s} = 3.773 \text{ GeV}$ with the BESIII detector, improved measurements of the semileptonic decays $D \rightarrow \bar{K}\ell^+\nu_\ell$ are performed. The absolute branching fractions of $D^0 \rightarrow K^-e^+\nu_e$, $D^0 \rightarrow K^-\mu^+\nu_\mu$, $D^+ \rightarrow \bar{K}^0e^+\nu_e$, and $D^+ \rightarrow \bar{K}^0\mu^+\nu_\mu$ are determined to be $(3.521 \pm 0.009_{\text{stat.}} \pm 0.016_{\text{syst.}})\%$, $(3.419 \pm 0.011_{\text{stat.}} \pm 0.016_{\text{syst.}})\%$, $(8.864 \pm 0.039_{\text{stat.}} \pm 0.082_{\text{syst.}})\%$ and $(8.665 \pm 0.046_{\text{stat.}} \pm 0.084_{\text{syst.}})\%$, respectively. Combining the branching fractions of semielectronic and semimuonic decays, we obtain the ratios of the two branching fractions $\frac{\mathcal{B}_{D^0 \rightarrow K^-\mu^+\nu_\mu}}{\mathcal{B}_{D^0 \rightarrow K^-e^+\nu_e}} = 0.971 \pm 0.004_{\text{stat.}} \pm 0.006_{\text{syst.}}$ and $\frac{\mathcal{B}_{D^+ \rightarrow \bar{K}^0\mu^+\nu_\mu}}{\mathcal{B}_{D^+ \rightarrow \bar{K}^0e^+\nu_e}} = 0.978 \pm 0.007_{\text{stat.}} \pm 0.013_{\text{syst.}}$, which are consistent with the theoretical calculation 0.975 ± 0.001 [45]. Our measurements support lepton flavor universality.

From the simultaneous fit to the partial decay rates of $D^0 \rightarrow K^-e^+\nu_e$, $D^0 \rightarrow K^-\mu^+\nu_\mu$, $D^+ \rightarrow \bar{K}^0e^+\nu_e$, and $D^+ \rightarrow \bar{K}^0\mu^+\nu_\mu$, the product of the hadronic form factor $f_+^K(0)$ and the modulus of the CKM matrix element $|V_{cs}|$ are determined to be $f_+^K(0)|V_{cs}| = 0.7171 \pm 0.0011_{\text{stat.}} \pm 0.0013_{\text{syst.}}$. Taking the value of $|V_{cs}| = 0.97349 \pm 0.00016$ given by the PDG [10] as input, we obtain the hadronic form factor $f_+^K(0) = 0.7366 \pm$

$0.0011_{\text{stat.}} \pm 0.0013_{\text{syst.}}$. Conversely, using the $f_+^K(0)$ calculated in LQCD [4], we obtain $|V_{cs}| = 0.9623 \pm 0.0015_{\text{stat.}} \pm 0.0017_{\text{syst.}} \pm 0.0040_{\text{LQCD}}$. The comparison of the $f_+^K(0)$ value obtained in this work with the theoretical and experimental calculations is shown in Fig. 6. For the experimental calculations, the values of $f_+^K(0)$ are updated by using the latest value of $|V_{cs}|$ as mentioned before. The hadronic form factor $f_+^K(0)$ measured in this work supersedes the previous BESIII results [21–24], with the better precision. This is important to test different models and help to improve the precision of theoretical calculations.

ACKNOWLEDGMENTS

The BESIII Collaboration thanks the staff of BEPCII and the IHEP computing center for their strong support. This work is supported in part by National Key R&D Program of China under Contracts Nos. 2020YFA0406000, 2023YFA1606400, 2020YFA0406300; National Natural Science Foundation of China (NSFC) under Contracts Nos. 11635010, 11735014, 11935015, 11935016, 11935018, 12025502, 12035009, 12035013, 12061131003, 12192260, 12192261, 12192262, 12192263, 12192264, 12192265, 12221005, 12225509, 12235017, 12361141819; the Chinese Academy of Sciences (CAS) Large-Scale Scientific Facility Program; the CAS Center for Excellence in Particle Physics (CCEPP); Joint Large-Scale Scientific Facility Funds of the NSFC and CAS under Contract No. U1832207; 100 Talents Program of CAS; The Institute of Nuclear and Particle Physics (INPAC) and Shanghai Key Laboratory for Particle Physics and Cosmology; German Research Foundation DFG under Contracts Nos. 455635585, FOR5327, GRK 2149; Istituto Nazionale di Fisica Nucleare, Italy; Ministry of Development of Turkey under Contract No. DPT2006K-120470; National Research Foundation of Korea under Contract No. NRF-2022R1A2C1092335; National Science and Technology fund of Mongolia; National Science Research and Innovation Fund (NSRF) via the Program Management Unit for Human Resources & Institutional Development, Research and Innovation of Thailand under Contracts Nos. B16F640076, B50G670107; Polish National Science Centre under Contract No. 2019/35/O/ST2/02907; The Swedish Research Council; U. S. Department of Energy under Contract No. DE-FG02-05ER41374.

[1] V. Lubicz *et al.*, *Phys. Rev. D* **96**, 054514 (2017).
 [2] B. Chakraborty *et al.* (HPQCD Collaboration), *Phys. Rev. D* **104**, 034505 (2021).
 [3] W. G. Parrott *et al.* (HPQCD collaboration), *Phys. Rev. D* **107**, 014510 (2023).
 [4] A. Bazavov *et al.* (Fermilab Lattice and MILC Collaborations), *Phys. Rev. D* **107**, 094516 (2023).

[5] Y. L. Wu, M. Zhong and Y. B. Zuo, *Int. J. Mod. Phys. A* **21**, 6125-6172 (2006).
 [6] R. C. Verma, *J. Phys. G* **39**, 025005 (2012).
 [7] M. A. Ivanov, J. G. Körner, J. N. Pandya, P. Santorelli, N. R. Soni and C. T. Tran, *Front. Phys. (Beijing)* **14**, 64401 (2019).
 [8] R. N. Faustov, V. O. Galkin and X. W. Kang,

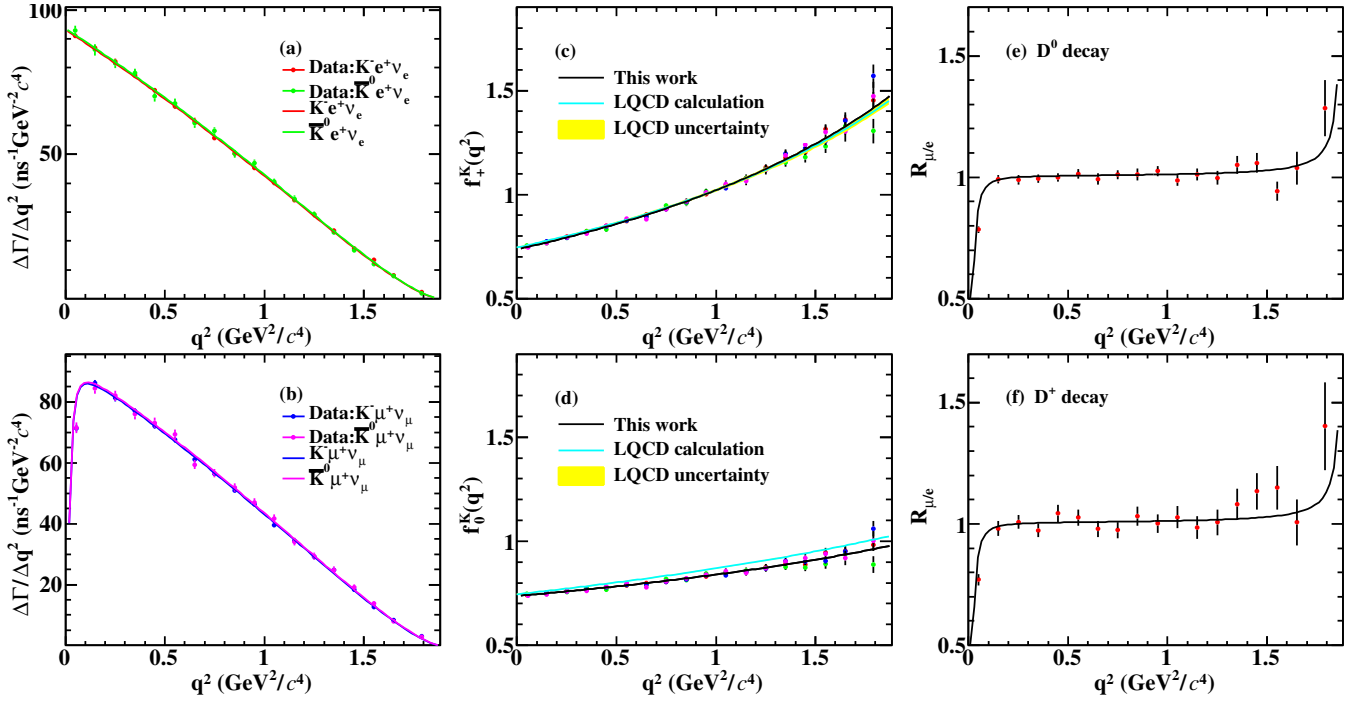


Fig. 5. (a)(b) Simultaneous fit to partial decay rates of $D^0(D^+) \rightarrow \bar{K}\ell^+\nu_\ell$. (c)(d) Projections of $f_+^K(q^2)$ and $f_0^K(q^2)$ as functions of q^2 of $D^0(D^+) \rightarrow \bar{K}\ell^+\nu_\ell$. (e)(f) The ratio of differential decay rates of $D^0 \rightarrow K^-\mu^+\nu_\mu$ over $D^0 \rightarrow K^-e^+\nu_e$ and the ratio of differential decay rates of $D^+ \rightarrow \bar{K}^0\mu^+\nu_\mu$ over $D^+ \rightarrow \bar{K}^0e^+\nu_e$ in each q^2 bin. The dots with error bars are data, and the solid lines are the results with the parameters of the simultaneous fit.

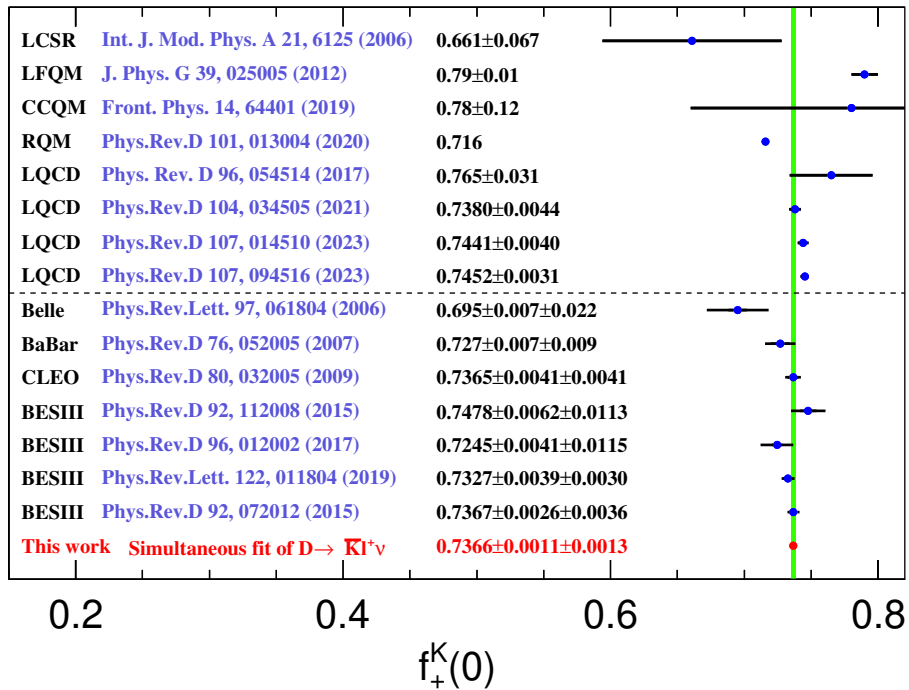


Fig. 6. Comparisons of the form factor $f_+^K(0)$ measured in this work with the theoretical and experimental calculations. The first and second uncertainties are statistical and systematic, respectively. The green band corresponds to the $\pm 1\sigma$ limit of the form factor calculated in this work.

- Phys. Rev. D **101**, 013004 (2020).
- [9] B. C. Ke, J. Koponen, H. B. Li and Y. Zheng, *Ann. Rev. Nucl. Part. Sci.* **73**, 285-314 (2023).
- [10] R. L. Workman *et al.* (Particle Data Group), *Prog. Theor. Exp. Phys.* **2022**, 083C01 (2022).
- [11] M. Ablikim *et al.* (BES Collaboration), *Phys. Lett. B* **597**, 39-46 (2004).
- [12] M. Ablikim *et al.* (BES Collaboration), *Phys. Lett. B* **608**, 24-30 (2005).
- [13] M. Ablikim *et al.* (BES Collaboration), *Phys. Lett. B* **644**, 20-24 (2007).
- [14] B. Aubert *et al.* (BaBar Collaboration), *Phys. Rev. D* **76**, 052005 (2007).
- [15] L. Widhalm *et al.* (Belle Collaboration), *Phys. Rev. Lett.* **97**, 061804 (2006).
- [16] G. S. Huang *et al.* (CLEO Collaboration), *Phys. Rev. Lett.* **95**, 181801 (2005).
- [17] T. E. Coan *et al.* (CLEO Collaboration), *Phys. Rev. Lett.* **95**, 181802 (2005).
- [18] S. Dobbs *et al.* (CLEO Collaboration), *Phys. Rev. D* **77**, 112005 (2008).
- [19] D. Besson *et al.* (CLEO Collaboration), *Phys. Rev. D* **80**, 032005 (2009).
- [20] M. Ablikim *et al.* (BESIII Collaboration), *Phys. Rev. D* **104**, 052008 (2021).
- [21] M. Ablikim *et al.* (BESIII Collaboration), *Phys. Rev. D* **92**, 072012 (2015).
- [22] M. Ablikim *et al.* (BESIII Collaboration), *Phys. Rev. Lett.* **122**, 011804 (2019).
- [23] M. Ablikim *et al.* (BESIII Collaboration), *Phys. Rev. D* **92**, 112008 (2015).
- [24] M. Ablikim *et al.* (BESIII Collaboration), *Phys. Rev. D* **96**, 012002 (2017).
- [25] M. Ablikim *et al.* (BESIII Collaboration), *Chin. Phys. C* **40**, 113001 (2016).
- [26] M. Ablikim *et al.* (BESIII Collaboration), *Eur. Phys. J. C* **76**, 369 (2016).
- [27] M. Ablikim *et al.* (BESIII Collaboration), [arXiv:2406.05827](https://arxiv.org/abs/2406.05827).
- [28] M. Ablikim *et al.* (BESIII Collaboration), *Nucl. Instrum. Meth. A* **614**, 345 (2010).
- [29] C. H. Yu *et al.*, *Proceedings of IPAC2016, Busan, Korea, 2016*, doi:10.18429/JACoW-IPAC2016-TUYA01.
- [30] M. Ablikim *et al.* (BESIII Collaboration), *Chin. Phys. C* **44**, 040001 (2020).
- [31] H. B. Li and X. R. Lyu, *Natl. Sci. Rev.* **8**, no.11, nwab181 (2021).
- [32] X. Li *et al.*, *Radiat. Detect. Technol. Methods* **1**, 13 (2017);
Y. X. Guo *et al.*, *Radiat. Detect. Technol. Methods* **1**, 15 (2017);
P. Cao *et al.*, *Nucl. Instrum. Meth. A* **953**, 163053 (2020).
- [33] S. Agostinelli *et al.* (GEANT4 Collaboration), *Nucl. Instrum. Meth. A* **506**, 250 (2003).
- [34] K. X. Huang, Z. J. Li, Z. Qian, J. Zhu, H. Y. Li, Y. M. Zhang, S. S. Sun and Z. Y. You, *Nucl. Sci. Tech.* **33**, 142 (2022).
- [35] S. Jadach, B. F. L. Ward and Z. Was, *Phys. Rev. D* **63**, 113009 (2001);
Comput. Phys. Commun. **130**, 260 (2000).
- [36] T. Becher and R. J. Hill, *Phys. Lett. B* **633**, 61 (2006).
- [37] D. J. Lange, *Nucl. Instrum. Meth. A* **462**, 152 (2001);
R. G. Ping, *Chin. Phys. C* **32**, 599 (2008).
- [38] J. C. Chen, G. S. Huang, X. R. Qi, D. H. Zhang and Y. S. Zhu, *Phys. Rev. D* **62**, 034003 (2000);
R. L. Yang, R. G. Ping and H. Chen, *Chin. Phys. Lett.* **31**, 061301 (2014).
- [39] E. Richter-Was, *Phys. Lett. B* **303**, 163 (1993).
- [40] R. M. Baltrusaitis *et al.* (MARK III Collaboration), *Phys. Rev. Lett.* **56**, 2140 (1986).
- [41] M. Ablikim *et al.* (BESIII Collaboration), *Phys. Lett. B* **734**, 227 (2014).
- [42] K. Cranmer *et al.* (ROOT Collaboration), [CERN-OPEN-2012-016](https://arxiv.org/abs/1207.7033).
- [43] H. Albrecht *et al.* (ARGUS Collaboration), *Phys. Lett. B* **241**, 278 (1990).
- [44] C. G. Boyd, B. Grinstein and R. F. Lebed, *Nucl. Phys. B* **461**, 493 (1996).
- [45] L. Riggio, G. Salerno and S. Simula, *Eur. Phys. J. C* **78**, no.6, 501 (2018).

APPENDIX

Tables 9, 10, 11, and 12 report the elements of the weighted efficiency matrices for $D^0 \rightarrow K^- e^+ \nu_e$, $D^0 \rightarrow K^- \mu^+ \nu_\mu$, $D^+ \rightarrow \bar{K}^0 e^+ \nu_e$, and $D^+ \rightarrow \bar{K}^0 \mu^+ \nu_\mu$, respectively.

Figures 7, 8, and 9 show the results of the fits to the U_{miss} distributions in the reconstructed q^2 intervals for $D^0 \rightarrow K^- \mu^+ \nu_\mu$, $D^+ \rightarrow \bar{K}^0 e^+ \nu_e$, and $D^+ \rightarrow \bar{K}^0 \mu^+ \nu_\mu$, respectively.

Table 13, 14, and 15 list the q^2 ranges, the fitted numbers of observed DT events (N_{DT}), the numbers of produced events (N_{prd}) calculated by the weighted efficiency matrix and the decay rates ($\Delta\Gamma$) of $D^0 \rightarrow K^- \mu^+ \nu_\mu$, $D^+ \rightarrow \bar{K}^0 e^+ \nu_e$, and $D^+ \rightarrow \bar{K}^0 \mu^+ \nu_\mu$ in individual q^2 intervals.

Tables 16, 17, 18, and 19 report the elements of the statistical covariance density matrices for $D^0 \rightarrow K^- e^+ \nu_e$, $D^0 \rightarrow K^- \mu^+ \nu_\mu$, $D^+ \rightarrow \bar{K}^0 e^+ \nu_e$, and $D^+ \rightarrow \bar{K}^0 \mu^+ \nu_\mu$, respectively.

Table 20, 21, and 22 show the systematic uncertainties σ_{sys} of $D^0 \rightarrow K^- \mu^+ \nu_\mu$, $D^+ \rightarrow \bar{K}^0 e^+ \nu_e$, and $D^+ \rightarrow \bar{K}^0 \mu^+ \nu_\mu$ in different q^2 intervals.

Tables 23, 24, 25 and 26 report the elements of the systematic covariance density matrices for $D^0 \rightarrow K^- e^+ \nu_e$, $D^0 \rightarrow K^- \mu^+ \nu_\mu$, $D^+ \rightarrow \bar{K}^0 e^+ \nu_e$, and $D^+ \rightarrow \bar{K}^0 \mu^+ \nu_\mu$, respectively.

Tables 27, 28, 29, and 30 report the elements of the covariance density matrix ρ_{ij} ($i = 0, 1, 2, \dots, 71, 72; j = 0, 1, 2, \dots, 71, 72;$) for the simultaneous fit.

Table 9. The weighted efficiency matrix (in %) for $D^0 \rightarrow K^- e^+ \nu_e$. The i denote the reconstructed bin, and the j represent the produced bin.

ε_{ij}	1	2	3	4	5	6	7	8	9	10	11	12	13	14	15	16	17	18
1	67.94	4.03	0.31	0.13	0.02	0.00	0.00	0.00	0.00	0.00	0.00	0.00	0.00	0.00	0.00	0.00	0.00	0.00
2	2.48	62.81	5.09	0.41	0.14	0.03	0.01	0.01	0.00	0.00	0.00	0.00	0.00	0.00	0.00	0.00	0.00	0.00
3	0.08	3.17	60.81	5.47	0.42	0.13	0.03	0.01	0.01	0.01	0.00	0.00	0.00	0.00	0.00	0.00	0.00	0.00
4	0.03	0.11	3.57	59.42	5.62	0.46	0.11	0.03	0.01	0.01	0.01	0.00	0.00	0.00	0.00	0.00	0.00	0.00
5	0.01	0.03	0.14	3.87	58.75	5.74	0.44	0.10	0.03	0.02	0.01	0.01	0.00	0.00	0.00	0.00	0.00	0.00
6	0.01	0.02	0.05	0.16	3.97	58.38	5.69	0.42	0.11	0.04	0.02	0.01	0.00	0.00	0.00	0.00	0.00	0.00
7	0.01	0.01	0.02	0.06	0.19	4.09	57.97	5.72	0.42	0.11	0.03	0.02	0.01	0.01	0.00	0.00	0.00	0.00
8	0.00	0.01	0.01	0.02	0.06	0.21	4.18	57.80	5.60	0.38	0.10	0.05	0.01	0.01	0.00	0.01	0.00	0.00
9	0.00	0.00	0.01	0.01	0.03	0.07	0.22	4.21	57.74	5.41	0.39	0.09	0.04	0.01	0.00	0.00	0.00	0.00
10	0.00	0.00	0.00	0.01	0.01	0.04	0.08	0.25	4.25	57.65	5.25	0.38	0.11	0.04	0.01	0.01	0.00	0.00
11	0.00	0.00	0.00	0.00	0.01	0.01	0.03	0.08	0.24	4.09	56.97	5.01	0.33	0.08	0.04	0.01	0.00	0.00
12	0.00	0.00	0.00	0.00	0.00	0.01	0.02	0.03	0.08	0.25	4.01	56.95	4.91	0.31	0.06	0.03	0.01	0.00
13	0.00	0.00	0.00	0.00	0.00	0.00	0.01	0.01	0.03	0.08	0.29	3.86	55.87	4.51	0.28	0.06	0.01	0.00
14	0.00	0.00	0.00	0.00	0.00	0.00	0.00	0.01	0.01	0.02	0.08	0.27	3.65	54.36	4.23	0.24	0.03	0.00
15	0.00	0.00	0.00	0.00	0.00	0.00	0.00	0.00	0.00	0.01	0.02	0.06	0.24	3.46	53.75	3.96	0.15	0.00
16	0.00	0.00	0.00	0.00	0.00	0.00	0.00	0.00	0.00	0.00	0.00	0.02	0.06	0.19	3.06	51.27	3.50	0.10
17	0.00	0.00	0.00	0.00	0.00	0.00	0.00	0.00	0.00	0.00	0.00	0.00	0.01	0.03	0.15	2.65	47.84	2.71
18	0.00	0.00	0.00	0.00	0.00	0.00	0.00	0.00	0.00	0.00	0.00	0.00	0.00	0.00	0.01	0.08	1.77	36.54

Table 10. The weighted efficiency matrix (in %) for $D^0 \rightarrow K^- \mu^+ \nu_\mu$. The i denote the reconstructed bin, and the j represent the produced bin.

ε_{ij}	1	2	3	4	5	6	7	8	9	10	11	12	13	14	15	16	17	18
1	38.04	1.14	0.02	0.00	0.00	0.00	0.00	0.00	0.00	0.00	0.00	0.00	0.00	0.00	0.00	0.00	0.00	0.00
2	1.52	38.87	1.79	0.03	0.01	0.00	0.00	0.00	0.00	0.00	0.00	0.00	0.00	0.00	0.00	0.00	0.00	0.00
3	0.04	1.71	40.76	2.28	0.05	0.01	0.00	0.00	0.00	0.00	0.00	0.00	0.00	0.00	0.00	0.00	0.00	0.00
4	0.01	0.05	2.17	43.37	2.71	0.08	0.02	0.01	0.00	0.00	0.00	0.00	0.00	0.00	0.00	0.00	0.00	0.00
5	0.01	0.02	0.08	2.61	46.18	3.14	0.13	0.03	0.02	0.01	0.00	0.00	0.00	0.00	0.00	0.00	0.00	0.00
6	0.01	0.01	0.03	0.10	2.99	49.00	3.46	0.15	0.05	0.02	0.01	0.00	0.00	0.00	0.00	0.00	0.00	0.00
7	0.00	0.01	0.02	0.03	0.14	3.33	51.75	3.70	0.18	0.06	0.03	0.01	0.00	0.00	0.00	0.00	0.00	0.00
8	0.00	0.00	0.01	0.02	0.06	0.18	3.65	53.83	3.88	0.21	0.06	0.02	0.01	0.01	0.00	0.00	0.00	0.00
9	0.00	0.00	0.00	0.01	0.02	0.05	0.18	3.80	55.97	3.93	0.23	0.08	0.04	0.02	0.00	0.00	0.00	0.00
10	0.00	0.00	0.00	0.01	0.01	0.03	0.07	0.23	3.85	57.24	3.97	0.27	0.08	0.03	0.01	0.01	0.00	0.00
11	0.00	0.00	0.00	0.00	0.01	0.02	0.03	0.07	0.24	3.97	58.22	3.82	0.23	0.07	0.03	0.01	0.00	0.00
12	0.00	0.00	0.00	0.00	0.01	0.01	0.01	0.03	0.07	0.25	3.90	58.46	3.73	0.23	0.08	0.02	0.00	0.00
13	0.00	0.00	0.00	0.00	0.00	0.00	0.01	0.01	0.03	0.08	0.28	3.76	57.18	3.58	0.20	0.05	0.01	0.00
14	0.00	0.00	0.00	0.00	0.00	0.00	0.00	0.00	0.01	0.02	0.07	0.28	3.47	56.01	3.29	0.17	0.03	0.01
15	0.00	0.00	0.00	0.00	0.00	0.00	0.00	0.00	0.00	0.01	0.02	0.06	0.25	3.26	54.77	3.09	0.12	0.02
16	0.00	0.00	0.00	0.00	0.00	0.00	0.00	0.00	0.00	0.00	0.01	0.01	0.05	0.19	2.95	52.16	2.87	0.05
17	0.00	0.00	0.00	0.00	0.00	0.00	0.00	0.00	0.00	0.00	0.00	0.00	0.01	0.03	0.14	2.42	48.84	2.01
18	0.00	0.00	0.00	0.00	0.00	0.00	0.00	0.00	0.00	0.00	0.00	0.00	0.00	0.00	0.02	0.07	1.70	37.02

Table 11. The weighted efficiency matrix (in %) for $D^+ \rightarrow \bar{K}^0 e^+ \nu_e$. The i denote the reconstructed bin, and the j represent the produced bin.

ε_{ij}	1	2	3	4	5	6	7	8	9	10	11	12	13	14	15	16	17	18
1	48.53	2.67	0.17	0.07	0.01	0.00	0.00	0.00	0.00	0.00	0.00	0.00	0.00	0.00	0.00	0.00	0.00	0.00
2	1.49	44.41	3.35	0.22	0.07	0.00	0.00	0.00	0.00	0.00	0.00	0.00	0.00	0.00	0.00	0.00	0.00	0.00
3	0.03	1.84	42.69	3.62	0.22	0.06	0.00	0.00	0.00	0.00	0.00	0.00	0.00	0.00	0.00	0.00	0.00	0.00
4	0.00	0.04	2.04	41.28	3.70	0.20	0.04	0.00	0.00	0.00	0.00	0.00	0.00	0.00	0.00	0.00	0.00	0.00
5	0.00	0.01	0.05	2.16	40.20	3.77	0.20	0.03	0.00	0.00	0.00	0.00	0.00	0.00	0.00	0.00	0.00	0.00
6	0.00	0.00	0.01	0.06	2.25	39.14	3.73	0.17	0.01	0.00	0.00	0.00	0.00	0.00	0.00	0.00	0.00	0.00
7	0.00	0.00	0.00	0.01	0.06	2.31	38.65	3.66	0.15	0.01	0.00	0.00	0.00	0.00	0.00	0.00	0.00	0.00
8	0.00	0.00	0.00	0.00	0.01	0.06	2.39	37.92	3.54	0.14	0.01	0.00	0.00	0.00	0.00	0.00	0.00	0.00
9	0.00	0.00	0.00	0.00	0.00	0.01	0.07	2.42	37.71	3.36	0.11	0.01	0.00	0.00	0.00	0.00	0.00	0.00
10	0.00	0.00	0.00	0.00	0.00	0.00	0.01	0.08	2.34	37.20	3.25	0.10	0.01	0.00	0.00	0.00	0.00	0.00
11	0.00	0.00	0.00	0.00	0.00	0.00	0.00	0.01	0.07	2.32	36.59	3.07	0.08	0.00	0.00	0.00	0.00	0.00
12	0.00	0.00	0.00	0.00	0.00	0.00	0.00	0.00	0.02	0.08	2.32	36.15	2.87	0.06	0.00	0.00	0.00	0.00
13	0.00	0.00	0.00	0.00	0.00	0.00	0.00	0.00	0.01	0.01	0.08	2.21	35.89	2.71	0.04	0.00	0.00	0.00
14	0.00	0.00	0.00	0.00	0.00	0.00	0.00	0.00	0.00	0.01	0.08	2.06	35.51	2.53	0.03	0.00	0.00	0.00
15	0.00	0.00	0.00	0.00	0.00	0.00	0.00	0.00	0.00	0.00	0.01	0.09	2.00	35.05	2.25	0.02	0.00	0.00
16	0.00	0.00	0.00	0.00	0.00	0.00	0.00	0.00	0.00	0.00	0.00	0.01	0.07	1.75	34.66	2.00	0.01	0.00
17	0.00	0.00	0.00	0.00	0.00	0.00	0.00	0.00	0.00	0.00	0.00	0.00	0.00	0.06	1.54	34.31	1.77	0.00
18	0.00	0.00	0.00	0.00	0.00	0.00	0.00	0.00	0.00	0.00	0.00	0.00	0.00	0.01	0.04	1.33	32.87	0.00

Table 12. The weighted efficiency matrix (in %) for $D^+ \rightarrow \bar{K}^0 \mu^+ \nu_\mu$. The i denote the reconstructed bin, and the j represent the produced bin.

ε_{ij}	1	2	3	4	5	6	7	8	9	10	11	12	13	14	15	16	17	18
1	31.24	0.90	0.00	0.00	0.00	0.00	0.00	0.00	0.00	0.00	0.00	0.00	0.00	0.00	0.00	0.00	0.01	0.01
2	1.05	30.73	1.36	0.01	0.00	0.00	0.00	0.00	0.00	0.00	0.00	0.00	0.00	0.00	0.01	0.01	0.01	0.00
3	0.02	1.12	31.34	1.67	0.01	0.00	0.00	0.00	0.00	0.00	0.00	0.00	0.00	0.00	0.00	0.00	0.01	0.01
4	0.00	0.02	1.42	32.64	2.01	0.03	0.00	0.00	0.00	0.00	0.00	0.00	0.00	0.00	0.00	0.00	0.00	0.01
5	0.00	0.00	0.02	1.62	33.99	2.16	0.02	0.00	0.00	0.00	0.00	0.00	0.00	0.00	0.00	0.00	0.00	0.00
6	0.00	0.00	0.00	0.03	1.86	35.12	2.31	0.02	0.00	0.00	0.00	0.00	0.00	0.00	0.00	0.01	0.02	0.01
7	0.00	0.00	0.00	0.00	0.04	2.01	36.06	2.44	0.04	0.00	0.00	0.01	0.00	0.00	0.01	0.01	0.03	0.02
8	0.00	0.00	0.00	0.00	0.01	0.04	2.19	36.89	2.50	0.03	0.01	0.00	0.00	0.01	0.01	0.01	0.01	0.01
9	0.00	0.00	0.00	0.00	0.01	0.01	0.05	2.28	37.36	2.52	0.04	0.01	0.00	0.00	0.00	0.01	0.01	0.00
10	0.00	0.00	0.00	0.00	0.00	0.00	0.01	0.07	2.24	37.14	2.44	0.02	0.01	0.01	0.01	0.01	0.00	0.00
11	0.00	0.00	0.00	0.00	0.00	0.01	0.01	0.02	0.06	2.26	37.01	2.34	0.03	0.01	0.00	0.01	0.01	0.00
12	0.00	0.00	0.00	0.00	0.00	0.00	0.00	0.01	0.02	0.07	2.21	36.36	2.11	0.03	0.01	0.01	0.00	0.00
13	0.00	0.00	0.00	0.00	0.01	0.01	0.00	0.01	0.00	0.01	0.07	2.12	36.27	2.08	0.02	0.01	0.00	0.00
14	0.00	0.00	0.00	0.00	0.01	0.00	0.00	0.01	0.01	0.01	0.01	0.08	2.04	36.00	1.91	0.01	0.00	0.00
15	0.00	0.01	0.00	0.00	0.00	0.00	0.01	0.01	0.01	0.01	0.02	0.02	0.06	1.93	35.32	1.78	0.01	0.00
16	0.00	0.00	0.00	0.00	0.01	0.00	0.01	0.01	0.00	0.01	0.01	0.01	0.01	0.05	1.69	34.99	1.61	0.00
17	0.00	0.01	0.00	0.00	0.01	0.01	0.01	0.01	0.01	0.00	0.00	0.00	0.00	0.01	0.05	1.56	34.29	1.28
18	0.01	0.01	0.01	0.01	0.01	0.01	0.00	0.00	0.00	0.00	0.00	0.00	0.00	0.00	0.01	0.03	1.13	32.84

Table 13. The observed yields (N_{DT}^i), the produced yields (N_{prd}^i) and the determined partial decay rates ($\Delta\Gamma$) of $D^0 \rightarrow K^- \mu^+ \nu_\mu$ in different q^2 intervals of data, where the uncertainties are statistical only.

q^2 (GeV $^2/c^4$)	N_{DT}^i	N_{prd}^i	$\Delta\Gamma$ (ns $^{-1}$)
(0.01, 0.10)	8165 ± 104	20612 ± 274	6.341 ± 0.084
(0.10, 0.20)	11686 ± 124	28015 ± 321	8.618 ± 0.099
(0.20, 0.30)	11845 ± 126	26431 ± 311	8.131 ± 0.096
(0.30, 0.40)	12107 ± 130	25037 ± 304	7.702 ± 0.093
(0.40, 0.50)	12238 ± 139	23450 ± 304	7.214 ± 0.094
(0.50, 0.60)	12231 ± 142	21968 ± 294	6.758 ± 0.090
(0.60, 0.70)	11779 ± 135	19861 ± 265	6.110 ± 0.081
(0.70, 0.80)	11329 ± 127	18313 ± 239	5.633 ± 0.073
(0.80, 0.90)	10646 ± 124	16544 ± 224	5.089 ± 0.069
(0.90, 1.00)	9895 ± 122	15090 ± 216	4.642 ± 0.066
(1.00, 1.10)	8619 ± 115	12877 ± 200	3.961 ± 0.061
(1.10, 1.20)	7495 ± 110	11213 ± 191	3.449 ± 0.059
(1.20, 1.30)	6177 ± 106	9438 ± 188	2.903 ± 0.058
(1.30, 1.40)	5077 ± 103	8035 ± 185	2.472 ± 0.057
(1.40, 1.50)	3692 ± 101	5962 ± 186	1.834 ± 0.057
(1.50, 1.60)	2420 ± 67	4107 ± 129	1.263 ± 0.040
(1.60, 1.70)	1475 ± 55	2719 ± 113	0.837 ± 0.035
(1.70, 1.88)	706 ± 46	1771 ± 124	0.545 ± 0.038

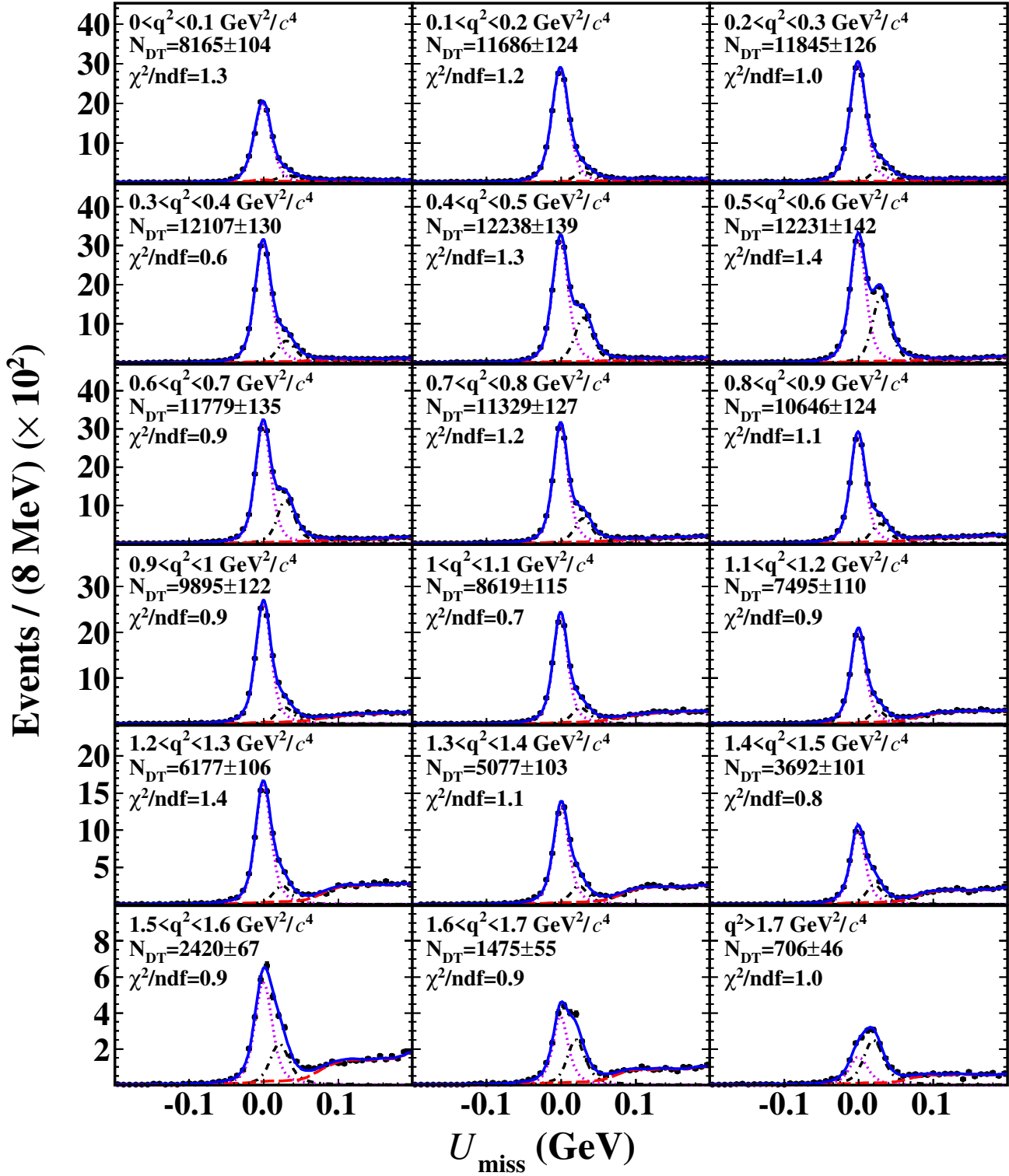


Fig. 7. Fits to the U_{miss} distributions of the accepted $D^0 \rightarrow K^- \mu^+ \nu_\mu$ candidates in different q^2 bins. The points with error bars are data. The blue solid curves are the fit results. The violet dotted curves are the signal shapes. The black dash-dotted curves are the peaking backgrounds. The red dashed curves are the fitted combinatorial background shapes.

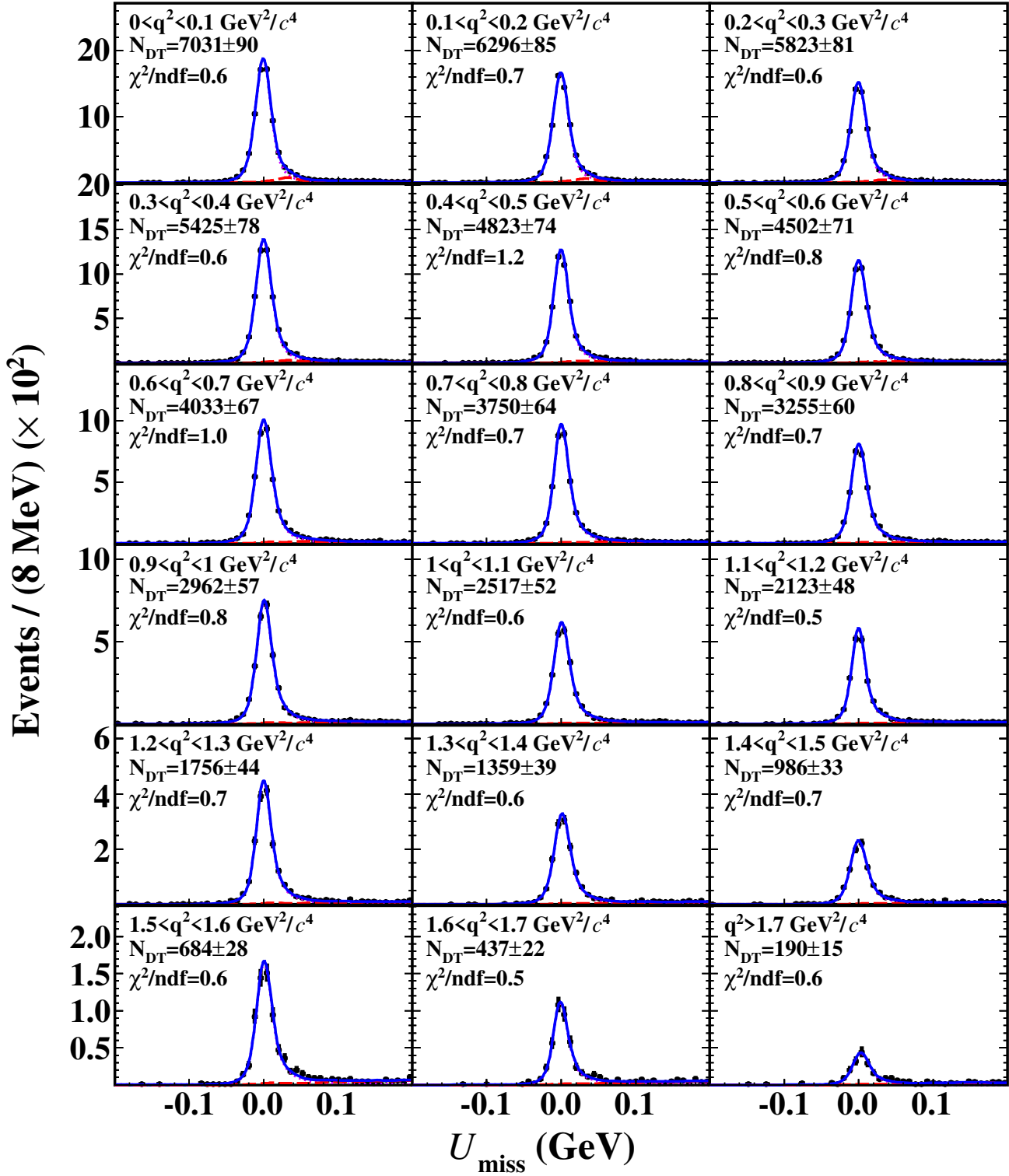


Fig. 8. Fits to the U_{miss} distributions of the accepted $D^+ \rightarrow \bar{K}^0 e^+ \nu_e$ candidates in different q^2 bins. The points with error bars are data. The blue solid curves are the fit results. The violet dotted curves are the signal shapes. The red dashed curves are the fitted combinatorial background shapes.

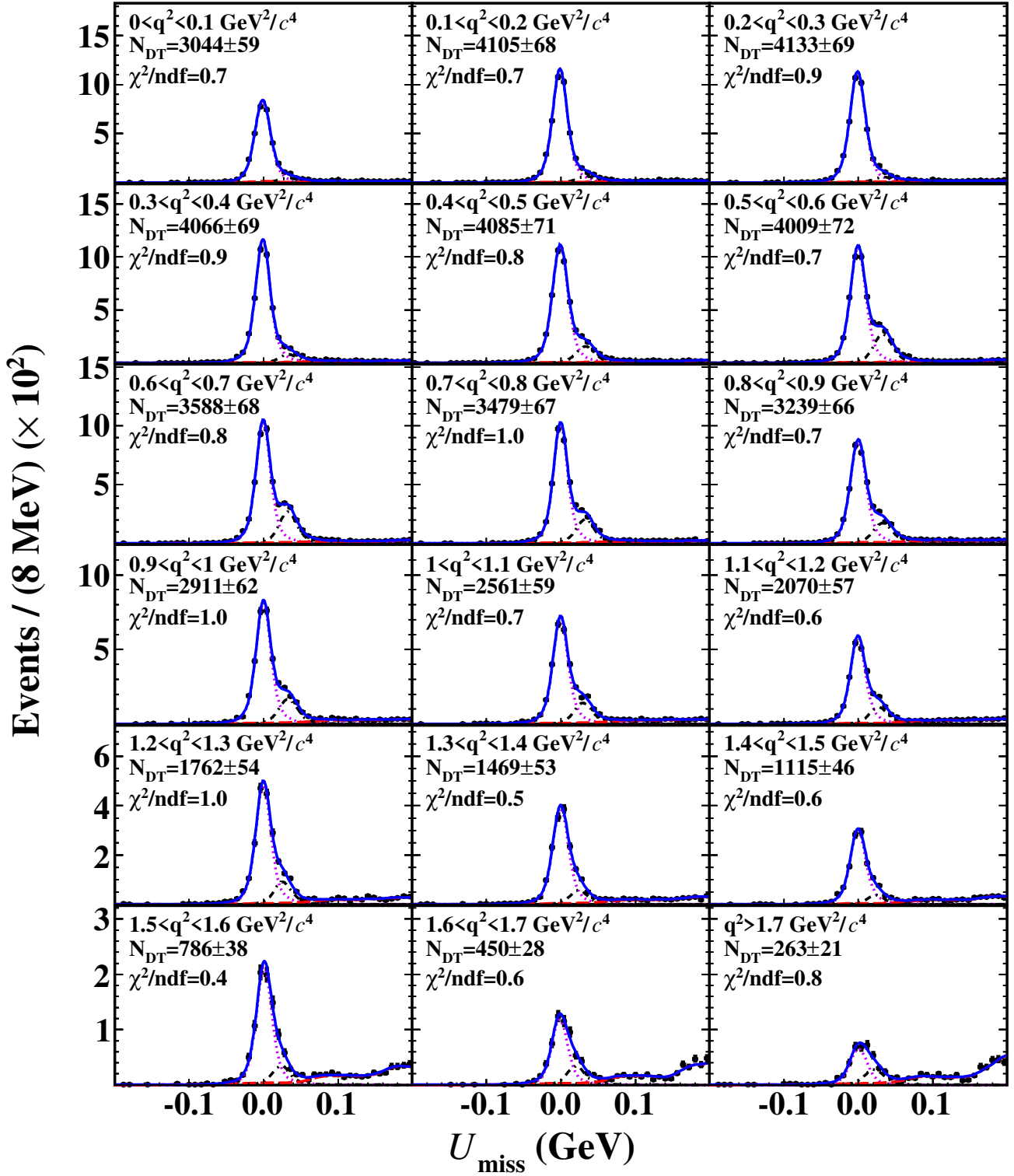


Fig. 9. Fits to the U_{miss} distributions of the accepted $D^+ \rightarrow \bar{K}^0 \mu^+ \nu_\mu$ candidates in different q^2 bins. The points with error bars are data. The blue solid curves are the fit results. The violet dotted curves are the signal shapes. The black dash-dotted curves are the peaking backgrounds. The red dashed curves are the fitted combinatorial background shapes. The bumps in the high q^2 region are mainly from the contributions of $D^+ \rightarrow K_S^0 \pi^+ \pi^0 \pi^0$ and $D^+ \rightarrow K_L^0 K_S^0 \pi^+$.

Table 14. The observed yields (N_{DT}^i), the produced yields (N_{prd}^i) and the determined partial decay rates ($\Delta\Gamma$) of $D^+ \rightarrow \bar{K}^0 e^+ \nu_e$ in different q^2 intervals of data, where the uncertainties are statistical only.

q^2 (GeV ² /c ⁴)	N_{DT}^i	N_{prd}^i	$\Delta\Gamma$ (ns ⁻¹)
(0.00, 0.10)	7031 ± 90	39669 ± 536	9.286 ± 0.126
(0.10, 0.20)	6296 ± 85	36805 ± 559	8.616 ± 0.131
(0.20, 0.30)	5823 ± 81	34781 ± 556	8.142 ± 0.130
(0.30, 0.40)	5425 ± 78	33376 ± 557	7.813 ± 0.130
(0.40, 0.50)	4823 ± 74	29974 ± 539	7.017 ± 0.126
(0.50, 0.60)	4502 ± 71	28876 ± 531	6.760 ± 0.124
(0.60, 0.70)	4033 ± 67	25941 ± 511	6.072 ± 0.120
(0.70, 0.80)	3750 ± 64	24813 ± 500	5.808 ± 0.117
(0.80, 0.90)	3255 ± 60	21458 ± 467	5.023 ± 0.109
(0.90, 1.00)	2962 ± 57	20048 ± 451	4.693 ± 0.105
(1.00, 1.10)	2517 ± 52	17291 ± 421	4.048 ± 0.098
(1.10, 1.20)	2123 ± 48	14805 ± 390	3.466 ± 0.091
(1.20, 1.30)	1756 ± 44	12433 ± 360	2.910 ± 0.084
(1.30, 1.40)	1359 ± 39	9787 ± 318	2.291 ± 0.074
(1.40, 1.50)	986 ± 33	7204 ± 276	1.686 ± 0.065
(1.50, 1.60)	684 ± 28	5118 ± 232	1.198 ± 0.054
(1.60, 1.70)	437 ± 22	3359 ± 187	0.786 ± 0.044
(1.70, 1.88)	190 ± 15	1523 ± 132	0.357 ± 0.031

Table 15. The observed yields (N_{DT}^i), the produced yields (N_{prd}^i) and the determined partial decay rates ($\Delta\Gamma$) of $D^+ \rightarrow \bar{K}^0 \mu^+ \nu_\mu$ in different q^2 intervals of data, where the uncertainties are statistical only.

q^2 (GeV ² /c ⁴)	N_{DT}^i	N_{prd}^i	$\Delta\Gamma$ (ns ⁻¹)
(0.01, 0.10)	3044 ± 59	27122 ± 547	6.349 ± 0.128
(0.10, 0.20)	4105 ± 68	36110 ± 642	8.453 ± 0.150
(0.20, 0.30)	4133 ± 69	35061 ± 640	8.208 ± 0.150
(0.30, 0.40)	4066 ± 69	32504 ± 612	7.609 ± 0.143
(0.40, 0.50)	4085 ± 71	31264 ± 608	7.319 ± 0.142
(0.50, 0.60)	4009 ± 72	29618 ± 603	6.933 ± 0.141
(0.60, 0.70)	3588 ± 68	25397 ± 550	5.945 ± 0.129
(0.70, 0.80)	3479 ± 67	24177 ± 530	5.660 ± 0.124
(0.80, 0.90)	3239 ± 66	22154 ± 520	5.186 ± 0.122
(0.90, 1.00)	2911 ± 62	20078 ± 486	4.700 ± 0.114
(1.00, 1.10)	2561 ± 59	17775 ± 469	4.161 ± 0.110
(1.10, 1.20)	2070 ± 57	14579 ± 462	3.413 ± 0.108
(1.20, 1.30)	1762 ± 54	12513 ± 433	2.929 ± 0.101
(1.30, 1.40)	1469 ± 53	10586 ± 428	2.478 ± 0.100
(1.40, 1.50)	1115 ± 46	8172 ± 383	1.913 ± 0.090
(1.50, 1.60)	786 ± 38	5881 ± 318	1.377 ± 0.075
(1.60, 1.70)	450 ± 28	3380 ± 233	0.791 ± 0.055
(1.70, 1.88)	263 ± 21	2136 ± 189	0.500 ± 0.044

Table 16. Statistical covariance density matrix for $D^0 \rightarrow K^- e^+ \nu_e$. The i denote the reconstructed bin, and the j represent the produced bin.

ρ_{ii}^{stat}	1	2	3	4	5	6	7	8	9	10	11	12	13	14	15	16	17	18
1	1.000	-0.099	0.004	-0.002	0.000	0.000	0.000	0.000	0.000	0.000	0.000	0.000	0.000	0.000	0.000	0.000	0.000	0.000
2	-0.099	1.000	-0.132	0.007	-0.002	0.000	0.000	0.000	0.000	0.000	0.000	0.000	0.000	0.000	0.000	0.000	0.000	0.000
3	0.004	-0.132	1.000	-0.148	0.009	-0.003	0.000	0.000	0.000	0.000	0.000	0.000	0.000	0.000	0.000	0.000	0.000	0.000
4	-0.002	0.007	-0.148	1.000	-0.158	0.010	-0.002	0.000	0.000	0.000	0.000	0.000	0.000	0.000	0.000	0.000	0.000	0.000
5	0.000	-0.002	0.009	-0.158	1.000	-0.162	0.011	-0.002	0.000	0.000	0.000	0.000	0.000	0.000	0.000	0.000	0.000	0.000
6	0.000	0.000	-0.003	0.010	-0.162	1.000	-0.165	0.011	-0.003	-0.001	0.000	0.000	0.000	0.000	0.000	0.000	0.000	0.000
7	0.000	0.000	0.000	-0.002	0.011	-0.165	1.000	-0.167	0.011	-0.003	0.000	0.000	0.000	0.000	0.000	0.000	0.000	0.000
8	0.000	0.000	0.000	0.000	-0.002	0.011	-0.167	1.000	-0.166	0.011	-0.003	-0.001	0.000	0.000	0.000	0.000	0.000	0.000
9	0.000	0.000	0.000	0.000	0.000	-0.003	0.011	-0.166	1.000	-0.164	0.010	-0.002	-0.001	0.000	0.000	0.000	0.000	0.000
10	0.000	0.000	0.000	0.000	0.000	-0.001	-0.003	0.011	-0.164	1.000	-0.160	0.009	-0.002	0.000	0.000	0.000	0.000	0.000
11	0.000	0.000	0.000	0.000	0.000	0.000	0.000	-0.003	0.010	-0.160	1.000	-0.155	0.008	-0.002	-0.001	0.000	0.000	0.000
12	0.000	0.000	0.000	0.000	0.000	0.000	0.000	-0.001	-0.002	0.009	-0.155	1.000	-0.152	0.007	-0.002	-0.001	0.000	0.000
13	0.000	0.000	0.000	0.000	0.000	0.000	0.000	0.000	-0.001	-0.002	0.008	-0.152	1.000	-0.145	0.007	-0.002	0.000	0.000
14	0.000	0.000	0.000	0.000	0.000	0.000	0.000	0.000	0.000	0.000	-0.002	0.007	-0.145	1.000	-0.140	0.006	-0.001	0.000
15	0.000	0.000	0.000	0.000	0.000	0.000	0.000	0.000	0.000	0.000	-0.001	-0.002	0.007	-0.140	1.000	-0.131	0.006	0.000
16	0.000	0.000	0.000	0.000	0.000	0.000	0.000	0.000	0.000	0.000	0.000	-0.001	-0.002	0.006	-0.131	1.000	-0.123	0.005
17	0.000	0.000	0.000	0.000	0.000	0.000	0.000	0.000	0.000	0.000	0.000	0.000	0.000	-0.001	0.006	-0.123	1.000	-0.105
18	0.000	0.000	0.000	0.000	0.000	0.000	0.000	0.000	0.000	0.000	0.000	0.000	0.000	0.000	0.000	0.005	-0.105	1.000

Table 17. Statistical covariance density matrix for $D^0 \rightarrow K^- \mu^+ \nu_\mu$. The i denote the reconstructed bin, and the j represent the produced bin.

ρ_{ii}^{stat}	1	2	3	4	5	6	7	8	9	10	11	12	13	14	15	16	17	18
1	1.000	-0.068	0.003	0.000	0.000	0.000	0.000	0.000	0.000	0.000	0.000	0.000	0.000	0.000	0.000	0.000	0.000	0.000
2	-0.068	1.000	-0.088	0.005	-0.001	0.000	0.000	0.000	0.000	0.000	0.000	0.000	0.000	0.000	0.000	0.000	0.000	0.000
3	0.003	-0.088	1.000	-0.105	0.007	-0.001	0.000	0.000	0.000	0.000	0.000	0.000	0.000	0.000	0.000	0.000	0.000	0.000
4	0.000	0.005	-0.105	1.000	-0.118	0.008	-0.001	0.000	0.000	0.000	0.000	0.000	0.000	0.000	0.000	0.000	0.000	0.000
5	0.000	-0.001	0.007	-0.118	1.000	-0.128	0.008	-0.002	0.000	0.000	0.000	0.000	0.000	0.000	0.000	0.000	0.000	0.000
6	0.000	0.000	-0.001	0.008	-0.128	1.000	-0.134	0.008	-0.002	-0.001	0.000	0.000	0.000	0.000	0.000	0.000	0.000	0.000
7	0.000	0.000	0.000	-0.001	0.008	-0.134	1.000	-0.138	0.008	-0.002	-0.001	0.000	0.000	0.000	0.000	0.000	0.000	0.000
8	0.000	0.000	0.000	0.000	-0.002	0.008	-0.138	1.000	-0.138	0.007	-0.002	0.000	0.000	0.000	0.000	0.000	0.000	0.000
9	0.000	0.000	0.000	0.000	0.000	-0.002	0.008	-0.138	1.000	-0.136	0.006	-0.002	-0.001	0.000	0.000	0.000	0.000	0.000
10	0.000	0.000	0.000	0.000	0.000	-0.001	-0.002	0.007	-0.136	1.000	-0.136	0.005	-0.002	0.000	0.000	0.000	0.000	0.000
11	0.000	0.000	0.000	0.000	0.000	0.000	-0.001	-0.002	0.006	-0.136	1.000	-0.131	0.004	-0.002	0.000	0.000	0.000	0.000
12	0.000	0.000	0.000	0.000	0.000	0.000	0.000	0.000	-0.002	0.005	-0.131	1.000	-0.128	0.003	-0.002	0.000	0.000	0.000
13	0.000	0.000	0.000	0.000	0.000	0.000	0.000	0.000	-0.001	-0.002	0.004	-0.128	1.000	-0.123	0.003	-0.001	0.000	0.000
14	0.000	0.000	0.000	0.000	0.000	0.000	0.000	0.000	0.000	0.000	-0.002	0.003	-0.123	1.000	-0.117	0.005	-0.001	0.000
15	0.000	0.000	0.000	0.000	0.000	0.000	0.000	0.000	0.000	0.000	0.000	-0.002	0.003	-0.117	1.000	-0.119	0.003	-0.001
16	0.000	0.000	0.000	0.000	0.000	0.000	0.000	0.000	0.000	0.000	0.000	0.000	-0.001	0.005	-0.119	1.000	-0.104	0.004
17	0.000	0.000	0.000	0.000	0.000	0.000	0.000	0.000	0.000	0.000	0.000	0.000	0.000	-0.001	0.003	-0.104	1.000	-0.087
18	0.000	0.000	0.000	0.000	0.000	0.000	0.000	0.000	0.000	0.000	0.000	0.000	0.000	0.000	-0.001	0.004	-0.087	1.000

Table 18. Statistical covariance density matrix for $D^+ \rightarrow \bar{K}^0 e^+ \nu_e$. The i denote the reconstructed bin, and the j represent the produced bin.

ρ_{ii}^{stat}	1	2	3	4	5	6	7	8	9	10	11	12	13	14	15	16	17	18
1	1.000	-0.089	0.004	-0.001	0.000	0.000	0.000	0.000	0.000	0.000	0.000	0.000	0.000	0.000	0.000	0.000	0.000	0.000
2	-0.089	1.000	-0.117	0.006	-0.002	0.000	0.000	0.000	0.000	0.000	0.000	0.000	0.000	0.000	0.000	0.000	0.000	0.000
3	0.004	-0.117	1.000	-0.133	0.009	-0.002	0.000	0.000	0.000	0.000	0.000	0.000	0.000	0.000	0.000	0.000	0.000	0.000
4	-0.001	0.006	-0.133	1.000	-0.141	0.010	-0.001	0.000	0.000	0.000	0.000	0.000	0.000	0.000	0.000	0.000	0.000	0.000
5	0.000	-0.002	0.009	-0.141	1.000	-0.149	0.012	-0.001	0.000	0.000	0.000	0.000	0.000	0.000	0.000	0.000	0.000	0.000
6	0.000	0.000	-0.002	0.010	-0.149	1.000	-0.152	0.013	-0.001	0.000	0.000	0.000	0.000	0.000	0.000	0.000	0.000	0.000
7	0.000	0.000	0.000	-0.001	0.012	-0.152	1.000	-0.156	0.013	-0.001	0.000	0.000	0.000	0.000	0.000	0.000	0.000	0.000
8	0.000	0.000	0.000	0.000	-0.001	0.013	-0.156	1.000	-0.155	0.012	-0.001	0.000	0.000	0.000	0.000	0.000	0.000	0.000
9	0.000	0.000	0.000	0.000	0.000	-0.001	0.013	-0.155	1.000	-0.150	0.013	-0.001	0.000	0.000	0.000	0.000	0.000	0.000
10	0.000	0.000	0.000	0.000	0.000	0.000	-0.001	0.012	-0.150	1.000	-0.148	0.012	-0.001	0.000	0.000	0.000	0.000	0.000
11	0.000	0.000	0.000	0.000	0.000	0.000	0.000	-0.001	0.013	-0.148	1.000	-0.146	0.011	-0.001	0.000	0.000	0.000	0.000
12	0.000	0.000	0.000	0.000	0.000	0.000	0.000	0.000	-0.001	0.012	-0.146	1.000	-0.139	0.010	-0.001	0.000	0.000	0.000
13	0.000	0.000	0.000	0.000	0.000	0.000	0.000	0.000	0.000	-0.001	0.011	-0.139	1.000	-0.132	0.009	-0.001	0.000	0.000
14	0.000	0.000	0.000	0.000	0.000	0.000	0.000	0.000	0.000	0.000	-0.001	0.010	-0.132	1.000	-0.127	0.008	0.000	0.000
15	0.000	0.000	0.000	0.000	0.000	0.000	0.000	0.000	0.000	0.000	0.000	-0.001	0.009	-0.127	1.000	-0.113	0.006	-0.001
16	0.000	0.000	0.000	0.000	0.000	0.000	0.000	0.000	0.000	0.000	0.000	0.000	-0.001	0.008	-0.113	1.000	-0.102	0.005
17	0.000	0.000	0.000	0.000	0.000	0.000	0.000	0.000	0.000	0.000	0.000	0.000	0.000	0.000	0.006	-0.102	1.000	-0.093
18	0.000	0.000	0.000	0.000	0.000	0.000	0.000	0.000	0.000	0.000	0.000	0.000	0.000	0.000	-0.001	0.005	-0.093	1.000

Table 19. Statistical covariance density matrix for $D^+ \rightarrow \bar{K}^0 \mu^+ \nu_\mu$. The i denote the reconstructed bin, and the j represent the produced bin.

ρ_{ii}^{stat}	1	2	3	4	5	6	7	8	9	10	11	12	13	14	15	16	17	18
1	1.000	-0.063	0.003	0.000	0.000	0.000	0.000	0.000	0.000	0.000	0.000	0.000	0.000	0.000	0.000	0.000	0.000	-0.001
2	-0.063	1.000	-0.080	0.005	0.000	0.000	0.000	0.000	0.000	0.000	0.000	0.000	0.000	0.000	-0.001	0.000	-0.001	-0.001
3	0.003	-0.080	1.000	-0.096	0.007	0.000	0.000	0.000	0.000	0.000	0.000	0.000	0.000	0.000	0.000	0.000	0.000	-0.001
4	0.000	0.005	-0.096	1.000	-0.109	0.008	0.000	0.000	0.000	0.000	0.000	0.000	0.000	0.000	0.000	0.000	0.000	-0.001
5	0.000	0.000	0.007	-0.109	1.000	-0.116	0.009	-0.001	0.000	0.000	0.000	0.000	0.000	0.000	0.000	-0.001	-0.001	-0.001
6	0.000	0.000	0.000	0.008	-0.116	1.000	-0.121	0.010	-0.001	0.000	0.000	0.000	0.000	0.000	0.000	0.000	-0.001	-0.001
7	0.000	0.000	0.000	0.000	0.009	-0.121	1.000	-0.126	0.010	-0.001	0.000	0.000	0.000	0.000	-0.001	0.000	-0.001	0.000
8	0.000	0.000	0.000	0.000	-0.001	0.010	-0.126	1.000	-0.128	0.010	-0.001	0.000	0.000	0.000	0.000	-0.001	-0.001	0.000
9	0.000	0.000	0.000	0.000	0.000	-0.001	0.010	-0.128	1.000	-0.127	0.009	-0.001	0.000	0.000	0.000	0.000	-0.001	0.000
10	0.000	0.000	0.000	0.000	0.000	0.000	-0.001	0.010	-0.127	1.000	-0.126	0.009	-0.001	0.000	0.000	-0.001	0.000	0.000
11	0.000	0.000	0.000	0.000	0.000	0.000	0.000	-0.001	0.009	-0.126	1.000	-0.123	0.008	-0.001	0.000	0.000	0.000	0.000
12	0.000	0.000	0.000	0.000	0.000	0.000	0.000	0.000	-0.001	0.009	-0.123	1.000	-0.116	0.007	-0.001	0.000	0.000	0.000
13	0.000	0.000	0.000	0.000	0.000	0.000	0.000	0.000	0.000	-0.001	0.008	-0.116	1.000	-0.114	0.007	-0.001	0.000	0.000
14	0.000	0.000	0.000	0.000	0.000	0.000	0.000	0.000	0.000	0.000	-0.001	0.007	-0.114	1.000	-0.108	0.006	-0.001	0.000
15	0.000	-0.001	0.000	0.000	0.000	0.000	-0.001	0.000	0.000	0.000	0.000	-0.001	0.007	-0.108	1.000	-0.100	0.005	-0.001
16	0.000	0.000	0.000	0.000	-0.001	0.000	0.000	-0.001	0.000	-0.001	0.000	0.000	-0.001	0.006	-0.100	1.000	-0.095	0.004
17	0.000	-0.001	0.000	0.000	-0.001	-0.001	-0.001	-0.001	-0.001	0.000	0.000	0.000	0.000	-0.001	0.005	-0.095	1.000	-0.073
18	-0.001	-0.001	-0.001	-0.001	-0.001	-0.001	0.000	0.000	0.000	0.000	0.000	0.000	0.000	0.000	-0.001	0.004	-0.073	1.000

Table 20. The systematic uncertainties (in %) of the measured decay rates of $D^0 \rightarrow K^- \mu^+ \nu_\mu$ in different q^2 bins.

i -th q^2 bin	1	2	3	4	5	6	7	8	9	10	11	12	13	14	15	16	17	18
N_{ST}	0.30	0.30	0.30	0.30	0.30	0.30	0.30	0.30	0.30	0.30	0.30	0.30	0.30	0.30	0.30	0.30	0.30	0.30
D^0 lifetime	0.24	0.24	0.24	0.24	0.24	0.24	0.24	0.24	0.24	0.24	0.24	0.24	0.24	0.24	0.24	0.24	0.24	0.24
MC statistics	0.25	0.21	0.20	0.20	0.20	0.20	0.20	0.20	0.21	0.21	0.23	0.24	0.27	0.31	0.36	0.44	0.58	0.93
MC model	0.18	0.21	0.71	0.44	0.20	0.23	0.28	0.06	0.19	0.20	0.16	0.74	1.03	0.87	0.21	0.74	1.02	1.06
K^- tracking	0.10	0.10	0.10	0.10	0.10	0.10	0.10	0.10	0.10	0.10	0.10	0.11	0.11	0.13	0.14	0.18	0.23	0.43
K^- PID	0.10	0.10	0.10	0.10	0.10	0.10	0.10	0.10	0.10	0.10	0.10	0.10	0.10	0.10	0.10	0.10	0.10	0.18
μ^+ tracking	0.10	0.10	0.10	0.10	0.10	0.10	0.10	0.10	0.10	0.10	0.10	0.10	0.10	0.10	0.10	0.10	0.10	0.10
μ^+ PID	0.20	0.20	0.19	0.18	0.18	0.17	0.17	0.17	0.16	0.17	0.17	0.18	0.18	0.19	0.19	0.20	0.22	0.23
U_{miss} fit	0.24	0.11	0.11	0.11	0.10	0.14	0.12	0.13	0.15	0.15	0.11	0.15	0.11	0.18	0.17	0.21	0.18	0.26
$E_{\text{extra}}^{\text{max}} \gamma$ and $N_{\text{extra}}^{\text{trk}}$ cut	0.10	0.10	0.10	0.10	0.10	0.10	0.10	0.10	0.10	0.10	0.10	0.10	0.10	0.10	0.10	0.10	0.10	0.10
Total	0.62	0.57	0.88	0.68	0.55	0.57	0.59	0.53	0.56	0.57	0.56	0.92	1.17	1.06	0.66	1.02	1.30	1.58

Table 21. The systematic uncertainties (in %) of the measured decay rates of $D^+ \rightarrow \bar{K}^0 e^+ \nu_e$ in different q^2 bins.

i -th q^2 bin	1	2	3	4	5	6	7	8	9	10	11	12	13	14	15	16	17	18
N_{tag}	0.30	0.30	0.30	0.30	0.30	0.30	0.30	0.30	0.30	0.30	0.30	0.30	0.30	0.30	0.30	0.30	0.30	0.30
D^+ lifetime	0.48	0.48	0.48	0.48	0.48	0.48	0.48	0.48	0.48	0.48	0.48	0.48	0.48	0.48	0.48	0.48	0.48	0.48
MC statistics	0.19	0.19	0.20	0.21	0.22	0.23	0.25	0.26	0.27	0.29	0.32	0.34	0.38	0.43	0.49	0.59	0.77	1.09
MC model	0.32	0.66	0.70	0.22	0.91	0.60	1.11	0.27	1.14	0.38	0.90	0.01	0.99	0.02	0.39	2.18	0.17	0.46
e^+ tracking	0.10	0.10	0.10	0.10	0.10	0.10	0.10	0.10	0.10	0.10	0.10	0.10	0.10	0.10	0.10	0.10	0.10	0.10
e^+ PID	0.10	0.10	0.10	0.10	0.10	0.10	0.10	0.10	0.10	0.10	0.10	0.10	0.10	0.10	0.10	0.10	0.10	0.10
U_{miss} fit	0.53	1.34	0.26	0.55	1.65	1.29	0.04	0.58	0.20	0.05	0.22	0.17	0.84	0.05	0.04	0.05	0.32	0.06
$E_{\text{extra}}^{\text{max}} \gamma$ and $N_{\text{extra}}^{\text{trk}}$ cut	0.10	0.10	0.10	0.10	0.10	0.10	0.10	0.10	0.10	0.10	0.10	0.10	0.10	0.10	0.10	0.10	0.10	0.10
K_S^0 reconstruction	0.75	0.72	0.68	0.65	0.60	0.60	0.70	0.82	0.95	1.11	1.31	1.44	1.48	1.55	1.62	1.72	1.75	1.93
Quoted branching fractions	0.07	0.07	0.07	0.07	0.07	0.07	0.07	0.07	0.07	0.07	0.07	0.07	0.07	0.07	0.07	0.07	0.07	0.07
Total	1.16	1.77	1.19	1.08	2.08	1.67	1.46	1.23	1.64	1.35	1.74	1.60	2.09	1.71	1.84	2.90	2.03	2.34

Table 22. The systematic uncertainties (in %) of the measured decay rates of $D^+ \rightarrow \bar{K}^0 \mu^+ \nu_\mu$ in different q^2 bins.

i -th q^2 bin	1	2	3	4	5	6	7	8	9	10	11	12	13	14	15	16	17	18
N_{tag}	0.30	0.30	0.30	0.30	0.30	0.30	0.30	0.30	0.30	0.30	0.30	0.30	0.30	0.30	0.30	0.30	0.30	0.30
D^+ lifetime	0.48	0.48	0.48	0.48	0.48	0.48	0.48	0.48	0.48	0.48	0.48	0.48	0.48	0.48	0.48	0.48	0.48	0.48
MC statistics	0.29	0.25	0.25	0.25	0.25	0.25	0.26	0.26	0.28	0.29	0.31	0.34	0.38	0.42	0.48	0.58	0.74	1.02
MC model	0.71	0.18	0.32	0.79	0.28	0.18	0.61	0.26	0.76	0.33	1.53	0.77	0.78	1.41	0.74	0.23	1.47	1.75
μ^+ tracking	0.10	0.10	0.10	0.10	0.10	0.10	0.10	0.10	0.10	0.10	0.10	0.10	0.10	0.10	0.10	0.10	0.10	0.10
μ^+ PID	0.17	0.17	0.17	0.17	0.16	0.16	0.16	0.16	0.16	0.16	0.17	0.17	0.18	0.19	0.18	0.19	0.22	0.25
U_{miss} fit	0.03	0.10	0.03	0.23	0.25	0.05	0.19	0.17	0.07	0.07	0.06	0.06	0.07	0.05	0.06	0.13	0.10	0.18
$E_{\text{extra}}^{\text{max}} \gamma$ and $N_{\text{extra}}^{\text{trk}}$ cut	0.10	0.10	0.10	0.10	0.10	0.10	0.10	0.10	0.10	0.10	0.10	0.10	0.10	0.10	0.10	0.10	0.10	0.10
K_S^0 reconstruction	1.05	0.71	0.68	0.65	0.60	0.60	0.70	0.82	0.95	1.11	1.30	1.44	1.48	1.55	1.62	1.72	1.77	1.96
Quoted branching fractions	0.07	0.07	0.07	0.07	0.07	0.07	0.07	0.07	0.07	0.07	0.07	0.07	0.07	0.07	0.07	0.07	0.07	0.07
Total	1.44	0.99	1.00	1.24	0.97	0.91	1.16	1.10	1.39	1.34	2.12	1.78	1.82	2.22	1.95	1.93	2.50	2.90

Table 23. Systematic covariance density matrix for $D^0 \rightarrow K^- e^+ \nu_e$, where i denotes the reconstructed bin, and the j represent the produced bin.

ρ_{ij}^{sys}	1	2	3	4	5	6	7	8	9	10	11	12	13	14	15	16	17	18
1	1.000	0.773	0.747	0.789	0.730	0.762	0.586	0.767	0.580	0.774	0.759	0.680	0.719	0.600	0.683	0.626	0.474	0.491
2	0.773	1.000	0.704	0.782	0.733	0.745	0.556	0.759	0.549	0.763	0.743	0.685	0.700	0.571	0.673	0.618	0.441	0.472
3	0.747	0.704	1.000	0.756	0.578	0.842	0.851	0.740	0.849	0.783	0.832	0.518	0.838	0.845	0.686	0.616	0.784	0.634
4	0.789	0.782	0.756	1.000	0.658	0.788	0.655	0.764	0.650	0.780	0.781	0.643	0.753	0.664	0.687	0.626	0.554	0.529
5	0.730	0.733	0.578	0.658	1.000	0.580	0.351	0.686	0.341	0.670	0.618	0.693	0.555	0.373	0.594	0.552	0.224	0.341
6	0.762	0.745	0.842	0.788	0.580	1.000	0.777	0.751	0.787	0.784	0.817	0.559	0.812	0.789	0.688	0.620	0.712	0.601
7	0.586	0.556	0.851	0.655	0.351	0.777	1.000	0.588	0.969	0.674	0.773	0.291	0.821	0.944	0.586	0.514	0.951	0.670
8	0.767	0.759	0.740	0.764	0.686	0.751	0.588	1.000	0.584	0.754	0.745	0.637	0.713	0.614	0.662	0.605	0.501	0.495
9	0.580	0.549	0.849	0.650	0.341	0.787	0.969	0.584	1.000	0.656	0.771	0.283	0.820	0.946	0.582	0.510	0.955	0.670
10	0.774	0.763	0.783	0.780	0.670	0.784	0.674	0.754	0.656	1.000	0.746	0.620	0.755	0.681	0.678	0.617	0.579	0.537
11	0.759	0.743	0.832	0.781	0.618	0.817	0.773	0.745	0.771	0.746	1.000	0.523	0.803	0.773	0.683	0.617	0.694	0.592
12	0.680	0.685	0.518	0.643	0.693	0.559	0.291	0.637	0.283	0.620	0.523	1.000	0.460	0.317	0.548	0.513	0.170	0.301
13	0.719	0.700	0.838	0.753	0.555	0.812	0.821	0.713	0.820	0.755	0.803	0.460	1.000	0.799	0.664	0.594	0.757	0.613
14	0.600	0.571	0.845	0.664	0.373	0.789	0.944	0.614	0.946	0.681	0.773	0.317	0.799	1.000	0.569	0.525	0.923	0.663
15	0.683	0.673	0.686	0.687	0.594	0.688	0.586	0.662	0.582	0.678	0.683	0.548	0.664	0.569	1.000	0.489	0.503	0.477
16	0.626	0.618	0.616	0.626	0.552	0.620	0.514	0.605	0.510	0.617	0.617	0.513	0.594	0.525	0.489	1.000	0.420	0.437
17	0.474	0.441	0.784	0.554	0.224	0.712	0.951	0.501	0.955	0.579	0.694	0.170	0.757	0.923	0.503	0.420	1.000	0.631
18	0.491	0.472	0.634	0.529	0.341	0.601	0.670	0.495	0.670	0.537	0.592	0.301	0.613	0.663	0.477	0.437	0.631	1.000

Table 24. Systematic covariance density matrix for $D^0 \rightarrow K^- \mu^+ \nu_\mu$, where i denotes the reconstructed bin, and the j represent the produced bin.

ρ_{ij}^{sys}	1	2	3	4	5	6	7	8	9	10	11	12	13	14	15	16	17	18
1	1.000	0.717	0.637	0.702	0.731	0.716	0.717	0.679	0.697	0.695	0.697	0.611	0.555	0.573	0.614	0.561	0.512	0.456
2	0.717	1.000	0.718	0.790	0.804	0.790	0.796	0.735	0.766	0.765	0.763	0.701	0.646	0.662	0.676	0.643	0.593	0.527
3	0.637	0.718	1.000	0.853	0.714	0.729	0.770	0.536	0.673	0.685	0.652	0.894	0.904	0.881	0.606	0.807	0.809	0.703
4	0.702	0.790	0.853	1.000	0.759	0.783	0.808	0.644	0.739	0.745	0.725	0.838	0.820	0.813	0.658	0.761	0.740	0.648
5	0.731	0.804	0.714	0.759	1.000	0.759	0.792	0.737	0.764	0.762	0.762	0.686	0.629	0.646	0.673	0.629	0.578	0.514
6	0.716	0.790	0.729	0.783	0.759	1.000	0.754	0.714	0.749	0.749	0.745	0.702	0.652	0.665	0.661	0.643	0.597	0.530
7	0.717	0.796	0.770	0.808	0.792	0.754	1.000	0.668	0.754	0.753	0.746	0.743	0.701	0.709	0.665	0.678	0.638	0.565
8	0.679	0.735	0.536	0.644	0.737	0.714	0.668	1.000	0.670	0.701	0.713	0.511	0.432	0.464	0.617	0.474	0.406	0.369
9	0.697	0.766	0.673	0.739	0.764	0.749	0.754	0.670	1.000	0.690	0.730	0.647	0.591	0.609	0.642	0.594	0.544	0.486
10	0.695	0.765	0.685	0.745	0.762	0.749	0.753	0.701	0.690	1.000	0.687	0.660	0.605	0.621	0.640	0.604	0.556	0.494
11	0.697	0.763	0.652	0.725	0.762	0.745	0.746	0.713	0.730	0.687	1.000	0.602	0.567	0.586	0.639	0.576	0.522	0.467
12	0.611	0.701	0.894	0.838	0.686	0.702	0.743	0.511	0.647	0.660	0.602	1.000	0.869	0.860	0.583	0.786	0.790	0.687
13	0.555	0.646	0.904	0.820	0.629	0.652	0.701	0.432	0.591	0.605	0.567	0.869	1.000	0.865	0.537	0.794	0.812	0.702
14	0.573	0.662	0.881	0.813	0.646	0.665	0.709	0.464	0.609	0.621	0.586	0.860	0.865	1.000	0.521	0.777	0.786	0.684
15	0.614	0.676	0.606	0.658	0.673	0.661	0.665	0.617	0.642	0.640	0.639	0.583	0.537	0.521	1.000	0.498	0.498	0.447
16	0.561	0.643	0.807	0.761	0.629	0.643	0.678	0.474	0.594	0.604	0.576	0.786	0.794	0.777	0.498	1.000	0.688	0.632
17	0.512	0.593	0.809	0.740	0.578	0.597	0.638	0.406	0.544	0.556	0.522	0.790	0.812	0.786	0.498	0.688	1.000	0.614
18	0.456	0.527	0.703	0.648	0.514	0.530	0.565	0.369	0.486	0.494	0.467	0.687	0.702	0.684	0.447	0.632	0.614	1.000

Table 25. Systematic covariance density matrix for $D^+ \rightarrow \bar{K}^0 e^+ \nu_e$, where i denotes the reconstructed bin, and the j represent the produced bin.

ρ_{ij}^{sys}	1	2	3	4	5	6	7	8	9	10	11	12	13	14	15	16	17	18
1	1.000	0.629	0.686	0.645	0.573	0.593	0.620	0.632	0.647	0.662	0.677	0.613	0.651	0.579	0.586	0.572	0.464	0.399
2	0.629	1.000	0.650	0.573	0.604	0.586	0.666	0.559	0.674	0.591	0.655	0.494	0.630	0.468	0.511	0.617	0.386	0.348
3	0.686	0.650	1.000	0.547	0.647	0.618	0.711	0.580	0.715	0.611	0.686	0.500	0.659	0.474	0.525	0.655	0.393	0.358
4	0.645	0.573	0.547	1.000	0.428	0.523	0.525	0.562	0.547	0.580	0.578	0.544	0.554	0.513	0.510	0.472	0.407	0.346
5	0.573	0.604	0.647	0.428	1.000	0.484	0.659	0.477	0.647	0.504	0.595	0.379	0.571	0.360	0.424	0.601	0.305	0.288
6	0.593	0.586	0.618	0.523	0.484	1.000	0.549	0.507	0.603	0.524	0.581	0.432	0.556	0.408	0.448	0.546	0.336	0.304
7	0.620	0.666	0.711	0.525	0.659	0.549	1.000	0.461	0.728	0.550	0.663	0.408	0.637	0.388	0.466	0.682	0.333	0.318
8	0.632	0.559	0.580	0.562	0.477	0.507	0.461	1.000	0.491	0.585	0.583	0.551	0.562	0.521	0.520	0.481	0.416	0.355
9	0.647	0.674	0.715	0.547	0.647	0.603	0.728	0.491	1.000	0.541	0.694	0.466	0.667	0.445	0.512	0.691	0.376	0.352
10	0.662	0.591	0.611	0.580	0.504	0.524	0.550	0.585	0.541	1.000	0.586	0.599	0.615	0.564	0.567	0.535	0.453	0.390
11	0.677	0.655	0.686	0.578	0.595	0.581	0.663	0.583	0.694	0.586	1.000	0.513	0.683	0.536	0.574	0.651	0.442	0.396
12	0.613	0.494	0.500	0.544	0.379	0.432	0.408	0.551	0.466	0.599	0.513	1.000	0.498	0.599	0.562	0.415	0.469	0.388
13	0.651	0.630	0.659	0.554	0.571	0.556	0.637	0.562	0.667	0.615	0.683	0.498	1.000	0.472	0.563	0.632	0.432	0.387
14	0.579	0.468	0.474	0.513	0.360	0.408	0.388	0.521	0.445	0.564	0.536	0.599	0.472	1.000	0.478	0.402	0.446	0.370
15	0.586	0.511	0.525	0.510	0.424	0.448	0.466	0.520	0.512	0.567	0.574	0.562	0.563	0.478	1.000	0.429	0.434	0.367
16	0.572	0.617	0.655	0.472	0.601	0.546	0.682	0.481	0.691	0.535	0.651	0.415	0.632	0.402	0.429	1.000	0.298	0.331
17	0.464	0.386	0.393	0.407	0.305	0.336	0.333	0.416	0.376	0.453	0.442	0.469	0.432	0.446	0.434	0.298	1.000	0.232
18	0.399	0.348	0.358	0.346	0.288	0.304	0.318	0.355	0.352	0.390	0.396	0.388	0.387	0.370	0.367	0.331	0.232	1.000

Table 26. Systematic covariance density matrix for $D^+ \rightarrow \bar{K}^0 \mu^+ \nu_\mu$, where i denotes the reconstructed bin, and the j represent the produced bin.

ρ_{ij}^{sys}	1	2	3	4	5	6	7	8	9	10	11	12	13	14	15	16	17	18
1	1.000	0.587	0.633	0.674	0.590	0.560	0.656	0.620	0.699	0.653	0.729	0.705	0.691	0.703	0.640	0.539	0.583	0.532
2	0.587	1.000	0.557	0.546	0.561	0.554	0.557	0.585	0.578	0.599	0.539	0.591	0.579	0.538	0.541	0.501	0.448	0.401
3	0.633	0.557	1.000	0.553	0.569	0.550	0.586	0.583	0.608	0.597	0.592	0.608	0.595	0.578	0.552	0.487	0.478	0.431
4	0.674	0.546	0.553	1.000	0.511	0.516	0.638	0.554	0.664	0.568	0.713	0.632	0.617	0.665	0.561	0.435	0.543	0.499
5	0.590	0.561	0.569	0.511	1.000	0.472	0.556	0.551	0.568	0.559	0.546	0.564	0.551	0.532	0.511	0.452	0.439	0.395
6	0.560	0.554	0.550	0.516	0.472	1.000	0.470	0.545	0.535	0.548	0.498	0.539	0.527	0.493	0.491	0.450	0.408	0.365
7	0.656	0.557	0.586	0.638	0.556	0.470	1.000	0.511	0.643	0.577	0.665	0.622	0.608	0.631	0.558	0.456	0.518	0.474
8	0.620	0.585	0.583	0.554	0.551	0.545	0.511	1.000	0.543	0.605	0.566	0.606	0.594	0.562	0.555	0.505	0.468	0.422
9	0.699	0.578	0.608	0.664	0.568	0.535	0.643	0.543	1.000	0.575	0.717	0.674	0.660	0.683	0.609	0.501	0.564	0.517
10	0.653	0.599	0.597	0.568	0.559	0.548	0.577	0.605	0.575	1.000	0.569	0.652	0.637	0.604	0.598	0.546	0.506	0.456
11	0.729	0.539	0.592	0.713	0.546	0.498	0.665	0.566	0.717	0.569	1.000	0.670	0.687	0.750	0.626	0.480	0.617	0.571
12	0.705	0.591	0.608	0.632	0.564	0.539	0.622	0.606	0.674	0.652	0.670	1.000	0.649	0.687	0.638	0.552	0.571	0.522
13	0.691	0.579	0.595	0.617	0.551	0.527	0.608	0.594	0.660	0.637	0.687	0.649	1.000	0.636	0.630	0.543	0.560	0.511
14	0.703	0.538	0.578	0.665	0.532	0.493	0.631	0.562	0.683	0.604	0.750	0.687	0.636	1.000	0.582	0.498	0.590	0.544
15	0.640	0.541	0.552	0.561	0.511	0.491	0.558	0.555	0.609	0.598	0.626	0.638	0.630	0.582	1.000	0.470	0.520	0.472
16	0.539	0.501	0.487	0.435	0.452	0.450	0.456	0.505	0.501	0.546	0.480	0.552	0.543	0.498	0.470	1.000	0.372	0.380
17	0.583	0.448	0.478	0.543	0.439	0.408	0.518	0.468	0.564	0.506	0.617	0.571	0.560	0.590	0.520	0.372	1.000	0.411
18	0.532	0.401	0.431	0.499	0.395	0.365	0.474	0.422	0.517	0.456	0.571	0.522	0.511	0.544	0.472	0.380	0.411	1.000

Table 30. The elements of the covariance density matrix $\rho_{ij}(i = 37, 38, 39, \dots, 71, 72; j = 37, 38, 39, \dots, 71, 72;)$ for the simultaneous fit.

ρ_{ij}	37	38	39	40	41	42	43	44	45	46	47	48	49	50	51	52	53	54	55	56	57	58	59	60	61	62	63	64	65	66	67	68	69	70	71	72	
37	1.000	0.038	0.129	0.109	0.085	0.085	0.088	0.072	0.080	0.077	0.069	0.096	0.096	0.080	0.039	0.058	0.053	0.035	0.005	0.007	0.006	0.006	0.006	0.006	0.005	0.005	0.005	0.005	0.004	0.004	0.003	0.003	0.003	0.002	0.002	0.001	
38	0.038	1.000	0.091	0.139	0.102	0.102	0.107	0.084	0.096	0.093	0.083	0.121	0.123	0.102	0.047	0.072	0.067	0.045	0.006	0.007	0.007	0.007	0.007	0.007	0.006	0.006	0.006	0.006	0.005	0.004	0.004	0.003	0.003	0.003	0.002	0.002	0.002
39	0.129	0.091	1.000	0.145	0.141	0.141	0.157	0.086	0.125	0.124	0.105	0.235	0.256	0.204	0.062	0.137	0.136	0.088	0.005	0.006	0.006	0.006	0.006	0.006	0.005	0.005	0.005	0.005	0.004	0.004	0.003	0.003	0.003	0.002	0.002	0.002	0.001
40	0.109	0.139	0.145	1.000	0.013	0.125	0.127	0.082	0.107	0.105	0.091	0.173	0.184	0.148	0.053	0.101	0.099	0.064	0.006	0.007	0.007	0.006	0.006	0.006	0.006	0.006	0.005	0.005	0.004	0.004	0.004	0.003	0.003	0.003	0.002	0.002	0.002
41	0.085	0.102	0.141	0.013	1.000	-0.028	0.100	0.072	0.082	0.080	0.072	0.103	0.104	0.086	0.040	0.061	0.057	0.038	0.006	0.007	0.007	0.006	0.006	0.006	0.006	0.006	0.005	0.005	0.004	0.004	0.004	0.003	0.003	0.003	0.002	0.002	0.001
42	0.085	0.102	0.141	0.125	-0.028	1.000	-0.028	0.079	0.081	0.079	0.071	0.108	0.110	0.091	0.040	0.064	0.060	0.040	0.005	0.007	0.006	0.006	0.006	0.006	0.006	0.005	0.005	0.005	0.005	0.004	0.004	0.003	0.003	0.003	0.002	0.002	0.001
43	0.088	0.107	0.157	0.127	0.100	-0.028	1.000	-0.054	0.093	0.082	0.074	0.120	0.124	0.102	0.042	0.071	0.067	0.044	0.005	0.007	0.006	0.006	0.006	0.006	0.005	0.005	0.005	0.005	0.004	0.004	0.003	0.003	0.003	0.002	0.002	0.002	0.001
44	0.072	0.084	0.086	0.082	0.072	0.079	-0.054	1.000	-0.059	0.072	0.059	0.064	0.059	0.052	0.033	0.039	0.034	0.024	0.006	0.007	0.007	0.006	0.006	0.006	0.006	0.005	0.005	0.004	0.004	0.004	0.003	0.003	0.003	0.002	0.002	0.002	0.001
45	0.080	0.096	0.125	0.107	0.082	0.081	0.093	-0.059	1.000	-0.051	0.073	0.094	0.095	0.079	0.038	0.057	0.053	0.035	0.005	0.006	0.006	0.006	0.006	0.006	0.005	0.005	0.005	0.005	0.004	0.004	0.003	0.003	0.003	0.002	0.002	0.002	0.001
46	0.077	0.093	0.124	0.105	0.080	0.079	0.082	0.072	-0.051	1.000	-0.063	0.099	0.093	0.079	0.036	0.056	0.052	0.035	0.005	0.006	0.006	0.006	0.006	0.006	0.005	0.005	0.005	0.005	0.004	0.003	0.003	0.003	0.002	0.002	0.002	0.002	0.001
47	0.069	0.083	0.105	0.091	0.072	0.071	0.074	0.059	0.073	-0.063	1.000	-0.035	0.082	0.065	0.032	0.047	0.044	0.029	0.005	0.006	0.006	0.005	0.005	0.005	0.005	0.005	0.004	0.004	0.004	0.003	0.003	0.003	0.002	0.002	0.002	0.002	0.001
48	0.096	0.121	0.235	0.173	0.103	0.108	0.120	0.064	0.094	0.099	-0.035	1.000	0.096	0.160	0.046	0.105	0.105	0.068	0.004	0.005	0.005	0.004	0.005	0.004	0.004	0.004	0.004	0.004	0.003	0.003	0.003	0.003	0.002	0.002	0.002	0.001	0.001
49	0.096	0.123	0.256	0.184	0.104	0.110	0.124	0.059	0.095	0.093	0.082	0.096	1.000	0.073	0.050	0.114	0.116	0.074	0.003	0.004	0.004	0.004	0.004	0.004	0.003	0.003	0.003	0.003	0.003	0.003	0.002	0.002	0.002	0.002	0.001	0.001	0.001
50	0.080	0.102	0.204	0.148	0.086	0.091	0.102	0.052	0.079	0.079	0.065	0.160	0.073	1.000	-0.068	0.096	0.091	0.059	0.003	0.004	0.004	0.003	0.003	0.003	0.003	0.003	0.003	0.003	0.003	0.002	0.002	0.002	0.002	0.002	0.001	0.001	0.001
51	0.039	0.047	0.062	0.053	0.040	0.040	0.042	0.033	0.038	0.036	0.032	0.046	0.050	-0.068	1.000	-0.086	0.029	0.017	0.002	0.003	0.003	0.003	0.003	0.003	0.003	0.002	0.002	0.002	0.002	0.002	0.002	0.001	0.001	0.001	0.001	0.001	0.001
52	0.058	0.072	0.137	0.101	0.061	0.064	0.071	0.039	0.057	0.056	0.047	0.105	0.114	0.096	-0.086	1.000	-0.036	0.044	0.002	0.003	0.003	0.003	0.003	0.003	0.002	0.002	0.002	0.002	0.002	0.002	0.001	0.001	0.001	0.001	0.001	0.001	0.001
53	0.053	0.067	0.136	0.099	0.057	0.060	0.067	0.034	0.053	0.052	0.044	0.105	0.116	0.091	0.029	-0.036	1.000	-0.042	0.002	0.002	0.002	0.002	0.002	0.002	0.002	0.002	0.002	0.002	0.002	0.001	0.001	0.001	0.001	0.001	0.001	0.000	0.000
54	0.035	0.045	0.088	0.064	0.038	0.040	0.044	0.024	0.035	0.035	0.029	0.068	0.074	0.059	0.017	0.044	-0.042	1.000	0.001	0.001	0.001	0.001	0.001	0.001	0.001	0.001	0.001	0.001	0.001	0.001	0.001	0.001	0.001	0.000	0.000	0.000	0.000
55	0.005	0.006	0.005	0.006	0.006	0.005	0.005	0.006	0.005	0.005	0.005	0.005	0.004	0.003	0.003	0.002	0.002	0.002	0.001	1.000	0.157	0.216	0.248	0.186	0.168	0.215	0.198	0.244	0.221	0.299	0.237	0.224	0.233	0.182	0.142	0.157	0.138
56	0.007	0.007	0.006	0.007	0.007	0.007	0.007	0.007	0.006	0.006	0.006	0.005	0.004	0.004	0.003	0.003	0.002	0.001	0.157	1.000	0.106	0.176	0.152	0.145	0.157	0.162	0.175	0.177	0.193	0.174	0.165	0.156	0.134	0.116	0.105	0.091	
57	0.006	0.007	0.006	0.007	0.007	0.006	0.006	0.007	0.006	0.006	0.006	0.005	0.004	0.004	0.003	0.003	0.002	0.001	0.216	0.106	1.000	0.110	0.159	0.142	0.166	0.161	0.184	0.175	0.212	0.178	0.168	0.167	0.137	0.112	0.113	0.098	
58	0.006	0.007	0.006	0.006	0.006	0.006	0.006	0.006	0.006	0.006	0.005	0.004	0.004	0.003	0.003	0.003	0.002	0.001	0.248	0.176	0.110	1.000	0.075	0.151	0.197	0.166	0.220	0.181	0.279	0.201	0.190	0.210	0.151	0.108	0.140	0.123	
59	0.006	0.007	0.006	0.006	0.006	0.006	0.006	0.006	0.006	0.006	0.005	0.005	0.004	0.003	0.003	0.003	0.002	0.001	0.186	0.152	0.159	0.075	1.000	0.026	0.153	0.141	0.160	0.153	0.182	0.154	0.145	0.144	0.118	0.097	0.096	0.084	
60	0.006	0.007	0.006	0.006	0.006	0.006	0.006	0.006	0.006	0.006	0.005	0.004	0.004	0.003	0.003	0.003	0.002	0.001	0.168	0.145	0.142	0.151	0.026	1.000	0.028	0.142	0.144	0.144	0.158	0.141	0.133	0.127	0.109	0.093	0.086	0.074	
61	0.005	0.006	0.005	0.006	0.006	0.005	0.005	0.006	0.005	0.005	0.005	0.004	0.003	0.003	0.002	0.002	0.002	0.001	0.215	0.157	0.166	0.197	0.153	0.028	1.000	0.044	0.196	0.163	0.231	0.176	0.167	0.177	0.133	0.101	0.118	0.105	
62	0.005	0.006	0.005	0.006	0.006	0.005	0.005	0.006	0.005	0.005	0.005	0.004	0.003	0.003	0.002	0.002	0.002	0.001	0.198	0.162	0.161	0.166	0.141	0.142	0.044	1.000	0.064	0.176	0.190	0.168	0.159	0.153	0.130	0.110	0.104	0.091	
63	0.005	0.006	0.005	0.005	0.005	0.005	0.005	0.005	0.005	0.005	0.004	0.004	0.003	0.003	0.002	0.002	0.002	0.001	0.244	0.175	0.184	0.220	0.160	0.144	0.196	0.064	1.000	0.086	0.271	0.203	0.193	0.204	0.155	0.119	0.137	0.121	
64	0.005	0.006	0.005	0.005	0.005	0.005	0.005	0.005	0.005	0.005	0.004	0.004	0.003	0.003	0.002	0.002	0.002	0.001	0.221	0.177	0.175	0.181	0.153	0.144	0.163	0.176	0.086	1.000	0.123	0.198	0.180	0.174	0.148	0.126	0.119	0.104	
65	0.004	0.005	0.004	0.004	0.004	0.004	0.004	0.004	0.004	0.004	0.004	0.003	0.002	0.002	0.002	0.002	0.001	0.001	0.299	0.193	0.212	0.279	0.182	0.158	0.231	0.190	0.271	1.000	0.159	0.240	0.261	0.187	0.133	0.175	0.157		
66	0.004	0.004	0.004	0.004	0.004	0.004	0.004	0.004	0.004	0.003	0.003	0.003	0.002	0.002	0.002	0.002	0.001	0.001	0.237	0.174	0.178	0.201	0.154	0.141	0.176	0.168	0.203	0.198	1.000	0.098	0.201	0.156	0.126	0.133	0.117		
67	0.003	0.004	0.003	0.004	0.004	0.003	0.003	0.003	0.003	0.003	0.003	0.002	0.002	0.002	0.002	0.001	0.001	0.001	0.224	0.165	0.168	0.190	0.145	0.133	0.167	0.159	0.193	0.180	0.240	0.098	1.000	0.094	0.155	0.119	0.126	0.111	
68	0.003	0.003	0.003	0.003	0.003	0.003	0.003	0.003	0.003	0.003	0.002	0.002	0.002	0.002	0.001	0.001	0.001	0.001	0.233	0.156	0.167	0.210	0.144	0.127	0.177												